

AFRL-AFOSR-VA-TR-2023-0292

Prediction of Basic Operation of Electro-Spray Thrusters Using High Fidelity Modeling

Boyd, Iain
REGENTS OF THE UNIVERSITY OF COLORADO
3100 MARINE ST 572 UCB
BOULDER, CO,
US

03/10/2023
Final Technical Report

DISTRIBUTION A: Distribution approved for public release.

Air Force Research Laboratory
Air Force Office of Scientific Research
Arlington, Virginia 22203
Air Force Materiel Command

REPORT DOCUMENTATION PAGE

PLEASE DO NOT RETURN YOUR FORM TO THE ABOVE ORGANIZATION.

1. REPORT DATE	2. REPORT TYPE	3. DATES COVERED	
20230310	Final	START DATE 20201201	END DATE 20221130

4. TITLE AND SUBTITLE
Prediction of Basic Operation of Electro-Spray Thrusters Using High Fidelity Modeling

5a. CONTRACT NUMBER	5b. GRANT NUMBER	5c. PROGRAM ELEMENT NUMBER
	FA9550-21-1-0045	61102F
5d. PROJECT NUMBER	**5e. TASK NUMBER**	**5f. WORK UNIT NUMBER**

6. AUTHOR(S)
Iain Boyd

7. PERFORMING ORGANIZATION NAME(S) AND ADDRESS(ES)
REGENTS OF THE UNIVERSITY OF COLORADO
3100 MARINE ST 572 UCB
BOULDER, CO
US

8. PERFORMING ORGANIZATION REPORT NUMBER

9. SPONSORING/MONITORING AGENCY NAME(S) AND ADDRESS(ES)	10. SPONSOR/MONITOR'S ACRONYM(S)	11. SPONSOR/MONITOR'S REPORT NUMBER(S)
Air Force Office of Scientific Research 875 N. Randolph St. Room 3112 Arlington, VA 22203	AFRL/AFOSR RTA1	AFRL-AFOSR-VA-TR-2023-0292

12. DISTRIBUTION/AVAILABILITY STATEMENT
A Distribution Unlimited: PB Public Release

13. SUPPLEMENTARY NOTES

14. ABSTRACT
Electro-spray (ES) thrusters for in-space propulsion operate using ionic liquids that may be colloidal or metal as propellant. Individual ES devices generate very small thrust and impulse bits that are ideal for fine pointing missions. The Air Force has a more significant need for large-scale thrust levels required for station keeping, orbit raising, and orbit transfer. ES systems are of interest because they provide a specific impulse that may be tailored by the propellant, high thrust through the application of many devices in parallel, and all achieved at potentially high efficiencies of about 80%. There are significant fundamental challenges for the integration of the large numbers of devices needed for Air Force missions including: (1) failure modes of ES thrusters; (2) determining the lifetime of ES thrusters; and (3) understanding any crosstalk between adjacent thrusters. We are pursuing a comprehensive research project to address these gaps:
- Model Development: The key developments needed to model electro-spray systems are treatment of ionic-liquid physics, consideration of multiple emission sites, and extension to three dimensions.
- Model Benchmarking

15. SUBJECT TERMS

16. SECURITY CLASSIFICATION OF:			17. LIMITATION OF ABSTRACT	18. NUMBER OF PAGES
a. REPORT U	b. ABSTRACT U	c. THIS PAGE U	UU	11

19a. NAME OF RESPONSIBLE PERSON	19b. PHONE NUMBER *(Include area code)*
DEREK BARBEE	000-0000

Standard Form 298 (Rev.5/2020)
Prescribed by ANSI Std. Z39.18

DISTRIBUTION A: Distribution approved for public release.

Final Technical Report

Prediction of Basic Operation of Electrospray Thrusters
Using High-Fidelity Modeling

AFOSR Grant FA9550-21-1-0045

Monitored by Mitat Birkan

Iain D. Boyd (PI), University of Colorado

Abstract

Electro-spray (ES) thrusters for in-space propulsion operate using ionic liquids that may be colloidal or metal as propellant. Individual ES devices generate very small thrust and impulse bits that are ideal for fine pointing missions. The Air Force has a more significant need for large-scale thrust levels required for station keeping, orbit raising, and orbit transfer. ES systems are of interest because they provide a specific impulse that may be tailored by the propellant, high thrust through the application of many devices in parallel, and all achieved at potentially high efficiencies of about 80%. There are significant fundamental challenges for the integration of the large numbers of devices needed for Air Force missions including: (1) failure modes of ES thrusters; (2) determining the lifetime of ES thrusters; and (3) understanding any crosstalk between adjacent thrusters. We are pursuing a comprehensive research project to address these gaps:

- Model Development: The key developments needed to model electro-spray systems are treatment of ionic-liquid physics, consideration of multiple emission sites, and extension to three dimensions.
- Model Benchmarking: Integration of high-fidelity modeling with empirical data is necessary to characterize life-limiting mechanisms and extrapolate performance in space environments. Direct comparisons will be made of model predictions with detailed plume measurements of AFRL porous-media flow emitters that are under way at the University of Michigan. Comparisons will also be made with all relevant data sets generated at the Air Force Research Laboratory in their current ES activities.
- Use the high-fidelity simulations to provide fundamental data needed for application of low-fidelity analysis of ES thrusters. For example, understanding the process and conditions for mode switching to the pure ionic regime is essential to meeting the USAF requirements for this technology.
- Analyses: Use the high-fidelity model for large arrays including assessment of coupling effects between multiple electro-spray emitters and prediction of primary failure modes.

This final report summarizes the progress made during the first and second years of the grant in terms of source and plume modeling.

DISTRIBUTION A: Distribution approved for public release.

1. Electrospray Model Description

A single porous electrospray emitter operating in a purely ionic emission regime is considered. The domain of interest spans from the emission site on the tip to the downstream plume between the extractor and accelerator electrodes. Computationally, this domain is partitioned into two two-dimensional subdomains: an Extraction Region where field emission from the electrohydrodynamic (EHD) meniscus is considered, and a Plume Region where the ion dynamics of the extracted species are considered. The Extraction Region is further decomposed into a vacuum and bulk liquid domain, Ω_{vac} and Ω_{liq} respectively, where Γ_{lv} denotes the intersection between them. A schematic of the global domain is presented in Fig. 1.

Within the bulk liquid, mass and momentum conservation are considered using the Navier-Stokes equations are the low Reynolds number limit, otherwise known as the Stokes equations,

$$\mu\nabla^2 v - \nabla \mathrm{p} = 0, \tag{1}$$
$$\nabla \cdot v = 0, \tag{2}$$

where μ is fluid viscosity, v is bulk fluid velocity, and p is pressure. Given the propellant is conductive, charge transport is considered as well. Convective charge transport is neglected and an Ohmic conduction model is chosen,

$$j = -K\nabla\phi_l, \tag{3}$$

where j is the current density, K is the electrical conductivity and ϕ_l is the electric potential in the bulk fluid. When charge conservation, $\nabla \cdot j = 0$, is considered with Eqn. (3) the electric potential can be shown to satisfy Laplace's equation,

$$\nabla^2\phi_l = 0. \tag{4}$$

Within the vacuum, space charge effects are negligible, and Laplace's equation is again used to determine the potential,

$$\nabla^2\phi_v = 0, \tag{5}$$

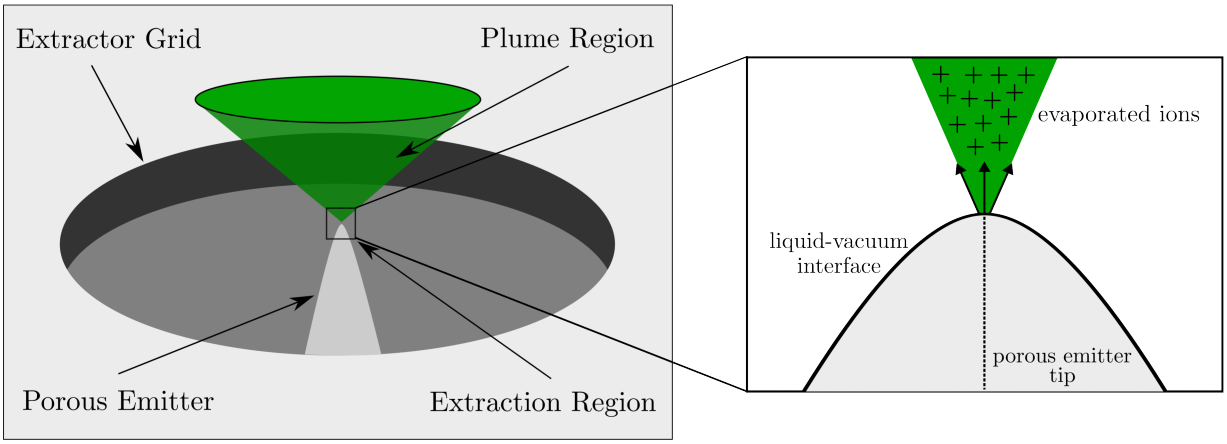


Figure 1. Domains of interest within a porous electrospray emitter.

where ϕ_v is the electric potential within the vacuum. At the liquid-vacuum interface, the free surface charge density is considered using the electrostatic condition,

$$(-\nabla\phi_v + \epsilon\nabla\phi_l)\cdot\hat{n} = \frac{\sigma}{\epsilon_0}, \tag{6}$$

where $\hat{n}$ is the unit vector normal to the interface, σ is the free surface charge density, ϵ is the relative permittivity, and ϵ_0 is the vacuum permittivity. Additionally, the free surface charge density satisfies the following steady-state transport equation,

$$v\cdot\nabla\sigma = \sigma\hat{n}\cdot\nabla v\cdot\hat{n} - K\nabla\phi_l\cdot\hat{n} - j\cdot\hat{n}. \tag{7}$$

Equation (7) states that the charge advected by the fluid flow is balanced by surface strain, the charge conducted to the surface, and the charge lost due to ion evaporation. Field emission of ions is described by the kinetic law,

$$j\cdot\hat{n} = \frac{k_b T}{h_c}\sigma\exp\left(\frac{-1}{k_b T}\left[\Delta G - \sqrt{\frac{\nabla\phi_v\cdot\hat{n}}{4\pi\epsilon_0/q^3}}\right]\right), \tag{8}$$

where k_b is the Boltzmann constant, h_c is the Planck constant, T is the temperature, q is the elementary charge and ΔG is the solvation energy of the ions. Additionally, force balance between the applied electric traction, viscous stresses, and surface tension is enforced at the liquid-vacuum interface,

$$\hat{t}\cdot(\tau_l - \tau_e)\cdot\hat{n} = 0, \tag{9}$$
$$\hat{n}\cdot(\tau_l - \tau_e)\cdot\hat{n} = -\gamma\nabla\cdot\hat{n}, \tag{10}$$

where $\hat{\boldsymbol{t}}$ is the unit vector tangent to the interface, τ_l is the viscous stress tensor, τ_e is the electrostatic Maxwell stress tensor, and γ is the surface tension. The normal and tangential projections of the Maxwell stress tensor on the interface satisfy the equations

$$\hat{t}\cdot\tau_e\cdot\hat{n} = -\sigma\nabla\phi_v\cdot\hat{t}, \tag{11}$$
$$\hat{n}\cdot\tau_e\cdot\hat{n} = \frac{1}{2}\epsilon_0((\nabla\phi_v\cdot\hat{n})^2 - \epsilon(\nabla\phi_l\cdot\hat{n})^2) + \frac{1}{2}\epsilon_0\big((\epsilon-1)(\nabla\phi_v\cdot\hat{t})^2\big). \tag{12}$$

A hybrid direct simulation Monte Carlo and particle-in-cell (DSMC–PIC) solver is implemented to simulate the downstream rarefied plume, of which a complete description of the solver can be found by Cai [1]. In summary, DSMC is a widely implemented particle method used to calculate collisional dynamics within dilute gases. Analogously for plasmas, PIC is a kinetic method used to simulate the dynamics of charged particles under the influence of external and self–induced electromagnetic fields. Simultaneous implementation of both methods within a

unified kinetic solver allows the study of gases characterized by both material and Coulombic interactions.

Within the multiscale model, the DSMC–PIC solver is used to initialize a distribution of charged macroparticles at the liquid–vacuum interface as well as simulate their motion within the computational vacuum domain. The initial distribution is a function of the ion number density determined by the EHD meniscus solver. The emission velocity is sampled from a biased Maxwellian based on the propellant temperature. From there, macroscopic plume properties that contribute to single emitter failure mechanisms can be calculated and simulations can be designed to study configurations that minimize these mechanisms. For example, the primary failure mode of electrosprays is overspray of propellant at the site of emission, resulting in impingement of the electrodes that ultimately contribute to shorting and power processing unit failure [2]. By conducting a sensitivity analysis, the proposed model may be able to elucidate what elements of the parameter space contribute most to the plume divergence angle, minimizing the probability of electrode impingement.

A complete schematic of the computational domain is presented in Fig. 2. Fig. 2a presents a macro-scale, two-dimensional domain of a single emitter tip below two extractor electrodes A voltage differential is applied between the emitter and electrodes to induce electric fields strengths on the order required for direct ion evaporation at the propellant free surface. Field emission at the interface is numerically treated within a separate sub-scale domain at the emitter apex and is coupled to the macro-scale domain via the Γ_{sub} intersection. Fig. 2b presents a sub-scale domain of an emission site at the emitter apex presented in Fig. 2a. Steady, open channel flow is assumed for the propellant in Ω_{liq}, where a fully developed velocity profile is imposed at the Γ_{inl} inlet boundary. Geometry of the EHD meniscus, Γ_{int}, is numerically perturbed to find configurations that satisfy mechanical equilibrium, a prerequisite to solve for steady-state emission characteristics.

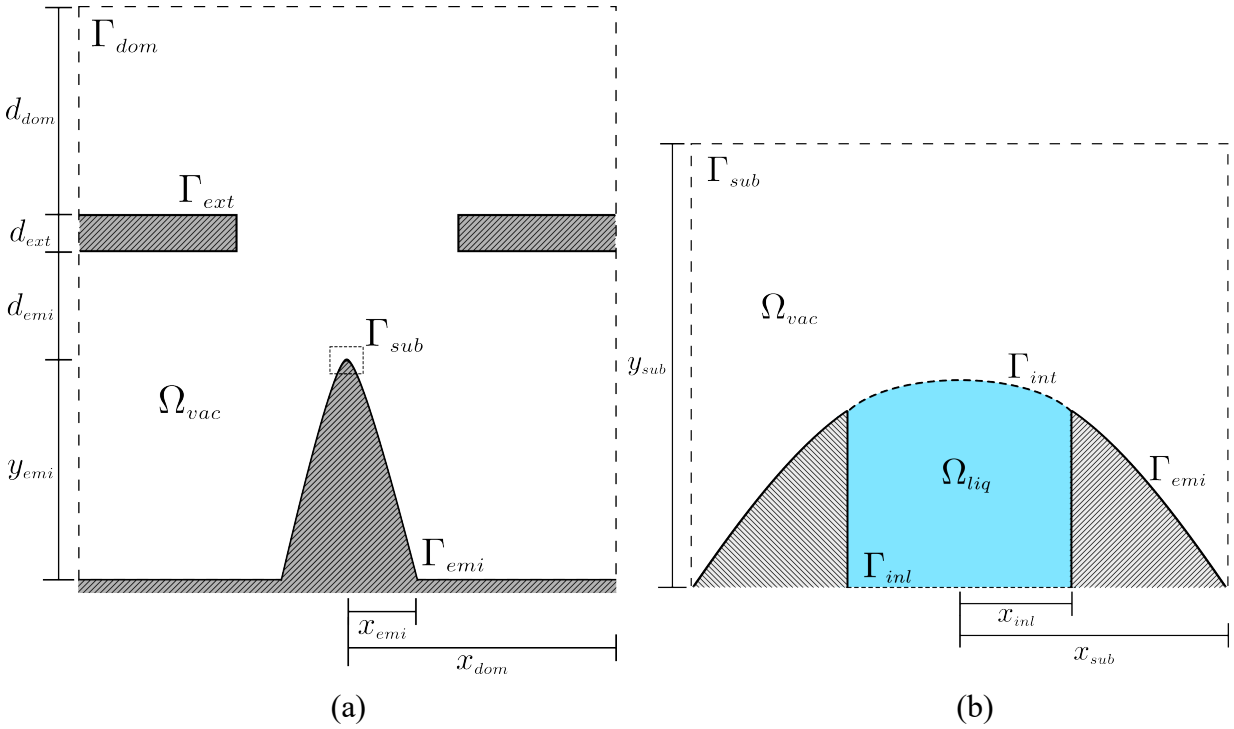


Figure 2. Computational domain.

2. Progress to Date

2.1 Numeric Implementation

The core developmental progress within the electrospray model has been within the Extraction Region. A finite element solver has been implemented using the Distributed and Unified Numerics Environment (DUNE), an open-source library for solving partial differential equations using grid-based methods. An algorithm has been developed that solves the coupled set of partial differential equations for a prescribed meniscus shape. The algorithm generally operates as follows:

The core Stokes and Laplace equations are solved in their respective domains. A multidomain module is configured to enforce boundary conditions that are dependent upon solutions across domains. An additional module is developed to enforce directionally dependent boundary conditions on the same interface. Consideration of electrostatic conditions, surface charge density transport, and stress balance at the free surface act as these unique multidomain boundary conditions. An iterative routine first solves the electric potential system until convergence, at which a global algorithm is implemented that solves the Stokes system and couples the domain together. A flowchart of this global algorithm is presented in Fig. 3. The result is a converged nonequilibrium solution for a prescribed meniscus shape. The current stage of development is expanding this to equilibrium solutions by including meniscus geometry perturbations in the global algorithm.

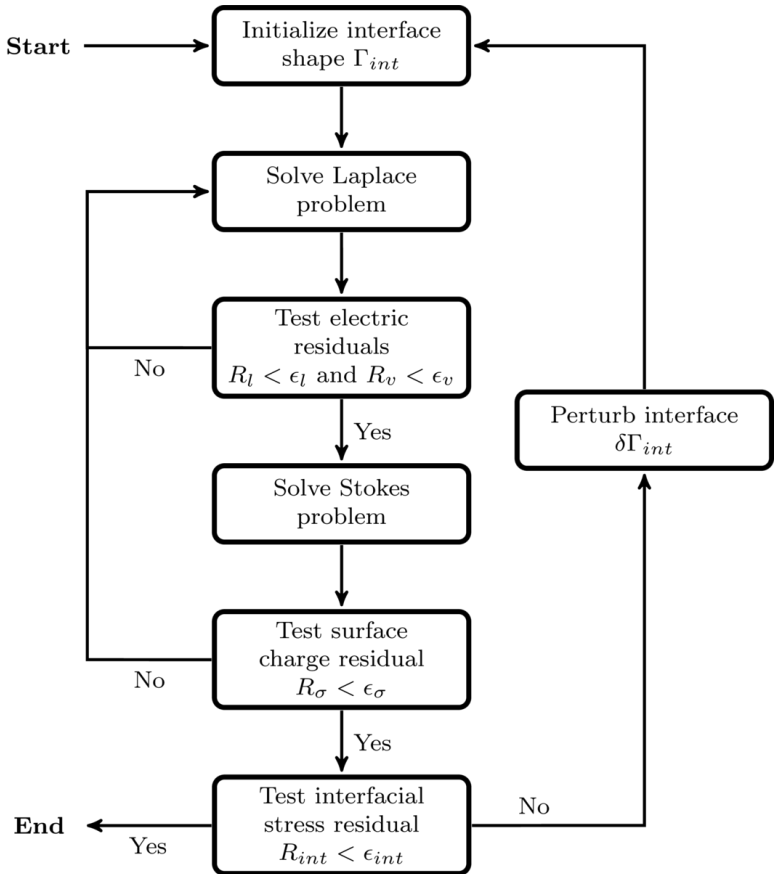


Figure 3. Algorithm to numerically solve for ion emission from the EHS meniscus within the Extraction Region.

2.2 Results

2.2.1 Simulation Parameters

Initial simulations within the Extraction and Plume region are conducted using similar operating parameters as those in [3]. Mapping of ion emission from the Extraction Region to the kinetic routine is not directly calculated. Experimental current values are used as input conditions into the kinetic routine via single cell injection at the emitter tip. The applied electric field condition within the EHD model is calibrated such that the integrated surface emission at the meniscus tip is of approximate order to the experimental current. Direct mapping of field emission from the EHD model within the Extraction Region to the kinetic model in the Plume Region is deferred to future work. A computational domain axial length of 0.1 μm and width of 0.1 μm is chosen for the Extraction Region, to emulate similar length scales of effective low paths within porous electrospray emitters. Meshes of the liquid and vacuum subdomains in the Extraction Region are shown in Fig. 3. A Taylor Cone angle of 49.29° is chosen for the emitter cone with a tip radius of 10 nm. Mesh elements at the emitter tip are refined in both subdomains to better resolve ion emission in this region. The computational domain of the Plume Region spans a radial distance of 500 μm and 1000 μm axially.

2.2.2 Electric Potentials

Electric potential distributions within the liquid and vacuum subdomains of the Extraction Region are presented in Fig. 4. A relatively linear progression is seen in the axial direction of both domains, with continuity between electric potentials at the interface. The potential within the liquid domain, Fig. 4a, can be seen enforced to zero where the fluid contacts the emitter electrode. A potential gradient tangential to the interface is also observed, suggesting a stronger electric field towards the meniscus center. This behavior is expected for a perturbed conductive fluid exposed to an external field, as the perturbation would result in a higher charge density at the tip and would result in a higher field strength. Continuity of electric potential across the liquid and vacuum domain interface is also observed. As the interfacial jump in electric displacement is innately enforced by the iteration scheme, all facets of the Laplace problem appear correctly represented within the semi-equilibrium potential distributions.

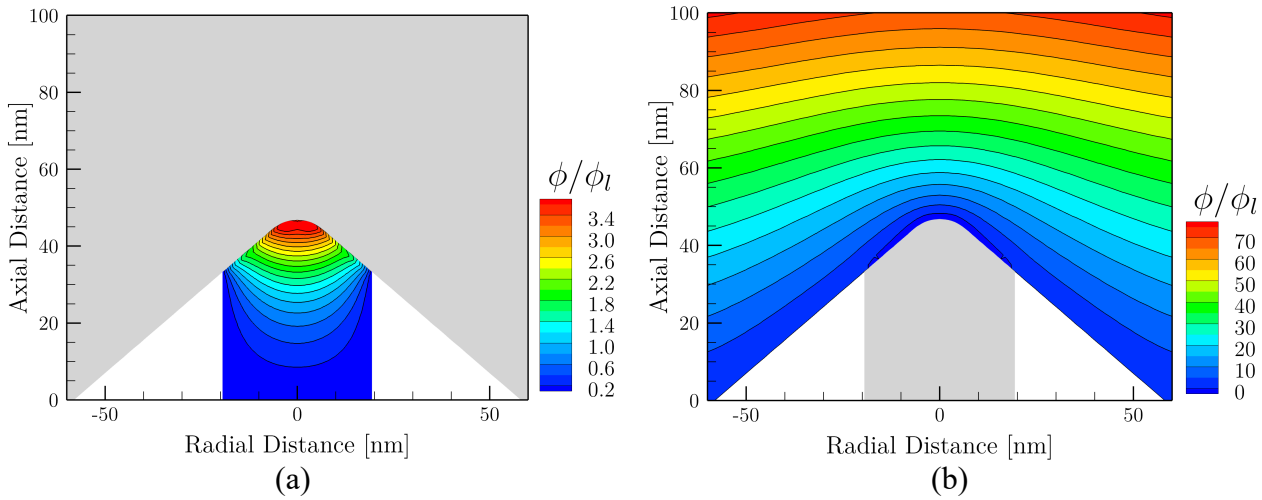


Figure 4. Electric potential distributions within the (a) liquid and (b) vacuum subdomains.

2.2.3 Stokes Flow and Ion Emission

Axial velocity contours within the liquid subdomain of the Extraction Region are presented in Fig. 5. Flow velocity of an ionic liquid meniscus operating in a purely ionic regime is known to scale with

$$v \sim \frac{I}{\pi\rho(q/m)(r^*)^2}, \tag{13}$$

where r^* is the characteristic length scale at the emitter tip and I is the emission current [4]. The Reynolds number scaling is then shown to be

$$Re \sim \frac{I}{\pi\mu(q/m)r^*} \sim 10^{-2}. \tag{14}$$

Using the single-emitter current for the -1562 V operational case ($I \approx 10^{-6}A$) in [3] and the fluid properties of EMI-BF_4 ($\mu \approx 10^{-2}$ Pa·s, $q/m \approx 10^6$ C/kg), the Reynolds number is shown to be significantly less than unity and thus Stokes flow is present. As mentioned, ion emission is only possible within a steady-state configuration if the normal fluid velocity at the intersection is nonzero. Field emission at the emitter tip is represented by arrows in the top-right plot of Fig. 5. It can be shown that the velocity at the emission tip is of approximate order to the emission velocity in the operational case, though it is important to note that the applied electric field, E_0, is adjusted in the Extraction Region to achieve this agreement.

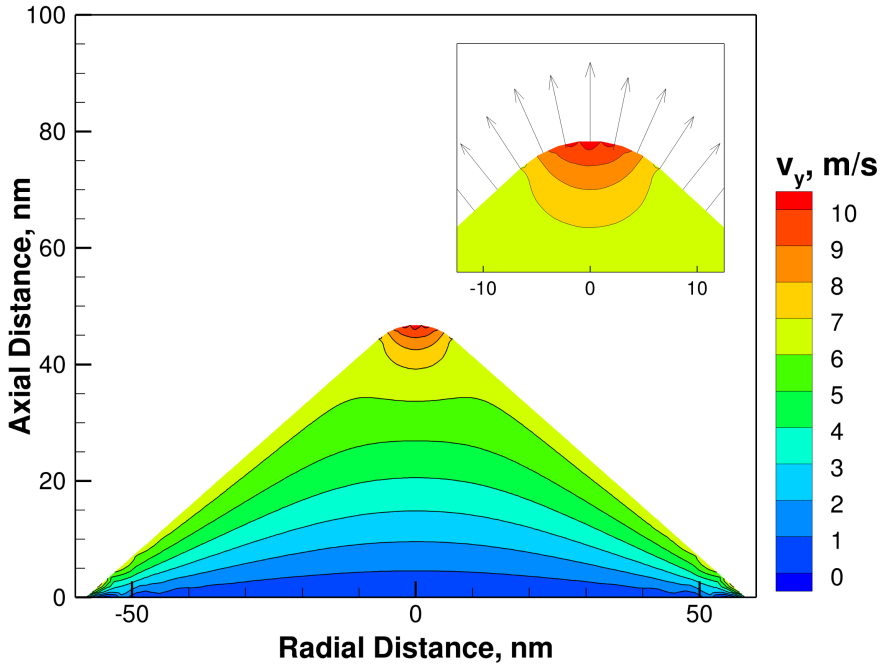


Figure 5. Axial velocity in the bulk fluid, with ion emission at the emitter tip shown in the inset.

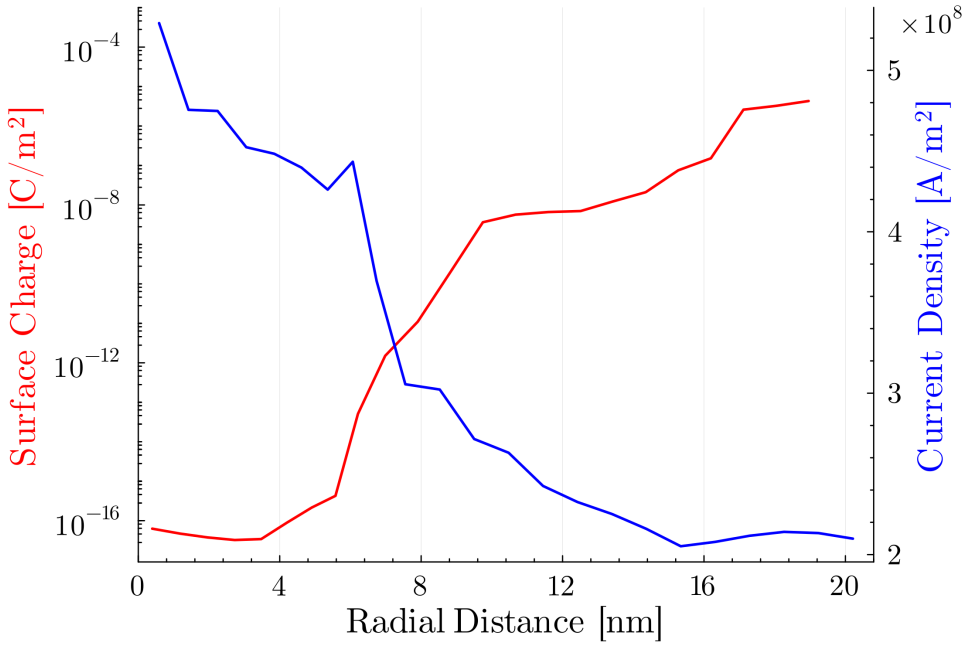


Figure 6. Interfacial surface charge and normal current density versus radial distance.

Characteristics of the Stokes problem can be observed through the interfacial current density, as it is linearly related to the normal fluid velocity at the meniscus. This current density in addition to the surface charge are plotted as a function of the radial distance in Fig. 6. As seen by the potential distribution, the emission centerline should correspond to the highest electric field, which in turn should result in the highest current density of emitted species. This is observed in Fig. 6, where the current density progressively declines with radial distance as the applied electric field weakens away from the centerline. The surface charge, on the other hand, appears to be inversely related to the current density with respect to radial distance. This is due to the continuity law of Eqn. (7), stating the surface charge represents the balance of current conducted to the interface and current evaporating from the interface. This balance is depicted in Fig. 6, where the surface charge is minimum at the interfacial locations corresponding to the highest ion emission, and vice versa. Additional quantitative validation of the EHD solver with occur once the interfacial perturbation scheme is implemented.

2.2.4 Plume Simulations

Independent simulations of the DSMC–PIC solver were conducted as well. As the coupling with the EHD meniscus solver has yet to be implemented, the simulations were initialized using experimental data of Natisin et al. [3]. Similarly, EMI-BF4 is chosen as the propellant. Within the simulation, the plume is assumed to consist of a 1:1 mixture of single-charged EMI^+ ions and EMI-BF4 neutrals. Ions colliding with any solid surfaces are reflected as neutral molecules. Emission current and thrust are calculated about the plane approximately 1000 μm away from the emitter base and are linearly scaled to match the experimental configuration where 576 emitters were operated in parallel. Within the plume, EMI^+ ion speeds (m/s) were calculated and are presented in Fig. 7, while comparisons of the numerical and measured values for emission current

and thrust are presented in Fig. 8. Agreement is shown between the numerical and experimental data across a range of extractor voltages, suggesting that downstream characteristics of the plume can be accurately simulated given sufficient initial conditions.

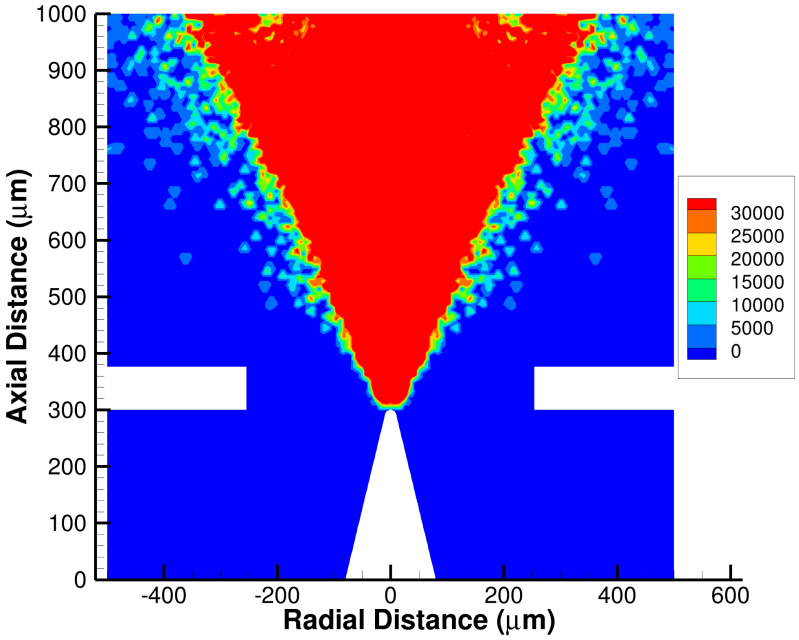


Figure 7. EMI+ ion speeds (m/s)

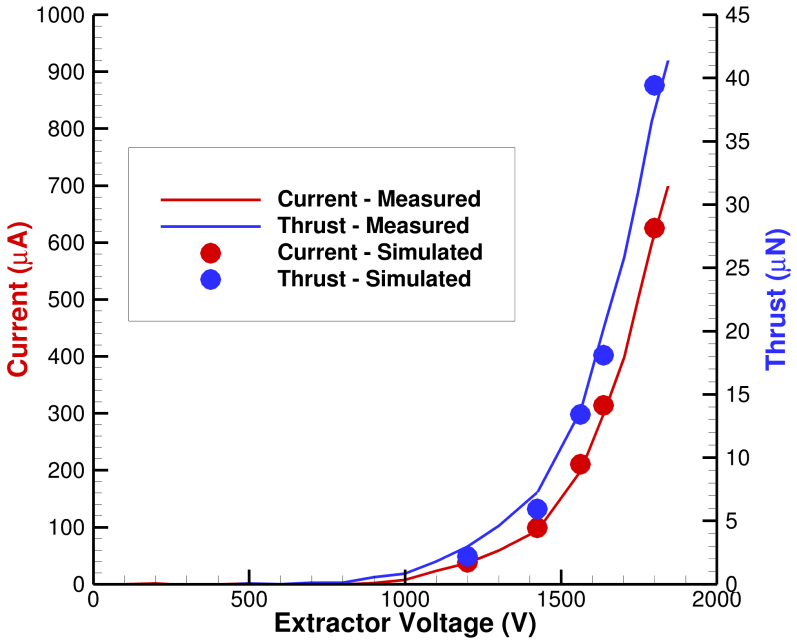


Figure 8. Comparison of emission current and thrust between experimental measurements by Natisin et al. [3] and DSMC–PIC simulation output.

3. Future Objectives

The majority of model development thus far has been within the Extraction Region. Implementing a normal stress balance routine at the interface, Eqn. (10), is the final module required for completion of the field emission model. This stress is a function of the surface tension, and thus the geometry of the meniscus. To complete this, a meniscus perturbation module must be developed that evolves the shape into one that satisfies equilibrium. Currently, the solver determines a nonequilibrium solution for a prescribed meniscus shape. With the addition of the meniscus perturbation module, the final equation of the field emission model is resolved, completing the Extraction Region component of the model. Development time for this module is estimated to take 1-2 months.

The kinetic model within the Plume Region is solved using an in-house direct simulation Monte-Carlo and particle-in-cell solver, and thus no core development is required. As such, the final task for the single emitter electrospray model is coupling the subscale routine in the Extraction Regime with the macroscale kinetic routine in the plume. To achieve a two-way coupling, the output of each submodel must be fed as boundary conditions to the other. Development time for this coupling module is estimated to take an additional month.

When the high-fidelity electrospray model is complete, its applications can be explored in parallel. First, the model must be benchmarked by comparing simulations with experimental measurements. Experimental measurements are nominally taken for electrosprays operating in arrays in the order of 100-1000, challenging validation of single emitter models as coupling effects cannot be accounted for. To overcome this, the Air Force Research Laboratory (AFRL) is conducting a Single Emitter Air Force Electrospray Thruster (SEAFET) program, providing data that can be directly used as validation for the single emitter model. The program has conducted a preliminary qualitative analysis of select emitters [5], with additional data to be made available in the coming months.

Further collaboration with the SEAFET program can allow exploration of the dependencies certain operating conditions have in life-limiting mechanisms. Once an initial benchmarking has been conducted, simulations spanning large parameter sweeps can be conducted to better quantify how perturbations in operations conditions such as geometry, voltage and material selection affect emission characteristics that directly contribute to failure modes. Experimental data could be taken for select configurations for calibration and further validation of the single emitter model. As the primary mechanism contributing to electrospray failure is emission impingement at the electrodes, exploring which facets of electrospray design and operation that directly contribute to overspraying at the grid will be the initial focus of the study.

The availability of both single emitter and multiplexed emitter data also allow for study of coupling effects within these systems. Experiments have demonstrated that emission characteristics of multiplexed arrays are not linear extrapolations of single emitter characteristics, alluding to possible inter-emitter dependencies. Once a single emitter model is validated, simulations can be configured to explore possible macroscopic effects that may occur from operating emitters in parallel. Again, these simulations may help elucidate what components of design and operation are contributing to this phenomenon by conducting parameter sweeps that are otherwise infeasible to perform experimentally. The results of which may then support select configurations of interest where experimentation can be conducted, optimizing the iterative routine towards building electrosprays whose mission capabilities vastly expand beyond those that are available today.

References

[1] C. Cai, "Theoretical and numerical studies of plume flows in vacuum chambers.," Ph.D. Dissertation, University of Michigan, Ann Arbor, 2005.

[2] A. Thuppul, P. L. Wright, A. L. Collins, J. K. Ziemer, and R. E. Wirz, "Lifetime Considerations for Electrospray Thrusters," *Aerospace*, vol. 7, no. 8, p. 108, Aug. 2020.

[3] M. Natisin, H. Zamora, W. McGehee, N. Arnold, Z. Holley, M. Holmes, and D. Eckhardt, "Fabrication and characterization of a fully conventionally machined, high-performance porous-media electrospray thruster," *Journal of Micromechanics and Microengineering*, vol. 30, no. 11, p. 115021, 2020.

[4] C. S. Coffman, "Electrically-assisted evaporation of charged fluids: Fundamental modeling and studies on ionic liquids," Ph.D. dissertation, Massachusetts Institute of Technology, 2016.

[5] W. A. McGehee, N. Arnold, M. R. Natisin, Z. A. Holley, and D. Eckhardt, "The single emitter air force electrospray thruster (SEAFET) Program: Goals and initial results," in *37th International Electric Propulsion Conference*, Massachusetts Institute of Technology, Cambridge, MA USA, Jun. 2022.

Final Technical Report

Prediction of Basic Operation of Electrospray Thrusters
Using High-Fidelity Modeling

AFOSR Grant FA9550-21-1-0045

Monitored by Mitat Birkan

Iain D. Boyd (PI), University of Colorado

Abstract

Electro-spray (ES) thrusters for in-space propulsion operate using ionic liquids that may be colloidal or metal as propellant. Individual ES devices generate very small thrust and impulse bits that are ideal for fine pointing missions. The Air Force has a more significant need for large-scale thrust levels required for station keeping, orbit raising, and orbit transfer. ES systems are of interest because they provide a specific impulse that may be tailored by the propellant, high thrust through the application of many devices in parallel, and all achieved at potentially high efficiencies of about 80%. There are significant fundamental challenges for the integration of the large numbers of devices needed for Air Force missions including: (1) failure modes of ES thrusters; (2) determining the lifetime of ES thrusters; and (3) understanding any crosstalk between adjacent thrusters. We are pursuing a comprehensive research project to address these gaps:

- Model Development: The key developments needed to model electro-spray systems are treatment of ionic-liquid physics, consideration of multiple emission sites, and extension to three dimensions.
- Model Benchmarking: Integration of high-fidelity modeling with empirical data is necessary to characterize life-limiting mechanisms and extrapolate performance in space environments. Direct comparisons will be made of model predictions with detailed plume measurements of AFRL porous-media flow emitters that are under way at the University of Michigan. Comparisons will also be made with all relevant data sets generated at the Air Force Research Laboratory in their current ES activities.
- Use the high-fidelity simulations to provide fundamental data needed for application of low-fidelity analysis of ES thrusters. For example, understanding the process and conditions for mode switching to the pure ionic regime is essential to meeting the USAF requirements for this technology.
- Analyses: Use the high-fidelity model for large arrays including assessment of coupling effects between multiple electro-spray emitters and prediction of primary failure modes.

This final report summarizes the progress made during the first and second years of the grant in terms of source and plume modeling.

DISTRIBUTION A: Distribution approved for public release.

1. Electrospray Model Description

A single porous electrospray emitter operating in a purely ionic emission regime is considered. The domain of interest spans from the emission site on the tip to the downstream plume between the extractor and accelerator electrodes. Computationally, this domain is partitioned into two two-dimensional subdomains: an Extraction Region where field emission from the electrohydrodynamic (EHD) meniscus is considered, and a Plume Region where the ion dynamics of the extracted species are considered. The Extraction Region is further decomposed into a vacuum and bulk liquid domain, Ω_{vac} and Ω_{liq} respectively, where Γ_{lv} denotes the intersection between them. A schematic of the global domain is presented in Fig. 1.

Within the bulk liquid, mass and momentum conservation are considered using the Navier-Stokes equations are the low Reynolds number limit, otherwise known as the Stokes equations,

$$\mu\nabla^2 v - \nabla \mathrm{p} = 0, \tag{1}$$
$$\nabla \cdot v = 0, \tag{2}$$

where μ is fluid viscosity, v is bulk fluid velocity, and p is pressure. Given the propellant is conductive, charge transport is considered as well. Convective charge transport is neglected and an Ohmic conduction model is chosen,

$$j = -K\nabla\phi_l, \tag{3}$$

where j is the current density, K is the electrical conductivity and ϕ_l is the electric potential in the bulk fluid. When charge conservation, $\nabla \cdot j = 0$, is considered with Eqn. (3) the electric potential can be shown to satisfy Laplace's equation,

$$\nabla^2\phi_l = 0. \tag{4}$$

Within the vacuum, space charge effects are negligible, and Laplace's equation is again used to determine the potential,

$$\nabla^2\phi_v = 0, \tag{5}$$

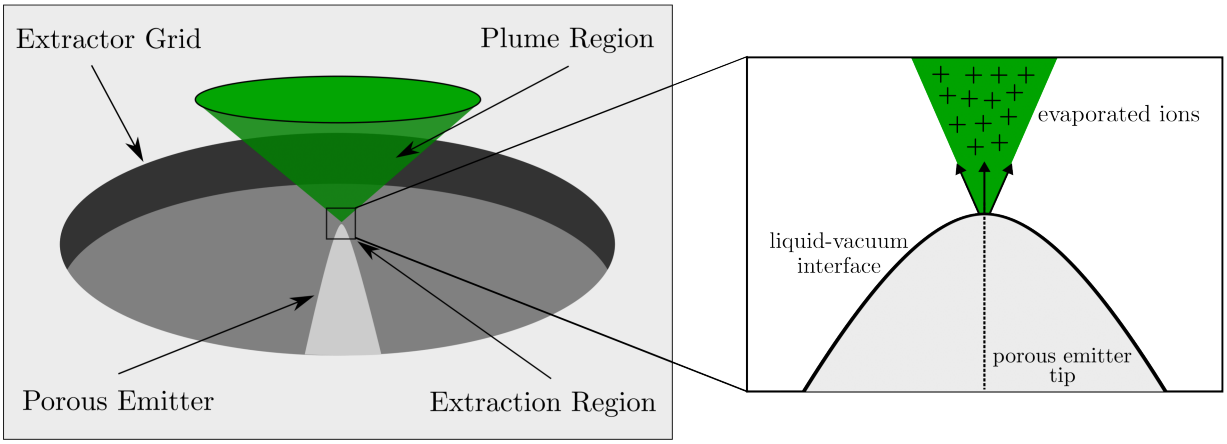


Figure 1. Domains of interest within a porous electrospray emitter.

DISTRIBUTION A: Distribution approved for public release.

where ϕ_v is the electric potential within the vacuum. At the liquid-vacuum interface, the free surface charge density is considered using the electrostatic condition,

$$(-\nabla\phi_v + \epsilon\nabla\phi_l)\cdot\hat{n} = \frac{\sigma}{\epsilon_0}, \tag{6}$$

where $\hat{n}$ is the unit vector normal to the interface, σ is the free surface charge density, ϵ is the relative permittivity, and ϵ_0 is the vacuum permittivity. Additionally, the free surface charge density satisfies the following steady-state transport equation,

$$v\cdot\nabla\sigma = \sigma\hat{n}\cdot\nabla v\cdot\hat{n} - K\nabla\phi_l\cdot\hat{n} - j\cdot\hat{n}. \tag{7}$$

Equation (7) states that the charge advected by the fluid flow is balanced by surface strain, the charge conducted to the surface, and the charge lost due to ion evaporation. Field emission of ions is described by the kinetic law,

$$j\cdot\hat{n} = \frac{k_b T}{h_c}\sigma\exp\left(\frac{-1}{k_b T}\left[\Delta G - \sqrt{\frac{\nabla\phi_v\cdot\hat{n}}{4\pi\epsilon_0/q^3}}\right]\right), \tag{8}$$

where k_b is the Boltzmann constant, h_c is the Planck constant, T is the temperature, q is the elementary charge and ΔG is the solvation energy of the ions. Additionally, force balance between the applied electric traction, viscous stresses, and surface tension is enforced at the liquid-vacuum interface,

$$\hat{t}\cdot(\tau_l - \tau_e)\cdot\hat{n} = 0, \tag{9}$$
$$\hat{n}\cdot(\tau_l - \tau_e)\cdot\hat{n} = -\gamma\nabla\cdot\hat{n}, \tag{10}$$

where $\hat{\boldsymbol{t}}$ is the unit vector tangent to the interface, τ_l is the viscous stress tensor, τ_e is the electrostatic Maxwell stress tensor, and γ is the surface tension. The normal and tangential projections of the Maxwell stress tensor on the interface satisfy the equations

$$\hat{t}\cdot\tau_e\cdot\hat{n} = -\sigma\nabla\phi_v\cdot\hat{t}, \tag{11}$$
$$\hat{n}\cdot\tau_e\cdot\hat{n} = \frac{1}{2}\epsilon_0((\nabla\phi_v\cdot\hat{n})^2 - \epsilon(\nabla\phi_l\cdot\hat{n})^2) + \frac{1}{2}\epsilon_0\big((\epsilon-1)(\nabla\phi_v\cdot\hat{t})^2\big). \tag{12}$$

A hybrid direct simulation Monte Carlo and particle-in-cell (DSMC–PIC) solver is implemented to simulate the downstream rarefied plume, of which a complete description of the solver can be found by Cai [1]. In summary, DSMC is a widely implemented particle method used to calculate collisional dynamics within dilute gases. Analogously for plasmas, PIC is a kinetic method used to simulate the dynamics of charged particles under the influence of external and self–induced electromagnetic fields. Simultaneous implementation of both methods within a

unified kinetic solver allows the study of gases characterized by both material and Coulombic interactions.

Within the multiscale model, the DSMC–PIC solver is used to initialize a distribution of charged macroparticles at the liquid–vacuum interface as well as simulate their motion within the computational vacuum domain. The initial distribution is a function of the ion number density determined by the EHD meniscus solver. The emission velocity is sampled from a biased Maxwellian based on the propellant temperature. From there, macroscopic plume properties that contribute to single emitter failure mechanisms can be calculated and simulations can be designed to study configurations that minimize these mechanisms. For example, the primary failure mode of electrosprays is overspray of propellant at the site of emission, resulting in impingement of the electrodes that ultimately contribute to shorting and power processing unit failure [2]. By conducting a sensitivity analysis, the proposed model may be able to elucidate what elements of the parameter space contribute most to the plume divergence angle, minimizing the probability of electrode impingement.

A complete schematic of the computational domain is presented in Fig. 2. Fig. 2a presents a macro-scale, two-dimensional domain of a single emitter tip below two extractor electrodes A voltage differential is applied between the emitter and electrodes to induce electric fields strengths on the order required for direct ion evaporation at the propellant free surface. Field emission at the interface is numerically treated within a separate sub-scale domain at the emitter apex and is coupled to the macro-scale domain via the Γ_{sub} intersection. Fig. 2b presents a sub-scale domain of an emission site at the emitter apex presented in Fig. 2a. Steady, open channel flow is assumed for the propellant in Ω_{liq}, where a fully developed velocity profile is imposed at the Γ_{inl} inlet boundary. Geometry of the EHD meniscus, Γ_{int}, is numerically perturbed to find configurations that satisfy mechanical equilibrium, a prerequisite to solve for steady-state emission characteristics.

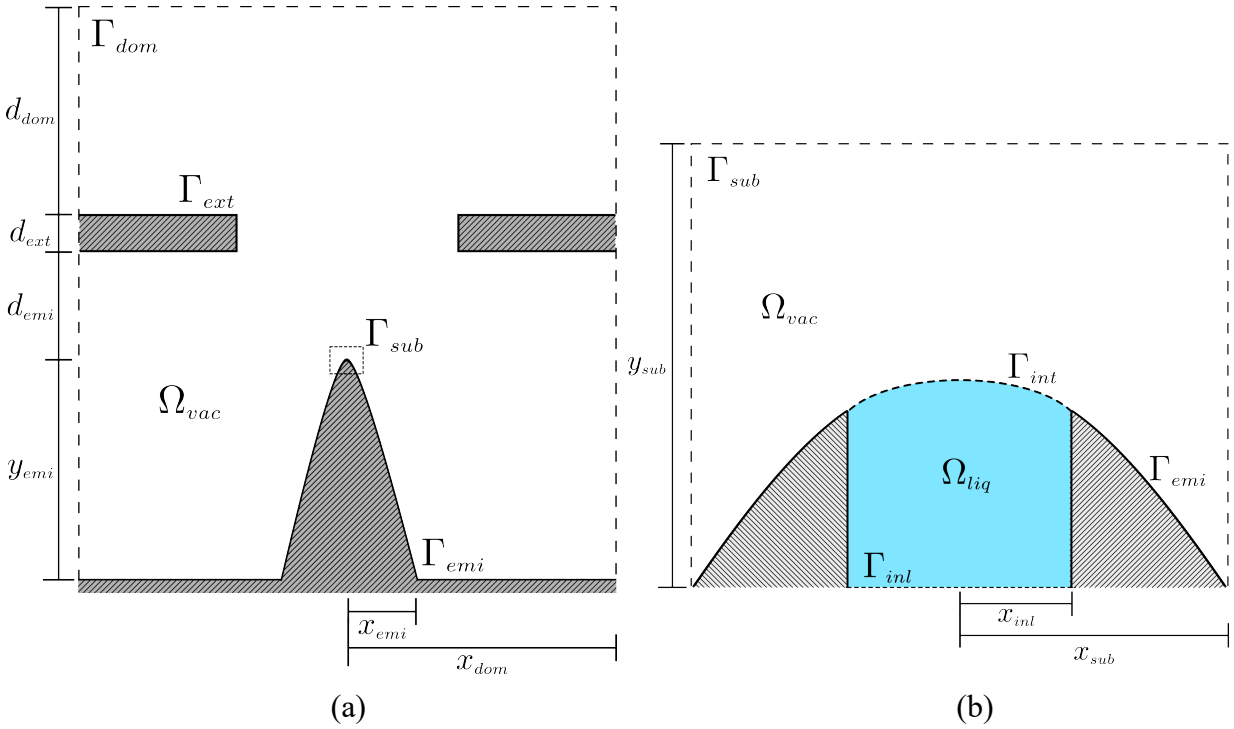


Figure 2. Computational domain.

2. Progress to Date

2.1 Numeric Implementation

The core developmental progress within the electrospray model has been within the Extraction Region. A finite element solver has been implemented using the Distributed and Unified Numerics Environment (DUNE), an open-source library for solving partial differential equations using grid-based methods. An algorithm has been developed that solves the coupled set of partial differential equations for a prescribed meniscus shape. The algorithm generally operates as follows:

The core Stokes and Laplace equations are solved in their respective domains. A multidomain module is configured to enforce boundary conditions that are dependent upon solutions across domains. An additional module is developed to enforce directionally dependent boundary conditions on the same interface. Consideration of electrostatic conditions, surface charge density transport, and stress balance at the free surface act as these unique multidomain boundary conditions. An iterative routine first solves the electric potential system until convergence, at which a global algorithm is implemented that solves the Stokes system and couples the domain together. A flowchart of this global algorithm is presented in Fig. 3. The result is a converged nonequilibrium solution for a prescribed meniscus shape. The current stage of development is expanding this to equilibrium solutions by including meniscus geometry perturbations in the global algorithm.

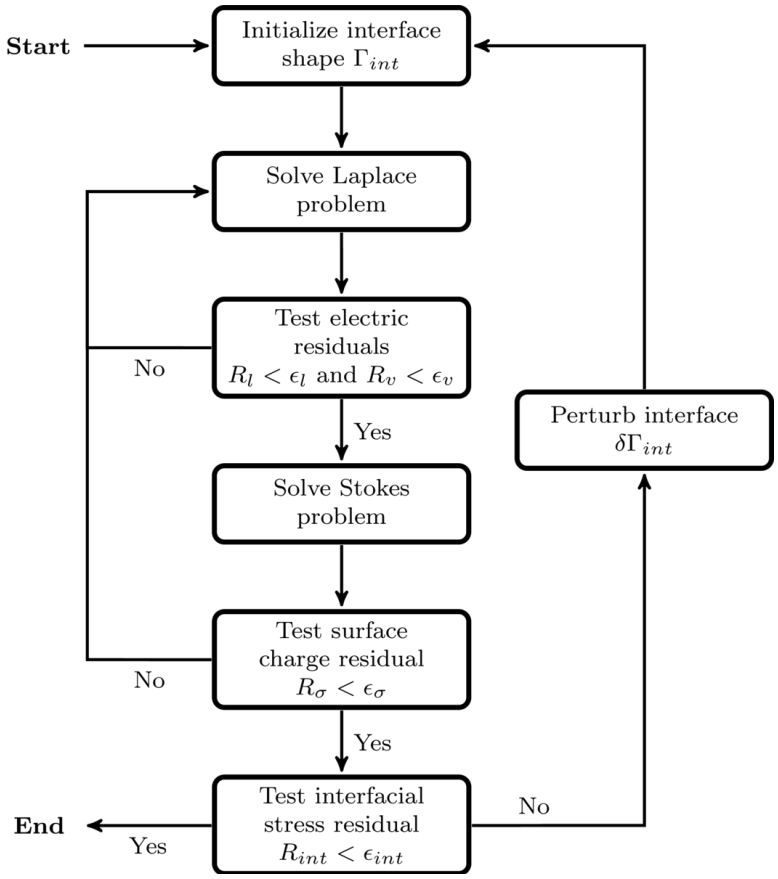


Figure 3. Algorithm to numerically solve for ion emission from the EHS meniscus within the Extraction Region.

2.2 Results

2.2.1 Simulation Parameters

Initial simulations within the Extraction and Plume region are conducted using similar operating parameters as those in [3]. Mapping of ion emission from the Extraction Region to the kinetic routine is not directly calculated. Experimental current values are used as input conditions into the kinetic routine via single cell injection at the emitter tip. The applied electric field condition within the EHD model is calibrated such that the integrated surface emission at the meniscus tip is of approximate order to the experimental current. Direct mapping of field emission from the EHD model within the Extraction Region to the kinetic model in the Plume Region is deferred to future work. A computational domain axial length of 0.1 μm and width of 0.1 μm is chosen for the Extraction Region, to emulate similar length scales of effective low paths within porous electrospray emitters. Meshes of the liquid and vacuum subdomains in the Extraction Region are shown in Fig. 3. A Taylor Cone angle of 49.29° is chosen for the emitter cone with a tip radius of 10 nm. Mesh elements at the emitter tip are refined in both subdomains to better resolve ion emission in this region. The computational domain of the Plume Region spans a radial distance of 500 μm and 1000 μm axially.

2.2.2 Electric Potentials

Electric potential distributions within the liquid and vacuum subdomains of the Extraction Region are presented in Fig. 4. A relatively linear progression is seen in the axial direction of both domains, with continuity between electric potentials at the interface. The potential within the liquid domain, Fig. 4a, can be seen enforced to zero where the fluid contacts the emitter electrode. A potential gradient tangential to the interface is also observed, suggesting a stronger electric field towards the meniscus center. This behavior is expected for a perturbed conductive fluid exposed to an external field, as the perturbation would result in a higher charge density at the tip and would result in a higher field strength. Continuity of electric potential across the liquid and vacuum domain interface is also observed. As the interfacial jump in electric displacement is innately enforced by the iteration scheme, all facets of the Laplace problem appear correctly represented within the semi-equilibrium potential distributions.

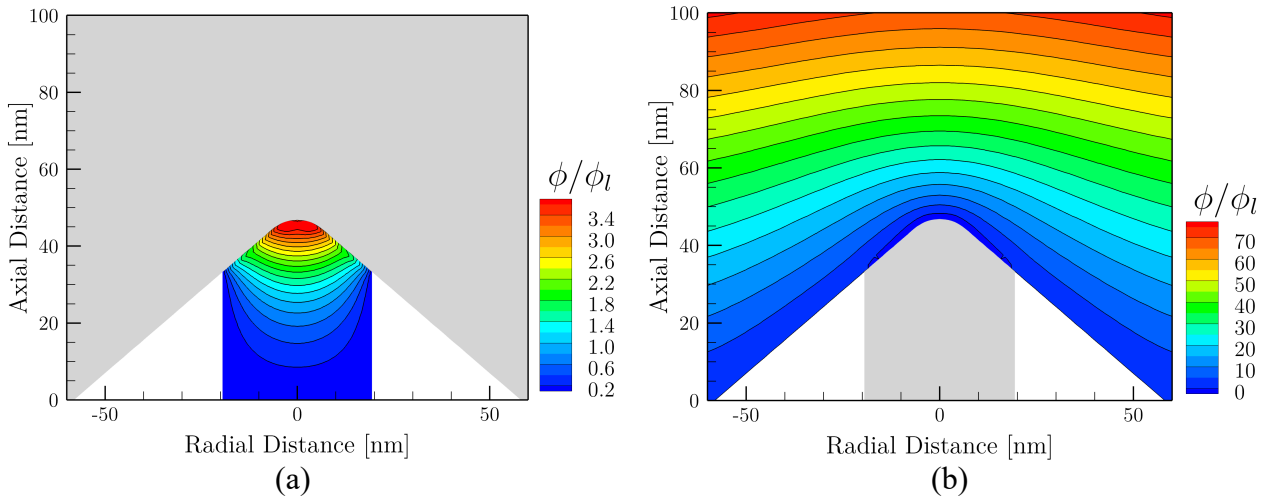


Figure 4. Electric potential distributions within the (a) liquid and (b) vacuum subdomains.

2.2.3 Stokes Flow and Ion Emission

Axial velocity contours within the liquid subdomain of the Extraction Region are presented in Fig. 5. Flow velocity of an ionic liquid meniscus operating in a purely ionic regime is known to scale with

$$v \sim \frac{I}{\pi\rho(q/m)(r^*)^2}, \tag{13}$$

where r^* is the characteristic length scale at the emitter tip and I is the emission current [4]. The Reynolds number scaling is then shown to be

$$Re \sim \frac{I}{\pi\mu(q/m)r^*} \sim 10^{-2}. \tag{14}$$

Using the single-emitter current for the -1562 V operational case ($I \approx 10^{-6}A$) in [3] and the fluid properties of EMI-BF_4 ($\mu \approx 10^{-2}$ Pa·s, $q/m \approx 10^6$ C/kg), the Reynolds number is shown to be significantly less than unity and thus Stokes flow is present. As mentioned, ion emission is only possible within a steady-state configuration if the normal fluid velocity at the intersection is nonzero. Field emission at the emitter tip is represented by arrows in the top-right plot of Fig. 5. It can be shown that the velocity at the emission tip is of approximate order to the emission velocity in the operational case, though it is important to note that the applied electric field, E_0, is adjusted in the Extraction Region to achieve this agreement.

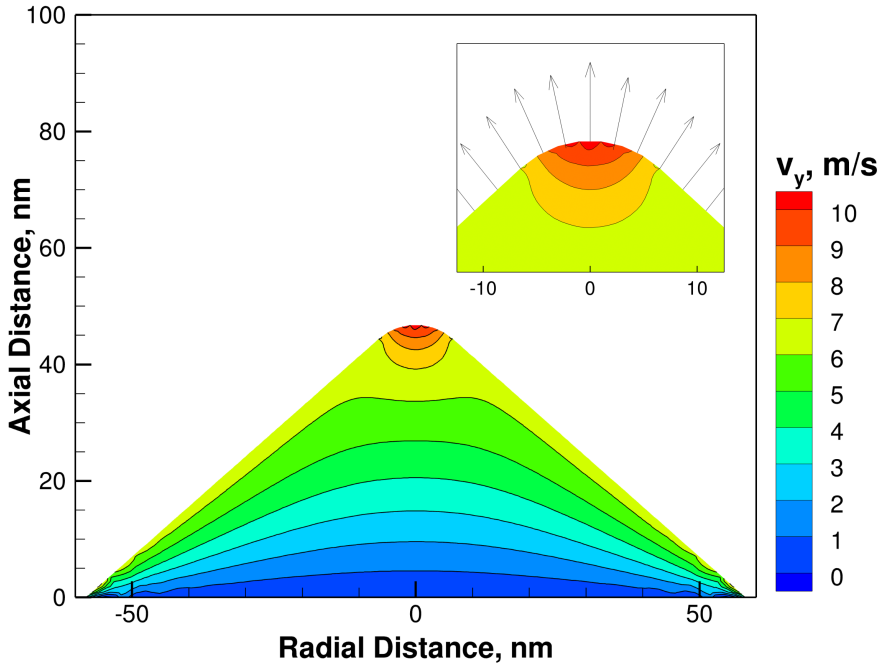


Figure 5. Axial velocity in the bulk fluid, with ion emission at the emitter tip shown in the inset.

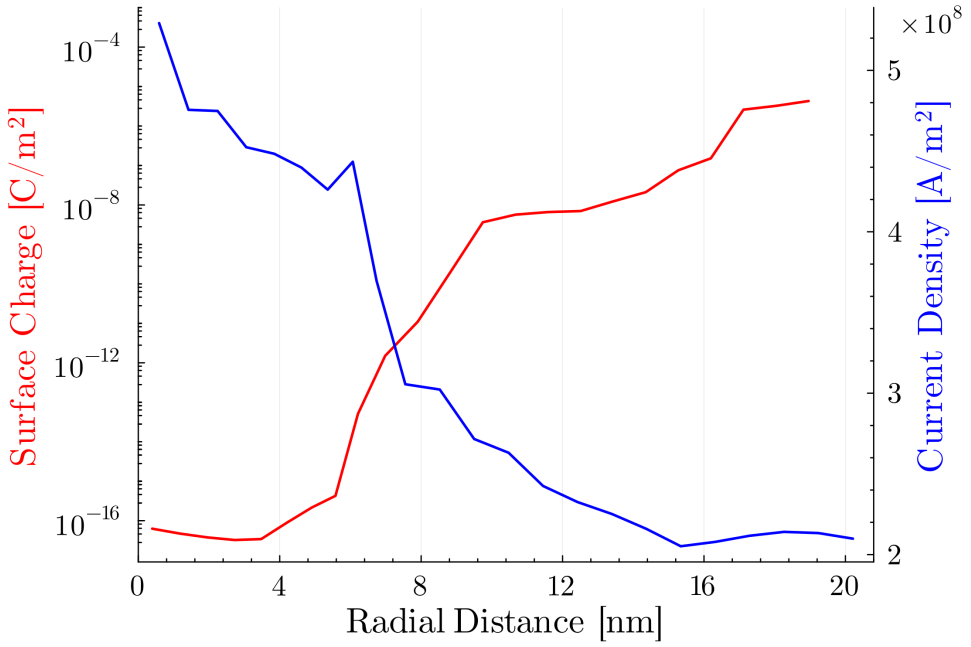


Figure 6. Interfacial surface charge and normal current density versus radial distance.

Characteristics of the Stokes problem can be observed through the interfacial current density, as it is linearly related to the normal fluid velocity at the meniscus. This current density in addition to the surface charge are plotted as a function of the radial distance in Fig. 6. As seen by the potential distribution, the emission centerline should correspond to the highest electric field, which in turn should result in the highest current density of emitted species. This is observed in Fig. 6, where the current density progressively declines with radial distance as the applied electric field weakens away from the centerline. The surface charge, on the other hand, appears to be inversely related to the current density with respect to radial distance. This is due to the continuity law of Eqn. (7), stating the surface charge represents the balance of current conducted to the interface and current evaporating from the interface. This balance is depicted in Fig. 6, where the surface charge is minimum at the interfacial locations corresponding to the highest ion emission, and vice versa. Additional quantitative validation of the EHD solver with occur once the interfacial perturbation scheme is implemented.

2.2.4 Plume Simulations

Independent simulations of the DSMC–PIC solver were conducted as well. As the coupling with the EHD meniscus solver has yet to be implemented, the simulations were initialized using experimental data of Natisin et al. [3]. Similarly, EMI-BF4 is chosen as the propellant. Within the simulation, the plume is assumed to consist of a 1:1 mixture of single-charged EMI^+ ions and EMI-BF4 neutrals. Ions colliding with any solid surfaces are reflected as neutral molecules. Emission current and thrust are calculated about the plane approximately 1000 μm away from the emitter base and are linearly scaled to match the experimental configuration where 576 emitters were operated in parallel. Within the plume, EMI^+ ion speeds (m/s) were calculated and are presented in Fig. 7, while comparisons of the numerical and measured values for emission current

and thrust are presented in Fig. 8. Agreement is shown between the numerical and experimental data across a range of extractor voltages, suggesting that downstream characteristics of the plume can be accurately simulated given sufficient initial conditions.

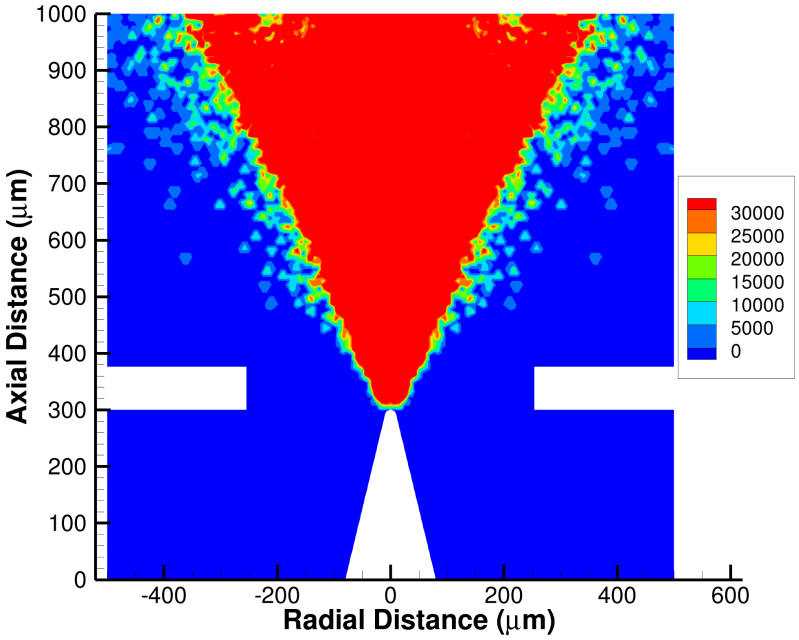


Figure 7. EMI+ ion speeds (m/s)

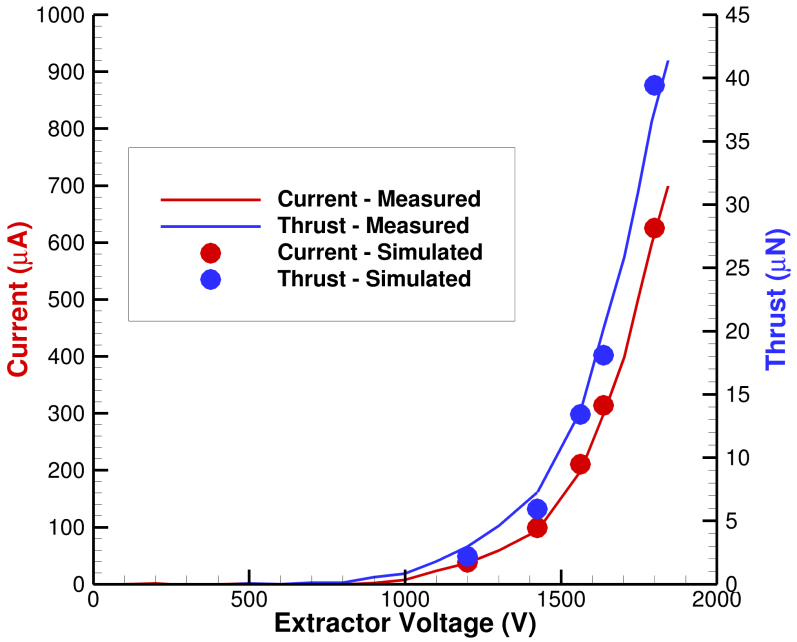


Figure 8. Comparison of emission current and thrust between experimental measurements by Natisin et al. [3] and DSMC–PIC simulation output.

3. Future Objectives

The majority of model development thus far has been within the Extraction Region. Implementing a normal stress balance routine at the interface, Eqn. (10), is the final module required for completion of the field emission model. This stress is a function of the surface tension, and thus the geometry of the meniscus. To complete this, a meniscus perturbation module must be developed that evolves the shape into one that satisfies equilibrium. Currently, the solver determines a nonequilibrium solution for a prescribed meniscus shape. With the addition of the meniscus perturbation module, the final equation of the field emission model is resolved, completing the Extraction Region component of the model. Development time for this module is estimated to take 1-2 months.

The kinetic model within the Plume Region is solved using an in-house direct simulation Monte-Carlo and particle-in-cell solver, and thus no core development is required. As such, the final task for the single emitter electrospray model is coupling the subscale routine in the Extraction Regime with the macroscale kinetic routine in the plume. To achieve a two-way coupling, the output of each submodel must be fed as boundary conditions to the other. Development time for this coupling module is estimated to take an additional month.

When the high-fidelity electrospray model is complete, its applications can be explored in parallel. First, the model must be benchmarked by comparing simulations with experimental measurements. Experimental measurements are nominally taken for electrosprays operating in arrays in the order of 100-1000, challenging validation of single emitter models as coupling effects cannot be accounted for. To overcome this, the Air Force Research Laboratory (AFRL) is conducting a Single Emitter Air Force Electrospray Thruster (SEAFET) program, providing data that can be directly used as validation for the single emitter model. The program has conducted a preliminary qualitative analysis of select emitters [5], with additional data to be made available in the coming months.

Further collaboration with the SEAFET program can allow exploration of the dependencies certain operating conditions have in life-limiting mechanisms. Once an initial benchmarking has been conducted, simulations spanning large parameter sweeps can be conducted to better quantify how perturbations in operations conditions such as geometry, voltage and material selection affect emission characteristics that directly contribute to failure modes. Experimental data could be taken for select configurations for calibration and further validation of the single emitter model. As the primary mechanism contributing to electrospray failure is emission impingement at the electrodes, exploring which facets of electrospray design and operation that directly contribute to overspraying at the grid will be the initial focus of the study.

The availability of both single emitter and multiplexed emitter data also allow for study of coupling effects within these systems. Experiments have demonstrated that emission characteristics of multiplexed arrays are not linear extrapolations of single emitter characteristics, alluding to possible inter-emitter dependencies. Once a single emitter model is validated, simulations can be configured to explore possible macroscopic effects that may occur from operating emitters in parallel. Again, these simulations may help elucidate what components of design and operation are contributing to this phenomenon by conducting parameter sweeps that are otherwise infeasible to perform experimentally. The results of which may then support select configurations of interest where experimentation can be conducted, optimizing the iterative routine towards building electrosprays whose mission capabilities vastly expand beyond those that are available today.

References

[1] C. Cai, "Theoretical and numerical studies of plume flows in vacuum chambers.," Ph.D. Dissertation, University of Michigan, Ann Arbor, 2005.

[2] A. Thuppul, P. L. Wright, A. L. Collins, J. K. Ziemer, and R. E. Wirz, "Lifetime Considerations for Electrospray Thrusters," *Aerospace*, vol. 7, no. 8, p. 108, Aug. 2020.

[3] M. Natisin, H. Zamora, W. McGehee, N. Arnold, Z. Holley, M. Holmes, and D. Eckhardt, "Fabrication and characterization of a fully conventionally machined, high-performance porous-media electrospray thruster," *Journal of Micromechanics and Microengineering*, vol. 30, no. 11, p. 115021, 2020.

[4] C. S. Coffman, "Electrically-assisted evaporation of charged fluids: Fundamental modeling and studies on ionic liquids," Ph.D. dissertation, Massachusetts Institute of Technology, 2016.

[5] W. A. McGehee, N. Arnold, M. R. Natisin, Z. A. Holley, and D. Eckhardt, "The single emitter air force electrospray thruster (SEAFET) Program: Goals and initial results," in *37th International Electric Propulsion Conference*, Massachusetts Institute of Technology, Cambridge, MA USA, Jun. 2022.

Final Technical Report

Prediction of Basic Operation of Electrospray Thrusters
Using High-Fidelity Modeling

AFOSR Grant FA9550-21-1-0045

Monitored by Mitat Birkan

Iain D. Boyd (PI), University of Colorado

Abstract

Electro-spray (ES) thrusters for in-space propulsion operate using ionic liquids that may be colloidal or metal as propellant. Individual ES devices generate very small thrust and impulse bits that are ideal for fine pointing missions. The Air Force has a more significant need for large-scale thrust levels required for station keeping, orbit raising, and orbit transfer. ES systems are of interest because they provide a specific impulse that may be tailored by the propellant, high thrust through the application of many devices in parallel, and all achieved at potentially high efficiencies of about 80%. There are significant fundamental challenges for the integration of the large numbers of devices needed for Air Force missions including: (1) failure modes of ES thrusters; (2) determining the lifetime of ES thrusters; and (3) understanding any crosstalk between adjacent thrusters. We are pursuing a comprehensive research project to address these gaps:

- Model Development: The key developments needed to model electro-spray systems are treatment of ionic-liquid physics, consideration of multiple emission sites, and extension to three dimensions.
- Model Benchmarking: Integration of high-fidelity modeling with empirical data is necessary to characterize life-limiting mechanisms and extrapolate performance in space environments. Direct comparisons will be made of model predictions with detailed plume measurements of AFRL porous-media flow emitters that are under way at the University of Michigan. Comparisons will also be made with all relevant data sets generated at the Air Force Research Laboratory in their current ES activities.
- Use the high-fidelity simulations to provide fundamental data needed for application of low-fidelity analysis of ES thrusters. For example, understanding the process and conditions for mode switching to the pure ionic regime is essential to meeting the USAF requirements for this technology.
- Analyses: Use the high-fidelity model for large arrays including assessment of coupling effects between multiple electro-spray emitters and prediction of primary failure modes.

This final report summarizes the progress made during the first and second years of the grant in terms of source and plume modeling.

DISTRIBUTION A: Distribution approved for public release.

1. Electrospray Model Description

A single porous electrospray emitter operating in a purely ionic emission regime is considered. The domain of interest spans from the emission site on the tip to the downstream plume between the extractor and accelerator electrodes. Computationally, this domain is partitioned into two two-dimensional subdomains: an Extraction Region where field emission from the electrohydrodynamic (EHD) meniscus is considered, and a Plume Region where the ion dynamics of the extracted species are considered. The Extraction Region is further decomposed into a vacuum and bulk liquid domain, Ω_{vac} and Ω_{liq} respectively, where Γ_{lv} denotes the intersection between them. A schematic of the global domain is presented in Fig. 1.

Within the bulk liquid, mass and momentum conservation are considered using the Navier-Stokes equations are the low Reynolds number limit, otherwise known as the Stokes equations,

$$\mu\nabla^2 v - \nabla \mathrm{p} = 0, \tag{1}$$
$$\nabla \cdot v = 0, \tag{2}$$

where μ is fluid viscosity, v is bulk fluid velocity, and p is pressure. Given the propellant is conductive, charge transport is considered as well. Convective charge transport is neglected and an Ohmic conduction model is chosen,

$$j = -K\nabla\phi_l, \tag{3}$$

where j is the current density, K is the electrical conductivity and ϕ_l is the electric potential in the bulk fluid. When charge conservation, $\nabla \cdot j = 0$, is considered with Eqn. (3) the electric potential can be shown to satisfy Laplace's equation,

$$\nabla^2\phi_l = 0. \tag{4}$$

Within the vacuum, space charge effects are negligible, and Laplace's equation is again used to determine the potential,

$$\nabla^2\phi_v = 0, \tag{5}$$

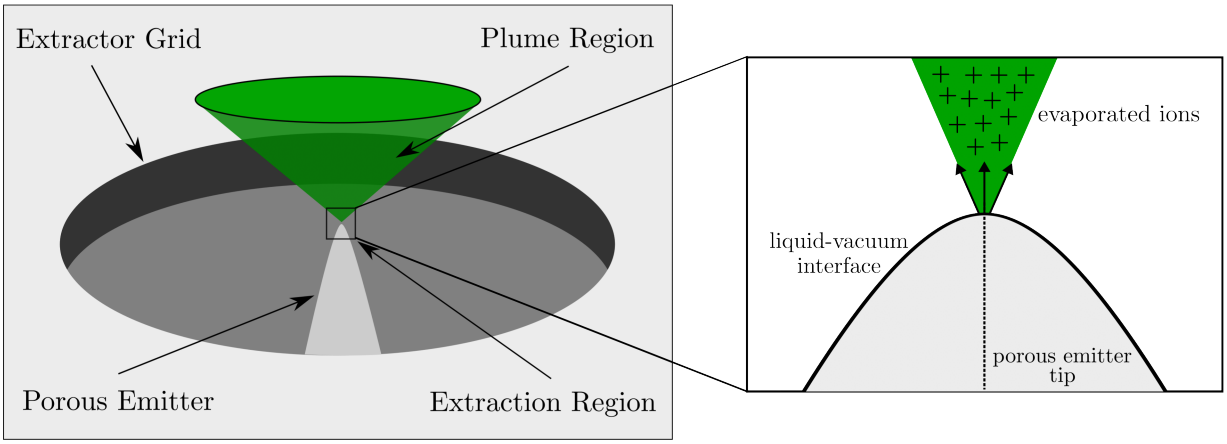


Figure 1. Domains of interest within a porous electrospray emitter.

DISTRIBUTION A: Distribution approved for public release.

where ϕ_v is the electric potential within the vacuum. At the liquid-vacuum interface, the free surface charge density is considered using the electrostatic condition,

$$(-\nabla\phi_v + \epsilon\nabla\phi_l)\cdot\hat{n} = \frac{\sigma}{\epsilon_0}, \tag{6}$$

where $\hat{n}$ is the unit vector normal to the interface, σ is the free surface charge density, ϵ is the relative permittivity, and ϵ_0 is the vacuum permittivity. Additionally, the free surface charge density satisfies the following steady-state transport equation,

$$v\cdot\nabla\sigma = \sigma\hat{n}\cdot\nabla v\cdot\hat{n} - K\nabla\phi_l\cdot\hat{n} - j\cdot\hat{n}. \tag{7}$$

Equation (7) states that the charge advected by the fluid flow is balanced by surface strain, the charge conducted to the surface, and the charge lost due to ion evaporation. Field emission of ions is described by the kinetic law,

$$j\cdot\hat{n} = \frac{k_b T}{h_c}\sigma\exp\left(\frac{-1}{k_b T}\left[\Delta G - \sqrt{\frac{\nabla\phi_v\cdot\hat{n}}{4\pi\epsilon_0/q^3}}\right]\right), \tag{8}$$

where k_b is the Boltzmann constant, h_c is the Planck constant, T is the temperature, q is the elementary charge and ΔG is the solvation energy of the ions. Additionally, force balance between the applied electric traction, viscous stresses, and surface tension is enforced at the liquid-vacuum interface,

$$\hat{t}\cdot(\tau_l - \tau_e)\cdot\hat{n} = 0, \tag{9}$$
$$\hat{n}\cdot(\tau_l - \tau_e)\cdot\hat{n} = -\gamma\nabla\cdot\hat{n}, \tag{10}$$

where $\hat{\boldsymbol{t}}$ is the unit vector tangent to the interface, τ_l is the viscous stress tensor, τ_e is the electrostatic Maxwell stress tensor, and γ is the surface tension. The normal and tangential projections of the Maxwell stress tensor on the interface satisfy the equations

$$\hat{t}\cdot\tau_e\cdot\hat{n} = -\sigma\nabla\phi_v\cdot\hat{t}, \tag{11}$$
$$\hat{n}\cdot\tau_e\cdot\hat{n} = \frac{1}{2}\epsilon_0((\nabla\phi_v\cdot\hat{n})^2 - \epsilon(\nabla\phi_l\cdot\hat{n})^2) + \frac{1}{2}\epsilon_0\big((\epsilon-1)(\nabla\phi_v\cdot\hat{t})^2\big). \tag{12}$$

A hybrid direct simulation Monte Carlo and particle-in-cell (DSMC–PIC) solver is implemented to simulate the downstream rarefied plume, of which a complete description of the solver can be found by Cai [1]. In summary, DSMC is a widely implemented particle method used to calculate collisional dynamics within dilute gases. Analogously for plasmas, PIC is a kinetic method used to simulate the dynamics of charged particles under the influence of external and self–induced electromagnetic fields. Simultaneous implementation of both methods within a

DISTRIBUTION A: Distribution approved for public release.

unified kinetic solver allows the study of gases characterized by both material and Coulombic interactions.

Within the multiscale model, the DSMC–PIC solver is used to initialize a distribution of charged macroparticles at the liquid–vacuum interface as well as simulate their motion within the computational vacuum domain. The initial distribution is a function of the ion number density determined by the EHD meniscus solver. The emission velocity is sampled from a biased Maxwellian based on the propellant temperature. From there, macroscopic plume properties that contribute to single emitter failure mechanisms can be calculated and simulations can be designed to study configurations that minimize these mechanisms. For example, the primary failure mode of electrosprays is overspray of propellant at the site of emission, resulting in impingement of the electrodes that ultimately contribute to shorting and power processing unit failure [2]. By conducting a sensitivity analysis, the proposed model may be able to elucidate what elements of the parameter space contribute most to the plume divergence angle, minimizing the probability of electrode impingement.

A complete schematic of the computational domain is presented in Fig. 2. Fig. 2a presents a macro-scale, two-dimensional domain of a single emitter tip below two extractor electrodes A voltage differential is applied between the emitter and electrodes to induce electric fields strengths on the order required for direct ion evaporation at the propellant free surface. Field emission at the interface is numerically treated within a separate sub-scale domain at the emitter apex and is coupled to the macro-scale domain via the Γ_{sub} intersection. Fig. 2b presents a sub-scale domain of an emission site at the emitter apex presented in Fig. 2a. Steady, open channel flow is assumed for the propellant in Ω_{liq}, where a fully developed velocity profile is imposed at the Γ_{inl} inlet boundary. Geometry of the EHD meniscus, Γ_{int}, is numerically perturbed to find configurations that satisfy mechanical equilibrium, a prerequisite to solve for steady-state emission characteristics.

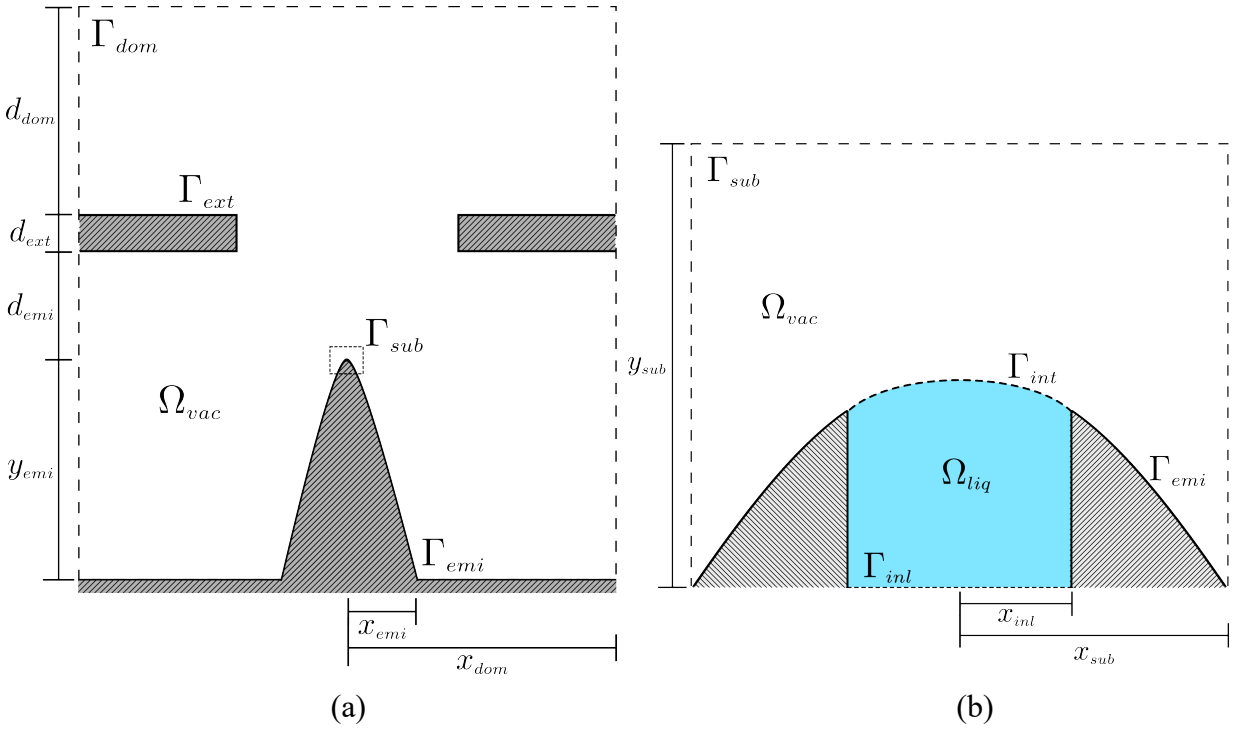


Figure 2. Computational domain.

2. Progress to Date

2.1 Numeric Implementation

The core developmental progress within the electrospray model has been within the Extraction Region. A finite element solver has been implemented using the Distributed and Unified Numerics Environment (DUNE), an open-source library for solving partial differential equations using grid-based methods. An algorithm has been developed that solves the coupled set of partial differential equations for a prescribed meniscus shape. The algorithm generally operates as follows:

The core Stokes and Laplace equations are solved in their respective domains. A multidomain module is configured to enforce boundary conditions that are dependent upon solutions across domains. An additional module is developed to enforce directionally dependent boundary conditions on the same interface. Consideration of electrostatic conditions, surface charge density transport, and stress balance at the free surface act as these unique multidomain boundary conditions. An iterative routine first solves the electric potential system until convergence, at which a global algorithm is implemented that solves the Stokes system and couples the domain together. A flowchart of this global algorithm is presented in Fig. 3. The result is a converged nonequilibrium solution for a prescribed meniscus shape. The current stage of development is expanding this to equilibrium solutions by including meniscus geometry perturbations in the global algorithm.

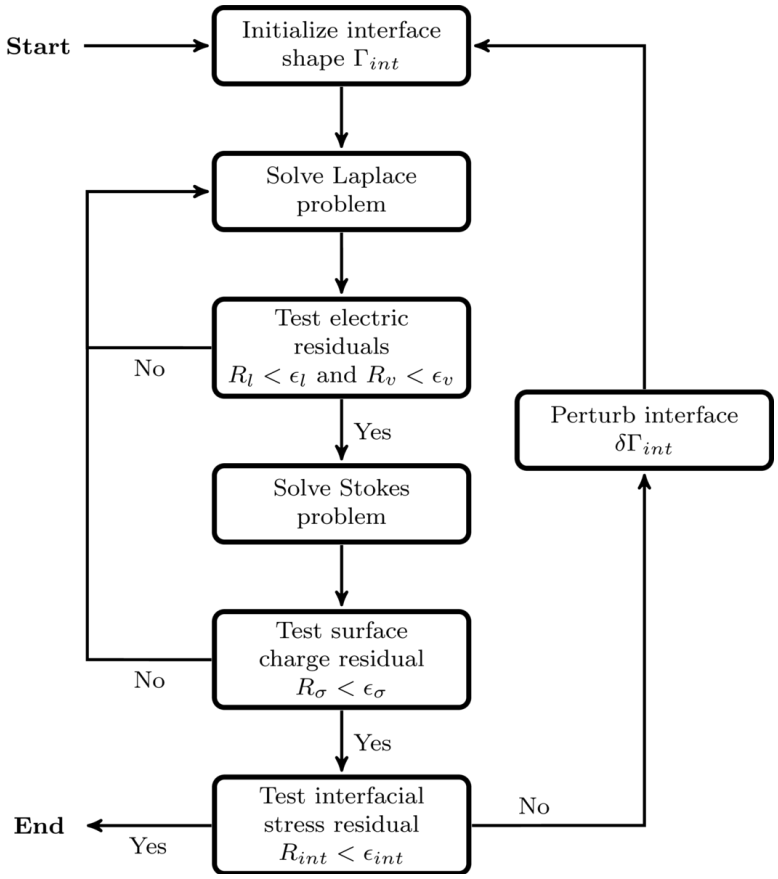


Figure 3. Algorithm to numerically solve for ion emission from the EHS meniscus within the Extraction Region.

2.2 Results

2.2.1 Simulation Parameters

Initial simulations within the Extraction and Plume region are conducted using similar operating parameters as those in [3]. Mapping of ion emission from the Extraction Region to the kinetic routine is not directly calculated. Experimental current values are used as input conditions into the kinetic routine via single cell injection at the emitter tip. The applied electric field condition within the EHD model is calibrated such that the integrated surface emission at the meniscus tip is of approximate order to the experimental current. Direct mapping of field emission from the EHD model within the Extraction Region to the kinetic model in the Plume Region is deferred to future work. A computational domain axial length of 0.1 μm and width of 0.1 μm is chosen for the Extraction Region, to emulate similar length scales of effective low paths within porous electrospray emitters. Meshes of the liquid and vacuum subdomains in the Extraction Region are shown in Fig. 3. A Taylor Cone angle of 49.29° is chosen for the emitter cone with a tip radius of 10 nm. Mesh elements at the emitter tip are refined in both subdomains to better resolve ion emission in this region. The computational domain of the Plume Region spans a radial distance of 500 μm and 1000 μm axially.

2.2.2 Electric Potentials

Electric potential distributions within the liquid and vacuum subdomains of the Extraction Region are presented in Fig. 4. A relatively linear progression is seen in the axial direction of both domains, with continuity between electric potentials at the interface. The potential within the liquid domain, Fig. 4a, can be seen enforced to zero where the fluid contacts the emitter electrode. A potential gradient tangential to the interface is also observed, suggesting a stronger electric field towards the meniscus center. This behavior is expected for a perturbed conductive fluid exposed to an external field, as the perturbation would result in a higher charge density at the tip and would result in a higher field strength. Continuity of electric potential across the liquid and vacuum domain interface is also observed. As the interfacial jump in electric displacement is innately enforced by the iteration scheme, all facets of the Laplace problem appear correctly represented within the semi-equilibrium potential distributions.

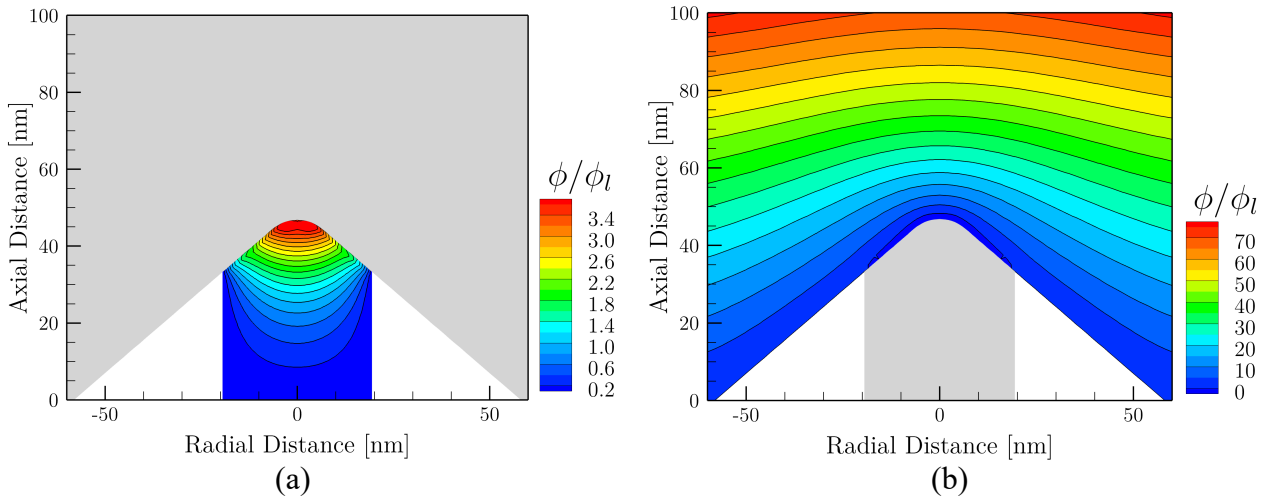


Figure 4. Electric potential distributions within the (a) liquid and (b) vacuum subdomains.

2.2.3 Stokes Flow and Ion Emission

Axial velocity contours within the liquid subdomain of the Extraction Region are presented in Fig. 5. Flow velocity of an ionic liquid meniscus operating in a purely ionic regime is known to scale with

$$v \sim \frac{I}{\pi\rho(q/m)(r^*)^2}, \tag{13}$$

where r^* is the characteristic length scale at the emitter tip and I is the emission current [4]. The Reynolds number scaling is then shown to be

$$Re \sim \frac{I}{\pi\mu(q/m)r^*} \sim 10^{-2}. \tag{14}$$

Using the single-emitter current for the -1562 V operational case ($I \approx 10^{-6}A$) in [3] and the fluid properties of EMI-BF_4 ($\mu \approx 10^{-2}$ Pa·s, $q/m \approx 10^6$ C/kg), the Reynolds number is shown to be significantly less than unity and thus Stokes flow is present. As mentioned, ion emission is only possible within a steady-state configuration if the normal fluid velocity at the intersection is nonzero. Field emission at the emitter tip is represented by arrows in the top-right plot of Fig. 5. It can be shown that the velocity at the emission tip is of approximate order to the emission velocity in the operational case, though it is important to note that the applied electric field, E_0, is adjusted in the Extraction Region to achieve this agreement.

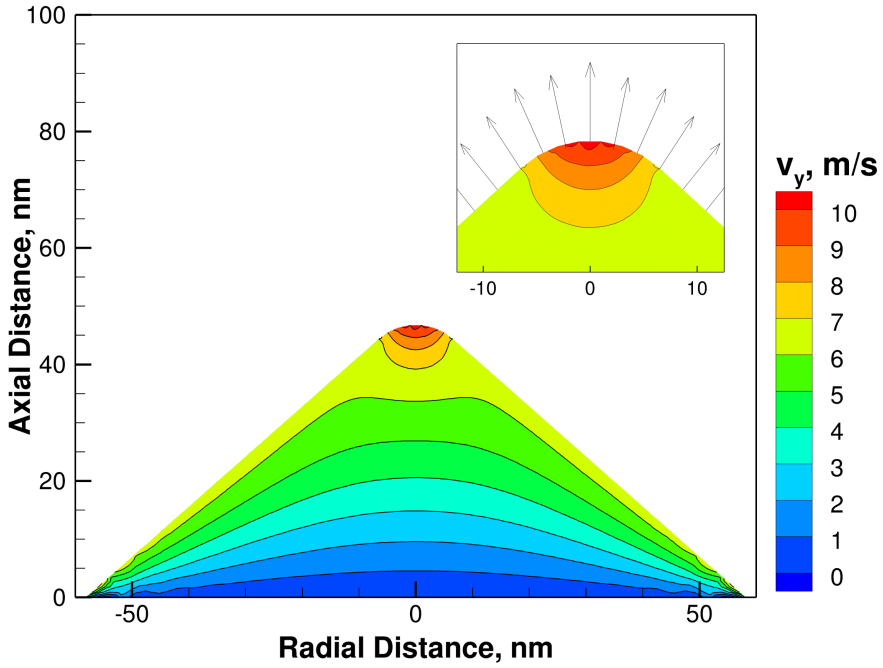


Figure 5. Axial velocity in the bulk fluid, with ion emission at the emitter tip shown in the inset.

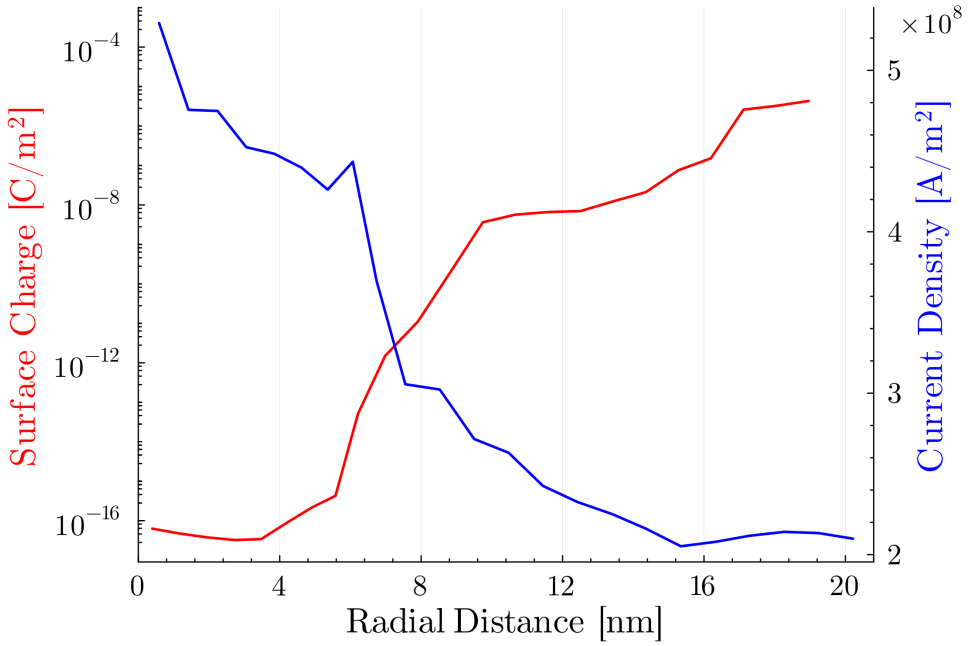


Figure 6. Interfacial surface charge and normal current density versus radial distance.

Characteristics of the Stokes problem can be observed through the interfacial current density, as it is linearly related to the normal fluid velocity at the meniscus. This current density in addition to the surface charge are plotted as a function of the radial distance in Fig. 6. As seen by the potential distribution, the emission centerline should correspond to the highest electric field, which in turn should result in the highest current density of emitted species. This is observed in Fig. 6, where the current density progressively declines with radial distance as the applied electric field weakens away from the centerline. The surface charge, on the other hand, appears to be inversely related to the current density with respect to radial distance. This is due to the continuity law of Eqn. (7), stating the surface charge represents the balance of current conducted to the interface and current evaporating from the interface. This balance is depicted in Fig. 6, where the surface charge is minimum at the interfacial locations corresponding to the highest ion emission, and vice versa. Additional quantitative validation of the EHD solver with occur once the interfacial perturbation scheme is implemented.

2.2.4 Plume Simulations

Independent simulations of the DSMC–PIC solver were conducted as well. As the coupling with the EHD meniscus solver has yet to be implemented, the simulations were initialized using experimental data of Natisin et al. [3]. Similarly, EMI-BF4 is chosen as the propellant. Within the simulation, the plume is assumed to consist of a 1:1 mixture of single-charged EMI^+ ions and EMI-BF4 neutrals. Ions colliding with any solid surfaces are reflected as neutral molecules. Emission current and thrust are calculated about the plane approximately 1000 μm away from the emitter base and are linearly scaled to match the experimental configuration where 576 emitters were operated in parallel. Within the plume, EMI^+ ion speeds (m/s) were calculated and are presented in Fig. 7, while comparisons of the numerical and measured values for emission current

and thrust are presented in Fig. 8. Agreement is shown between the numerical and experimental data across a range of extractor voltages, suggesting that downstream characteristics of the plume can be accurately simulated given sufficient initial conditions.

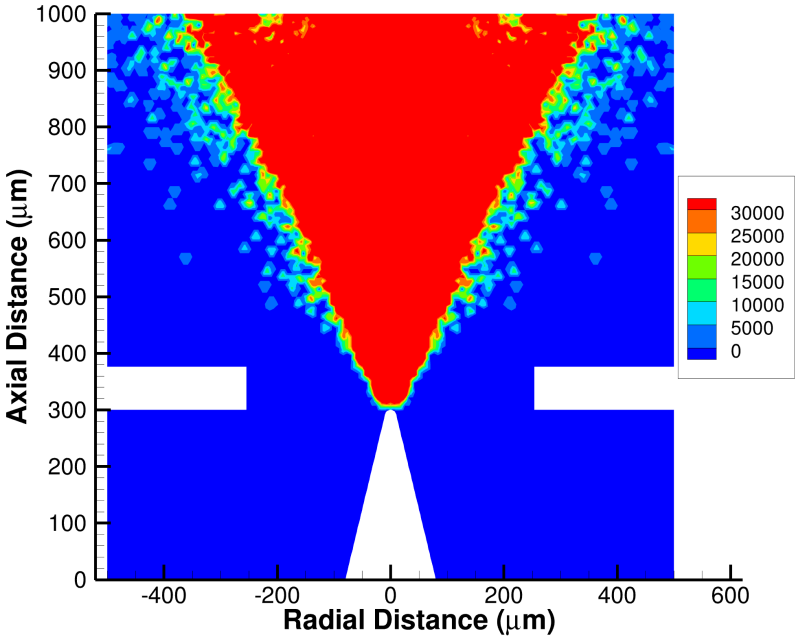


Figure 7. EMI+ ion speeds (m/s)

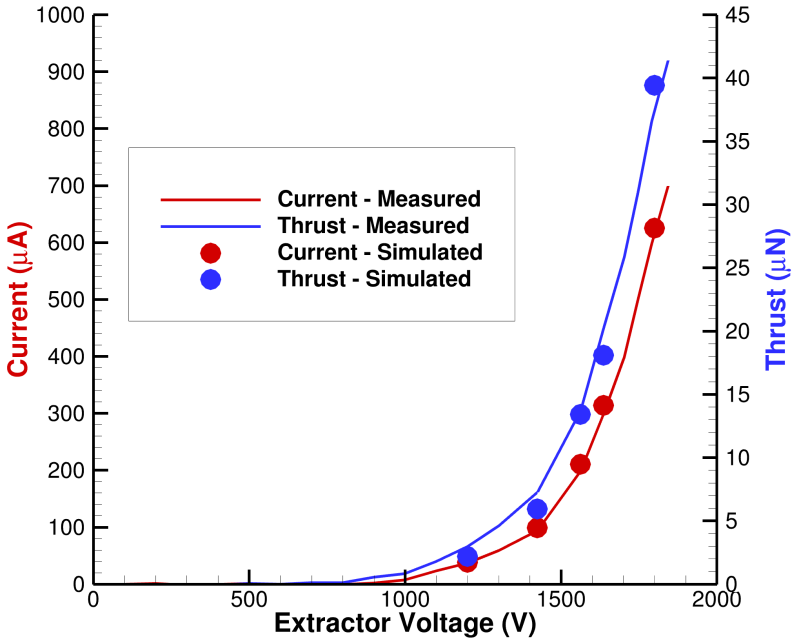


Figure 8. Comparison of emission current and thrust between experimental measurements by Natisin et al. [3] and DSMC–PIC simulation output.

3. Future Objectives

The majority of model development thus far has been within the Extraction Region. Implementing a normal stress balance routine at the interface, Eqn. (10), is the final module required for completion of the field emission model. This stress is a function of the surface tension, and thus the geometry of the meniscus. To complete this, a meniscus perturbation module must be developed that evolves the shape into one that satisfies equilibrium. Currently, the solver determines a nonequilibrium solution for a prescribed meniscus shape. With the addition of the meniscus perturbation module, the final equation of the field emission model is resolved, completing the Extraction Region component of the model. Development time for this module is estimated to take 1-2 months.

The kinetic model within the Plume Region is solved using an in-house direct simulation Monte-Carlo and particle-in-cell solver, and thus no core development is required. As such, the final task for the single emitter electrospray model is coupling the subscale routine in the Extraction Regime with the macroscale kinetic routine in the plume. To achieve a two-way coupling, the output of each submodel must be fed as boundary conditions to the other. Development time for this coupling module is estimated to take an additional month.

When the high-fidelity electrospray model is complete, its applications can be explored in parallel. First, the model must be benchmarked by comparing simulations with experimental measurements. Experimental measurements are nominally taken for electrosprays operating in arrays in the order of 100-1000, challenging validation of single emitter models as coupling effects cannot be accounted for. To overcome this, the Air Force Research Laboratory (AFRL) is conducting a Single Emitter Air Force Electrospray Thruster (SEAFET) program, providing data that can be directly used as validation for the single emitter model. The program has conducted a preliminary qualitative analysis of select emitters [5], with additional data to be made available in the coming months.

Further collaboration with the SEAFET program can allow exploration of the dependencies certain operating conditions have in life-limiting mechanisms. Once an initial benchmarking has been conducted, simulations spanning large parameter sweeps can be conducted to better quantify how perturbations in operations conditions such as geometry, voltage and material selection affect emission characteristics that directly contribute to failure modes. Experimental data could be taken for select configurations for calibration and further validation of the single emitter model. As the primary mechanism contributing to electrospray failure is emission impingement at the electrodes, exploring which facets of electrospray design and operation that directly contribute to overspraying at the grid will be the initial focus of the study.

The availability of both single emitter and multiplexed emitter data also allow for study of coupling effects within these systems. Experiments have demonstrated that emission characteristics of multiplexed arrays are not linear extrapolations of single emitter characteristics, alluding to possible inter-emitter dependencies. Once a single emitter model is validated, simulations can be configured to explore possible macroscopic effects that may occur from operating emitters in parallel. Again, these simulations may help elucidate what components of design and operation are contributing to this phenomenon by conducting parameter sweeps that are otherwise infeasible to perform experimentally. The results of which may then support select configurations of interest where experimentation can be conducted, optimizing the iterative routine towards building electrosprays whose mission capabilities vastly expand beyond those that are available today.

References

[1] C. Cai, "Theoretical and numerical studies of plume flows in vacuum chambers.," Ph.D. Dissertation, University of Michigan, Ann Arbor, 2005.

[2] A. Thuppul, P. L. Wright, A. L. Collins, J. K. Ziemer, and R. E. Wirz, "Lifetime Considerations for Electrospray Thrusters," *Aerospace*, vol. 7, no. 8, p. 108, Aug. 2020.

[3] M. Natisin, H. Zamora, W. McGehee, N. Arnold, Z. Holley, M. Holmes, and D. Eckhardt, "Fabrication and characterization of a fully conventionally machined, high-performance porous-media electrospray thruster," *Journal of Micromechanics and Microengineering*, vol. 30, no. 11, p. 115021, 2020.

[4] C. S. Coffman, "Electrically-assisted evaporation of charged fluids: Fundamental modeling and studies on ionic liquids," Ph.D. dissertation, Massachusetts Institute of Technology, 2016.

[5] W. A. McGehee, N. Arnold, M. R. Natisin, Z. A. Holley, and D. Eckhardt, "The single emitter air force electrospray thruster (SEAFET) Program: Goals and initial results," in *37th International Electric Propulsion Conference*, Massachusetts Institute of Technology, Cambridge, MA USA, Jun. 2022.

Final Technical Report

Prediction of Basic Operation of Electrospray Thrusters
Using High-Fidelity Modeling

AFOSR Grant FA9550-21-1-0045

Monitored by Mitat Birkan

Iain D. Boyd (PI), University of Colorado

Abstract

Electro-spray (ES) thrusters for in-space propulsion operate using ionic liquids that may be colloidal or metal as propellant. Individual ES devices generate very small thrust and impulse bits that are ideal for fine pointing missions. The Air Force has a more significant need for large-scale thrust levels required for station keeping, orbit raising, and orbit transfer. ES systems are of interest because they provide a specific impulse that may be tailored by the propellant, high thrust through the application of many devices in parallel, and all achieved at potentially high efficiencies of about 80%. There are significant fundamental challenges for the integration of the large numbers of devices needed for Air Force missions including: (1) failure modes of ES thrusters; (2) determining the lifetime of ES thrusters; and (3) understanding any crosstalk between adjacent thrusters. We are pursuing a comprehensive research project to address these gaps:

- Model Development: The key developments needed to model electro-spray systems are treatment of ionic-liquid physics, consideration of multiple emission sites, and extension to three dimensions.
- Model Benchmarking: Integration of high-fidelity modeling with empirical data is necessary to characterize life-limiting mechanisms and extrapolate performance in space environments. Direct comparisons will be made of model predictions with detailed plume measurements of AFRL porous-media flow emitters that are under way at the University of Michigan. Comparisons will also be made with all relevant data sets generated at the Air Force Research Laboratory in their current ES activities.
- Use the high-fidelity simulations to provide fundamental data needed for application of low-fidelity analysis of ES thrusters. For example, understanding the process and conditions for mode switching to the pure ionic regime is essential to meeting the USAF requirements for this technology.
- Analyses: Use the high-fidelity model for large arrays including assessment of coupling effects between multiple electro-spray emitters and prediction of primary failure modes.

This final report summarizes the progress made during the first and second years of the grant in terms of source and plume modeling.

DISTRIBUTION A: Distribution approved for public release.

1. Electrospray Model Description

A single porous electrospray emitter operating in a purely ionic emission regime is considered. The domain of interest spans from the emission site on the tip to the downstream plume between the extractor and accelerator electrodes. Computationally, this domain is partitioned into two two-dimensional subdomains: an Extraction Region where field emission from the electrohydrodynamic (EHD) meniscus is considered, and a Plume Region where the ion dynamics of the extracted species are considered. The Extraction Region is further decomposed into a vacuum and bulk liquid domain, Ω_{vac} and Ω_{liq} respectively, where Γ_{lv} denotes the intersection between them. A schematic of the global domain is presented in Fig. 1.

Within the bulk liquid, mass and momentum conservation are considered using the Navier-Stokes equations are the low Reynolds number limit, otherwise known as the Stokes equations,

$$\mu\nabla^2 v - \nabla \mathrm{p} = 0, \tag{1}$$
$$\nabla \cdot v = 0, \tag{2}$$

where μ is fluid viscosity, v is bulk fluid velocity, and p is pressure. Given the propellant is conductive, charge transport is considered as well. Convective charge transport is neglected and an Ohmic conduction model is chosen,

$$j = -K\nabla\phi_l, \tag{3}$$

where j is the current density, K is the electrical conductivity and ϕ_l is the electric potential in the bulk fluid. When charge conservation, $\nabla \cdot j = 0$, is considered with Eqn. (3) the electric potential can be shown to satisfy Laplace's equation,

$$\nabla^2\phi_l = 0. \tag{4}$$

Within the vacuum, space charge effects are negligible, and Laplace's equation is again used to determine the potential,

$$\nabla^2\phi_v = 0, \tag{5}$$

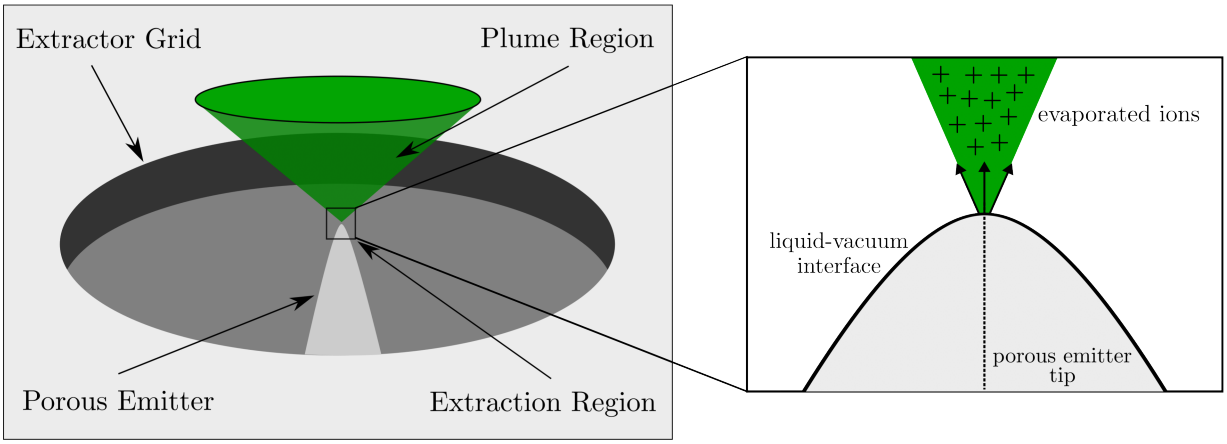


Figure 1. Domains of interest within a porous electrospray emitter.

DISTRIBUTION A: Distribution approved for public release.

where ϕ_v is the electric potential within the vacuum. At the liquid-vacuum interface, the free surface charge density is considered using the electrostatic condition,

$$(-\nabla\phi_v + \epsilon\nabla\phi_l)\cdot\hat{n} = \frac{\sigma}{\epsilon_0}, \tag{6}$$

where $\hat{n}$ is the unit vector normal to the interface, σ is the free surface charge density, ϵ is the relative permittivity, and ϵ_0 is the vacuum permittivity. Additionally, the free surface charge density satisfies the following steady-state transport equation,

$$v\cdot\nabla\sigma = \sigma\hat{n}\cdot\nabla v\cdot\hat{n} - K\nabla\phi_l\cdot\hat{n} - j\cdot\hat{n}. \tag{7}$$

Equation (7) states that the charge advected by the fluid flow is balanced by surface strain, the charge conducted to the surface, and the charge lost due to ion evaporation. Field emission of ions is described by the kinetic law,

$$j\cdot\hat{n} = \frac{k_b T}{h_c}\sigma\exp\left(\frac{-1}{k_b T}\left[\Delta G - \sqrt{\frac{\nabla\phi_v\cdot\hat{n}}{4\pi\epsilon_0/q^3}}\right]\right), \tag{8}$$

where k_b is the Boltzmann constant, h_c is the Planck constant, T is the temperature, q is the elementary charge and ΔG is the solvation energy of the ions. Additionally, force balance between the applied electric traction, viscous stresses, and surface tension is enforced at the liquid-vacuum interface,

$$\hat{t}\cdot(\tau_l - \tau_e)\cdot\hat{n} = 0, \tag{9}$$
$$\hat{n}\cdot(\tau_l - \tau_e)\cdot\hat{n} = -\gamma\nabla\cdot\hat{n}, \tag{10}$$

where $\hat{\boldsymbol{t}}$ is the unit vector tangent to the interface, τ_l is the viscous stress tensor, τ_e is the electrostatic Maxwell stress tensor, and γ is the surface tension. The normal and tangential projections of the Maxwell stress tensor on the interface satisfy the equations

$$\hat{t}\cdot\tau_e\cdot\hat{n} = -\sigma\nabla\phi_v\cdot\hat{t}, \tag{11}$$
$$\hat{n}\cdot\tau_e\cdot\hat{n} = \frac{1}{2}\epsilon_0((\nabla\phi_v\cdot\hat{n})^2 - \epsilon(\nabla\phi_l\cdot\hat{n})^2) + \frac{1}{2}\epsilon_0\big((\epsilon-1)(\nabla\phi_v\cdot\hat{t})^2\big). \tag{12}$$

A hybrid direct simulation Monte Carlo and particle-in-cell (DSMC–PIC) solver is implemented to simulate the downstream rarefied plume, of which a complete description of the solver can be found by Cai [1]. In summary, DSMC is a widely implemented particle method used to calculate collisional dynamics within dilute gases. Analogously for plasmas, PIC is a kinetic method used to simulate the dynamics of charged particles under the influence of external and self–induced electromagnetic fields. Simultaneous implementation of both methods within a

DISTRIBUTION A: Distribution approved for public release.

unified kinetic solver allows the study of gases characterized by both material and Coulombic interactions.

Within the multiscale model, the DSMC–PIC solver is used to initialize a distribution of charged macroparticles at the liquid–vacuum interface as well as simulate their motion within the computational vacuum domain. The initial distribution is a function of the ion number density determined by the EHD meniscus solver. The emission velocity is sampled from a biased Maxwellian based on the propellant temperature. From there, macroscopic plume properties that contribute to single emitter failure mechanisms can be calculated and simulations can be designed to study configurations that minimize these mechanisms. For example, the primary failure mode of electrosprays is overspray of propellant at the site of emission, resulting in impingement of the electrodes that ultimately contribute to shorting and power processing unit failure [2]. By conducting a sensitivity analysis, the proposed model may be able to elucidate what elements of the parameter space contribute most to the plume divergence angle, minimizing the probability of electrode impingement.

A complete schematic of the computational domain is presented in Fig. 2. Fig. 2a presents a macro-scale, two-dimensional domain of a single emitter tip below two extractor electrodes A voltage differential is applied between the emitter and electrodes to induce electric fields strengths on the order required for direct ion evaporation at the propellant free surface. Field emission at the interface is numerically treated within a separate sub-scale domain at the emitter apex and is coupled to the macro-scale domain via the Γ_{sub} intersection. Fig. 2b presents a sub-scale domain of an emission site at the emitter apex presented in Fig. 2a. Steady, open channel flow is assumed for the propellant in Ω_{liq}, where a fully developed velocity profile is imposed at the Γ_{inl} inlet boundary. Geometry of the EHD meniscus, Γ_{int}, is numerically perturbed to find configurations that satisfy mechanical equilibrium, a prerequisite to solve for steady-state emission characteristics.

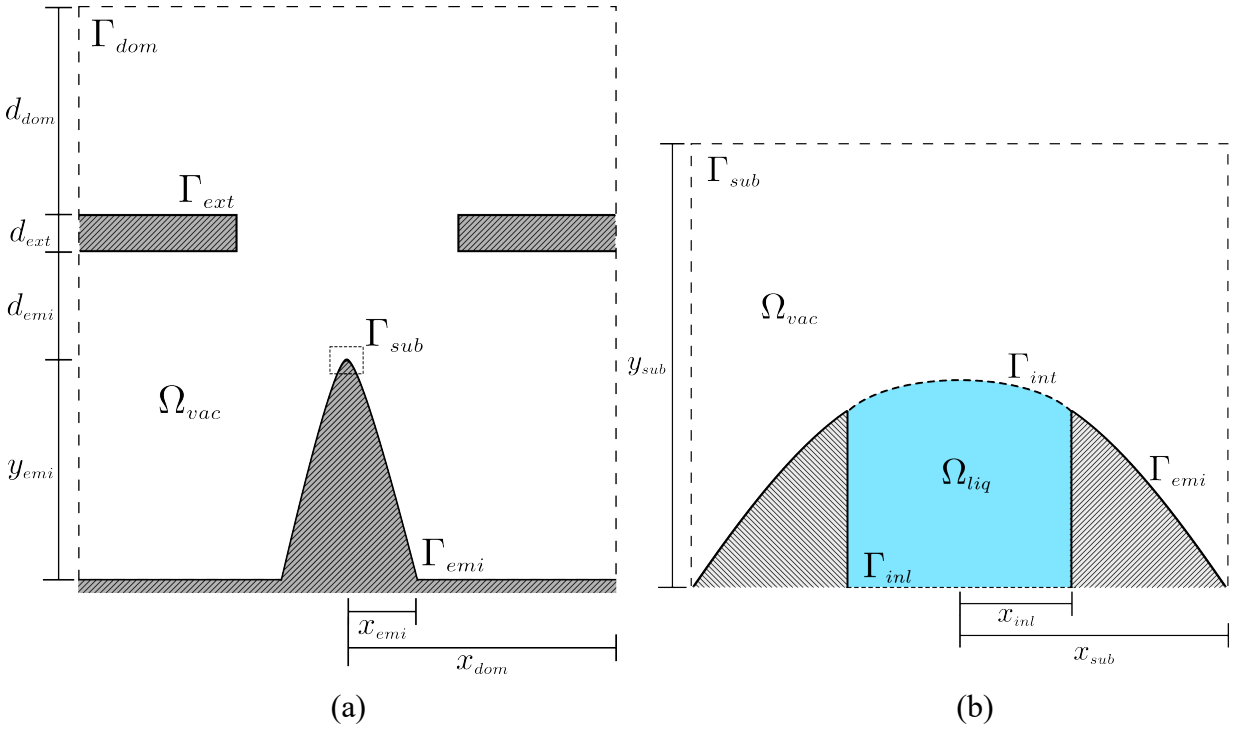


Figure 2. Computational domain.

DISTRIBUTION A: Distribution approved for public release.

2. Progress to Date

2.1 Numeric Implementation

The core developmental progress within the electrospray model has been within the Extraction Region. A finite element solver has been implemented using the Distributed and Unified Numerics Environment (DUNE), an open-source library for solving partial differential equations using grid-based methods. An algorithm has been developed that solves the coupled set of partial differential equations for a prescribed meniscus shape. The algorithm generally operates as follows:

The core Stokes and Laplace equations are solved in their respective domains. A multidomain module is configured to enforce boundary conditions that are dependent upon solutions across domains. An additional module is developed to enforce directionally dependent boundary conditions on the same interface. Consideration of electrostatic conditions, surface charge density transport, and stress balance at the free surface act as these unique multidomain boundary conditions. An iterative routine first solves the electric potential system until convergence, at which a global algorithm is implemented that solves the Stokes system and couples the domain together. A flowchart of this global algorithm is presented in Fig. 3. The result is a converged nonequilibrium solution for a prescribed meniscus shape. The current stage of development is expanding this to equilibrium solutions by including meniscus geometry perturbations in the global algorithm.

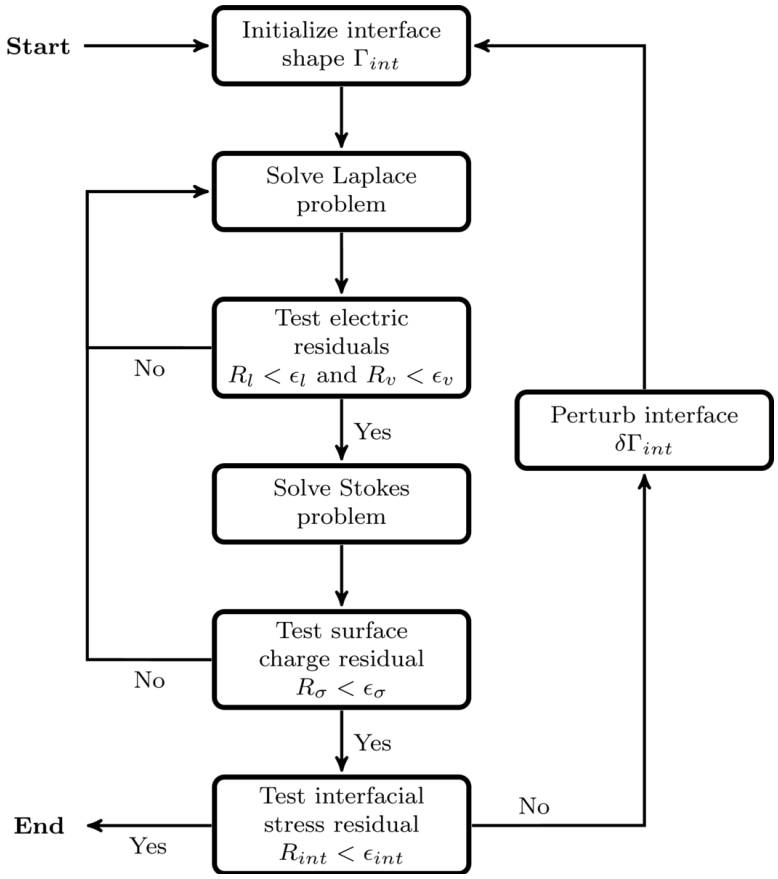


Figure 3. Algorithm to numerically solve for ion emission from the EHS meniscus within the Extraction Region.

2.2 Results

2.2.1 Simulation Parameters

Initial simulations within the Extraction and Plume region are conducted using similar operating parameters as those in [3]. Mapping of ion emission from the Extraction Region to the kinetic routine is not directly calculated. Experimental current values are used as input conditions into the kinetic routine via single cell injection at the emitter tip. The applied electric field condition within the EHD model is calibrated such that the integrated surface emission at the meniscus tip is of approximate order to the experimental current. Direct mapping of field emission from the EHD model within the Extraction Region to the kinetic model in the Plume Region is deferred to future work. A computational domain axial length of 0.1 μm and width of 0.1 μm is chosen for the Extraction Region, to emulate similar length scales of effective low paths within porous electrospray emitters. Meshes of the liquid and vacuum subdomains in the Extraction Region are shown in Fig. 3. A Taylor Cone angle of 49.29° is chosen for the emitter cone with a tip radius of 10 nm. Mesh elements at the emitter tip are refined in both subdomains to better resolve ion emission in this region. The computational domain of the Plume Region spans a radial distance of 500 μm and 1000 μm axially.

2.2.2 Electric Potentials

Electric potential distributions within the liquid and vacuum subdomains of the Extraction Region are presented in Fig. 4. A relatively linear progression is seen in the axial direction of both domains, with continuity between electric potentials at the interface. The potential within the liquid domain, Fig. 4a, can be seen enforced to zero where the fluid contacts the emitter electrode. A potential gradient tangential to the interface is also observed, suggesting a stronger electric field towards the meniscus center. This behavior is expected for a perturbed conductive fluid exposed to an external field, as the perturbation would result in a higher charge density at the tip and would result in a higher field strength. Continuity of electric potential across the liquid and vacuum domain interface is also observed. As the interfacial jump in electric displacement is innately enforced by the iteration scheme, all facets of the Laplace problem appear correctly represented within the semi-equilibrium potential distributions.

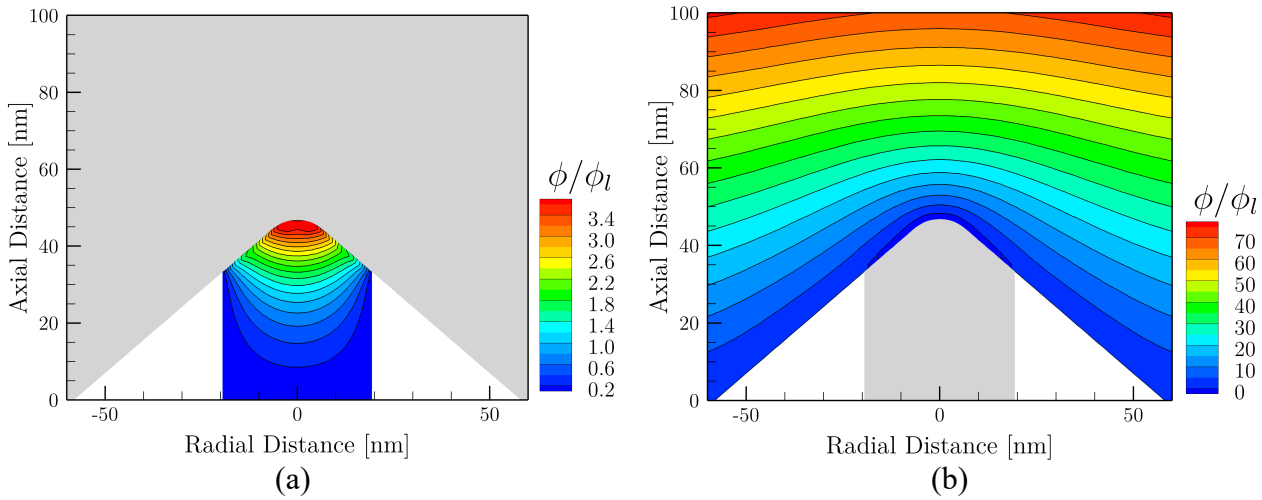


Figure 4. Electric potential distributions within the (a) liquid and (b) vacuum subdomains.

2.2.3 Stokes Flow and Ion Emission

Axial velocity contours within the liquid subdomain of the Extraction Region are presented in Fig. 5. Flow velocity of an ionic liquid meniscus operating in a purely ionic regime is known to scale with

$$v \sim \frac{I}{\pi\rho(q/m)(r^*)^2}, \tag{13}$$

where r^* is the characteristic length scale at the emitter tip and I is the emission current [4]. The Reynolds number scaling is then shown to be

$$Re \sim \frac{I}{\pi\mu(q/m)r^*} \sim 10^{-2}. \tag{14}$$

Using the single-emitter current for the -1562 V operational case ($I \approx 10^{-6}A$) in [3] and the fluid properties of EMI-BF_4 ($\mu \approx 10^{-2}$ Pa·s, $q/m \approx 10^6$ C/kg), the Reynolds number is shown to be significantly less than unity and thus Stokes flow is present. As mentioned, ion emission is only possible within a steady-state configuration if the normal fluid velocity at the intersection is nonzero. Field emission at the emitter tip is represented by arrows in the top-right plot of Fig. 5. It can be shown that the velocity at the emission tip is of approximate order to the emission velocity in the operational case, though it is important to note that the applied electric field, E_0, is adjusted in the Extraction Region to achieve this agreement.

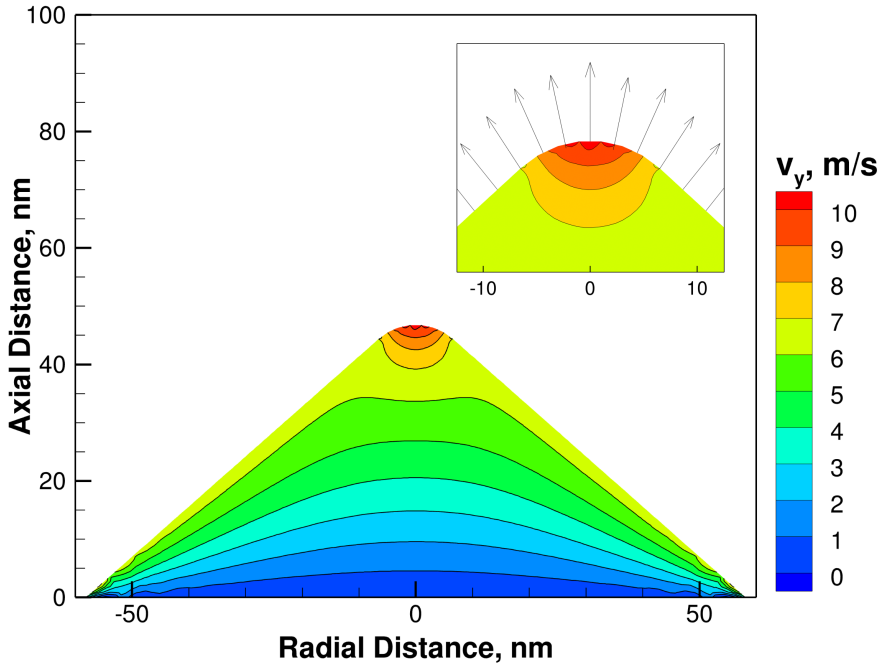


Figure 5. Axial velocity in the bulk fluid, with ion emission at the emitter tip shown in the inset.

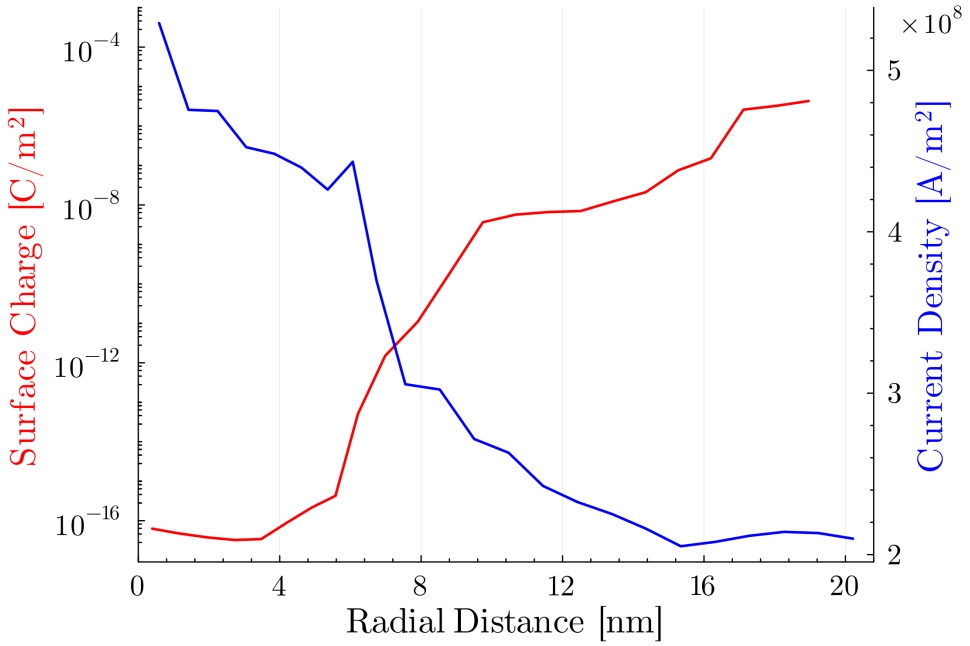


Figure 6. Interfacial surface charge and normal current density versus radial distance.

Characteristics of the Stokes problem can be observed through the interfacial current density, as it is linearly related to the normal fluid velocity at the meniscus. This current density in addition to the surface charge are plotted as a function of the radial distance in Fig. 6. As seen by the potential distribution, the emission centerline should correspond to the highest electric field, which in turn should result in the highest current density of emitted species. This is observed in Fig. 6, where the current density progressively declines with radial distance as the applied electric field weakens away from the centerline. The surface charge, on the other hand, appears to be inversely related to the current density with respect to radial distance. This is due to the continuity law of Eqn. (7), stating the surface charge represents the balance of current conducted to the interface and current evaporating from the interface. This balance is depicted in Fig. 6, where the surface charge is minimum at the interfacial locations corresponding to the highest ion emission, and vice versa. Additional quantitative validation of the EHD solver with occur once the interfacial perturbation scheme is implemented.

2.2.4 Plume Simulations

Independent simulations of the DSMC–PIC solver were conducted as well. As the coupling with the EHD meniscus solver has yet to be implemented, the simulations were initialized using experimental data of Natisin et al. [3]. Similarly, EMI-BF4 is chosen as the propellant. Within the simulation, the plume is assumed to consist of a 1:1 mixture of single-charged EMI^+ ions and EMI-BF4 neutrals. Ions colliding with any solid surfaces are reflected as neutral molecules. Emission current and thrust are calculated about the plane approximately 1000 μm away from the emitter base and are linearly scaled to match the experimental configuration where 576 emitters were operated in parallel. Within the plume, EMI^+ ion speeds (m/s) were calculated and are presented in Fig. 7, while comparisons of the numerical and measured values for emission current

and thrust are presented in Fig. 8. Agreement is shown between the numerical and experimental data across a range of extractor voltages, suggesting that downstream characteristics of the plume can be accurately simulated given sufficient initial conditions.

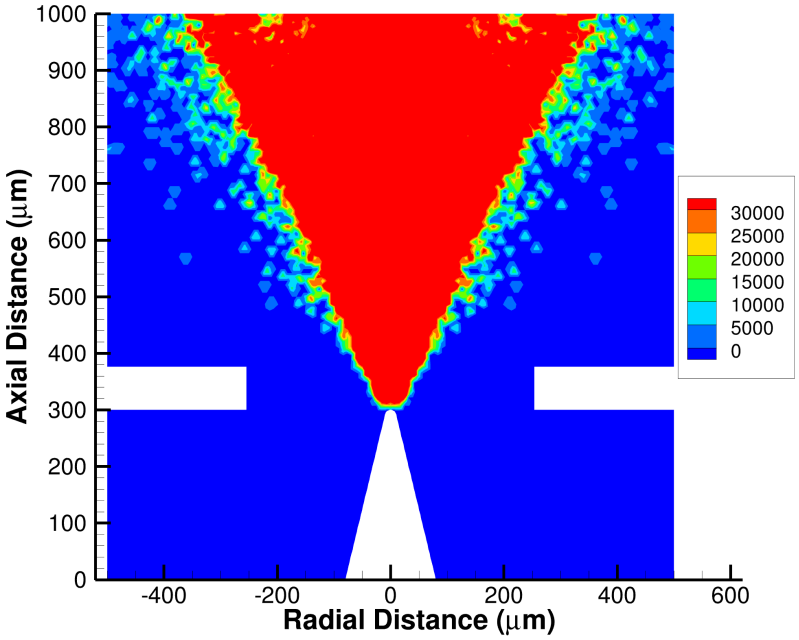


Figure 7. EMI+ ion speeds (m/s)

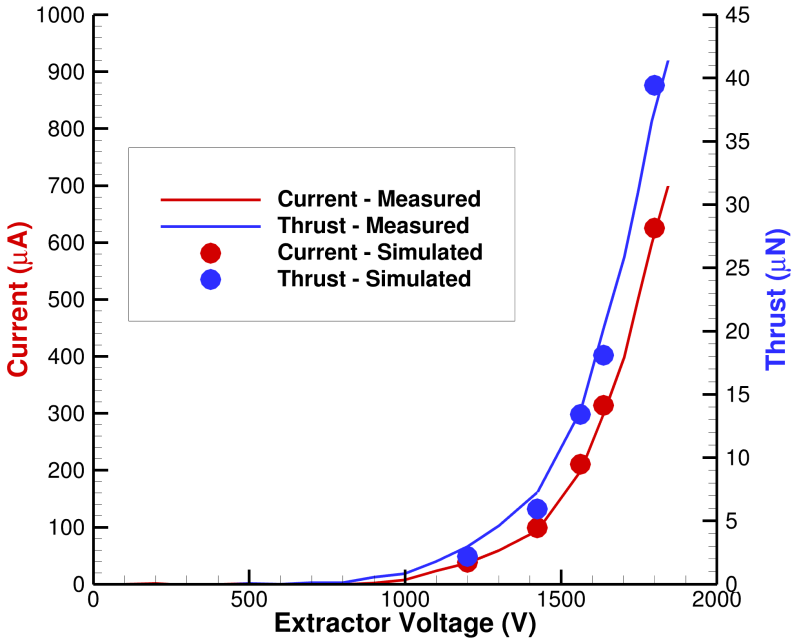


Figure 8. Comparison of emission current and thrust between experimental measurements by Natisin et al. [3] and DSMC–PIC simulation output.

3. Future Objectives

The majority of model development thus far has been within the Extraction Region. Implementing a normal stress balance routine at the interface, Eqn. (10), is the final module required for completion of the field emission model. This stress is a function of the surface tension, and thus the geometry of the meniscus. To complete this, a meniscus perturbation module must be developed that evolves the shape into one that satisfies equilibrium. Currently, the solver determines a nonequilibrium solution for a prescribed meniscus shape. With the addition of the meniscus perturbation module, the final equation of the field emission model is resolved, completing the Extraction Region component of the model. Development time for this module is estimated to take 1-2 months.

The kinetic model within the Plume Region is solved using an in-house direct simulation Monte-Carlo and particle-in-cell solver, and thus no core development is required. As such, the final task for the single emitter electrospray model is coupling the subscale routine in the Extraction Regime with the macroscale kinetic routine in the plume. To achieve a two-way coupling, the output of each submodel must be fed as boundary conditions to the other. Development time for this coupling module is estimated to take an additional month.

When the high-fidelity electrospray model is complete, its applications can be explored in parallel. First, the model must be benchmarked by comparing simulations with experimental measurements. Experimental measurements are nominally taken for electrosprays operating in arrays in the order of 100-1000, challenging validation of single emitter models as coupling effects cannot be accounted for. To overcome this, the Air Force Research Laboratory (AFRL) is conducting a Single Emitter Air Force Electrospray Thruster (SEAFET) program, providing data that can be directly used as validation for the single emitter model. The program has conducted a preliminary qualitative analysis of select emitters [5], with additional data to be made available in the coming months.

Further collaboration with the SEAFET program can allow exploration of the dependencies certain operating conditions have in life-limiting mechanisms. Once an initial benchmarking has been conducted, simulations spanning large parameter sweeps can be conducted to better quantify how perturbations in operations conditions such as geometry, voltage and material selection affect emission characteristics that directly contribute to failure modes. Experimental data could be taken for select configurations for calibration and further validation of the single emitter model. As the primary mechanism contributing to electrospray failure is emission impingement at the electrodes, exploring which facets of electrospray design and operation that directly contribute to overspraying at the grid will be the initial focus of the study.

The availability of both single emitter and multiplexed emitter data also allow for study of coupling effects within these systems. Experiments have demonstrated that emission characteristics of multiplexed arrays are not linear extrapolations of single emitter characteristics, alluding to possible inter-emitter dependencies. Once a single emitter model is validated, simulations can be configured to explore possible macroscopic effects that may occur from operating emitters in parallel. Again, these simulations may help elucidate what components of design and operation are contributing to this phenomenon by conducting parameter sweeps that are otherwise infeasible to perform experimentally. The results of which may then support select configurations of interest where experimentation can be conducted, optimizing the iterative routine towards building electrosprays whose mission capabilities vastly expand beyond those that are available today.

References

[1] C. Cai, "Theoretical and numerical studies of plume flows in vacuum chambers.," Ph.D. Dissertation, University of Michigan, Ann Arbor, 2005.

[2] A. Thuppul, P. L. Wright, A. L. Collins, J. K. Ziemer, and R. E. Wirz, "Lifetime Considerations for Electrospray Thrusters," *Aerospace*, vol. 7, no. 8, p. 108, Aug. 2020.

[3] M. Natisin, H. Zamora, W. McGehee, N. Arnold, Z. Holley, M. Holmes, and D. Eckhardt, "Fabrication and characterization of a fully conventionally machined, high-performance porous-media electrospray thruster," *Journal of Micromechanics and Microengineering*, vol. 30, no. 11, p. 115021, 2020.

[4] C. S. Coffman, "Electrically-assisted evaporation of charged fluids: Fundamental modeling and studies on ionic liquids," Ph.D. dissertation, Massachusetts Institute of Technology, 2016.

[5] W. A. McGehee, N. Arnold, M. R. Natisin, Z. A. Holley, and D. Eckhardt, "The single emitter air force electrospray thruster (SEAFET) Program: Goals and initial results," in *37th International Electric Propulsion Conference*, Massachusetts Institute of Technology, Cambridge, MA USA, Jun. 2022.

Final Technical Report

Prediction of Basic Operation of Electrospray Thrusters
Using High-Fidelity Modeling

AFOSR Grant FA9550-21-1-0045

Monitored by Mitat Birkan

Iain D. Boyd (PI), University of Colorado

Abstract

Electro-spray (ES) thrusters for in-space propulsion operate using ionic liquids that may be colloidal or metal as propellant. Individual ES devices generate very small thrust and impulse bits that are ideal for fine pointing missions. The Air Force has a more significant need for large-scale thrust levels required for station keeping, orbit raising, and orbit transfer. ES systems are of interest because they provide a specific impulse that may be tailored by the propellant, high thrust through the application of many devices in parallel, and all achieved at potentially high efficiencies of about 80%. There are significant fundamental challenges for the integration of the large numbers of devices needed for Air Force missions including: (1) failure modes of ES thrusters; (2) determining the lifetime of ES thrusters; and (3) understanding any crosstalk between adjacent thrusters. We are pursuing a comprehensive research project to address these gaps:

- Model Development: The key developments needed to model electro-spray systems are treatment of ionic-liquid physics, consideration of multiple emission sites, and extension to three dimensions.
- Model Benchmarking: Integration of high-fidelity modeling with empirical data is necessary to characterize life-limiting mechanisms and extrapolate performance in space environments. Direct comparisons will be made of model predictions with detailed plume measurements of AFRL porous-media flow emitters that are under way at the University of Michigan. Comparisons will also be made with all relevant data sets generated at the Air Force Research Laboratory in their current ES activities.
- Use the high-fidelity simulations to provide fundamental data needed for application of low-fidelity analysis of ES thrusters. For example, understanding the process and conditions for mode switching to the pure ionic regime is essential to meeting the USAF requirements for this technology.
- Analyses: Use the high-fidelity model for large arrays including assessment of coupling effects between multiple electro-spray emitters and prediction of primary failure modes.

This final report summarizes the progress made during the first and second years of the grant in terms of source and plume modeling.

DISTRIBUTION A: Distribution approved for public release.

1. Electrospray Model Description

A single porous electrospray emitter operating in a purely ionic emission regime is considered. The domain of interest spans from the emission site on the tip to the downstream plume between the extractor and accelerator electrodes. Computationally, this domain is partitioned into two two-dimensional subdomains: an Extraction Region where field emission from the electrohydrodynamic (EHD) meniscus is considered, and a Plume Region where the ion dynamics of the extracted species are considered. The Extraction Region is further decomposed into a vacuum and bulk liquid domain, Ω_{vac} and Ω_{liq} respectively, where Γ_{lv} denotes the intersection between them. A schematic of the global domain is presented in Fig. 1.

Within the bulk liquid, mass and momentum conservation are considered using the Navier-Stokes equations are the low Reynolds number limit, otherwise known as the Stokes equations,

$$\mu\nabla^2 v - \nabla \mathrm{p} = 0, \tag{1}$$
$$\nabla \cdot v = 0, \tag{2}$$

where μ is fluid viscosity, v is bulk fluid velocity, and p is pressure. Given the propellant is conductive, charge transport is considered as well. Convective charge transport is neglected and an Ohmic conduction model is chosen,

$$j = -K\nabla\phi_l, \tag{3}$$

where j is the current density, K is the electrical conductivity and ϕ_l is the electric potential in the bulk fluid. When charge conservation, $\nabla \cdot j = 0$, is considered with Eqn. (3) the electric potential can be shown to satisfy Laplace's equation,

$$\nabla^2\phi_l = 0. \tag{4}$$

Within the vacuum, space charge effects are negligible, and Laplace's equation is again used to determine the potential,

$$\nabla^2\phi_v = 0, \tag{5}$$

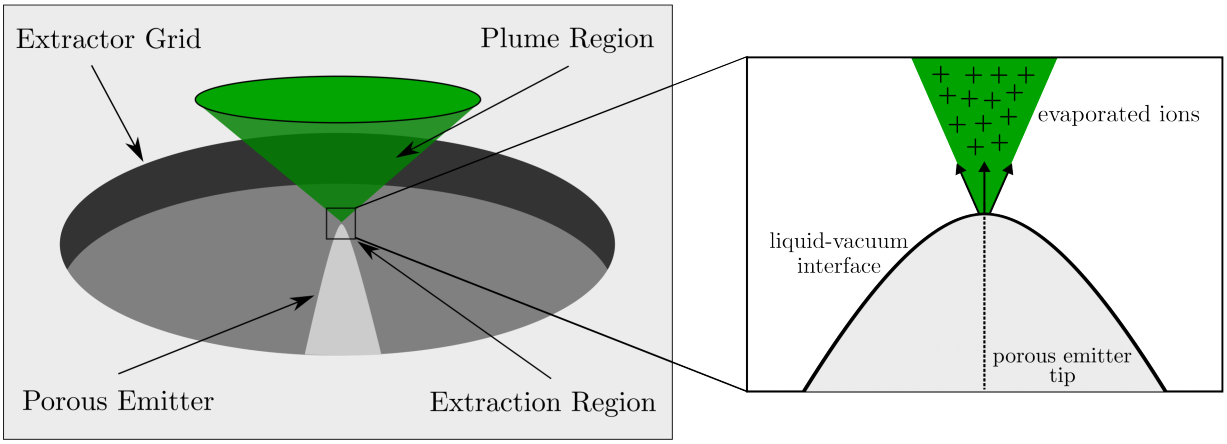


Figure 1. Domains of interest within a porous electrospray emitter.

DISTRIBUTION A: Distribution approved for public release.

where ϕ_v is the electric potential within the vacuum. At the liquid-vacuum interface, the free surface charge density is considered using the electrostatic condition,

$$(-\nabla\phi_v + \epsilon\nabla\phi_l)\cdot\hat{n} = \frac{\sigma}{\epsilon_0}, \tag{6}$$

where $\hat{n}$ is the unit vector normal to the interface, σ is the free surface charge density, ϵ is the relative permittivity, and ϵ_0 is the vacuum permittivity. Additionally, the free surface charge density satisfies the following steady-state transport equation,

$$v\cdot\nabla\sigma = \sigma\hat{n}\cdot\nabla v\cdot\hat{n} - K\nabla\phi_l\cdot\hat{n} - j\cdot\hat{n}. \tag{7}$$

Equation (7) states that the charge advected by the fluid flow is balanced by surface strain, the charge conducted to the surface, and the charge lost due to ion evaporation. Field emission of ions is described by the kinetic law,

$$j\cdot\hat{n} = \frac{k_b T}{h_c}\sigma\exp\left(\frac{-1}{k_b T}\left[\Delta G - \sqrt{\frac{\nabla\phi_v\cdot\hat{n}}{4\pi\epsilon_0/q^3}}\right]\right), \tag{8}$$

where k_b is the Boltzmann constant, h_c is the Planck constant, T is the temperature, q is the elementary charge and ΔG is the solvation energy of the ions. Additionally, force balance between the applied electric traction, viscous stresses, and surface tension is enforced at the liquid-vacuum interface,

$$\hat{t}\cdot(\tau_l - \tau_e)\cdot\hat{n} = 0, \tag{9}$$
$$\hat{n}\cdot(\tau_l - \tau_e)\cdot\hat{n} = -\gamma\nabla\cdot\hat{n}, \tag{10}$$

where $\hat{\boldsymbol{t}}$ is the unit vector tangent to the interface, τ_l is the viscous stress tensor, τ_e is the electrostatic Maxwell stress tensor, and γ is the surface tension. The normal and tangential projections of the Maxwell stress tensor on the interface satisfy the equations

$$\hat{t}\cdot\tau_e\cdot\hat{n} = -\sigma\nabla\phi_v\cdot\hat{t}, \tag{11}$$
$$\hat{n}\cdot\tau_e\cdot\hat{n} = \frac{1}{2}\epsilon_0((\nabla\phi_v\cdot\hat{n})^2 - \epsilon(\nabla\phi_l\cdot\hat{n})^2) + \frac{1}{2}\epsilon_0\big((\epsilon-1)(\nabla\phi_v\cdot\hat{t})^2\big). \tag{12}$$

A hybrid direct simulation Monte Carlo and particle-in-cell (DSMC–PIC) solver is implemented to simulate the downstream rarefied plume, of which a complete description of the solver can be found by Cai [1]. In summary, DSMC is a widely implemented particle method used to calculate collisional dynamics within dilute gases. Analogously for plasmas, PIC is a kinetic method used to simulate the dynamics of charged particles under the influence of external and self–induced electromagnetic fields. Simultaneous implementation of both methods within a

DISTRIBUTION A: Distribution approved for public release.

unified kinetic solver allows the study of gases characterized by both material and Coulombic interactions.

Within the multiscale model, the DSMC–PIC solver is used to initialize a distribution of charged macroparticles at the liquid–vacuum interface as well as simulate their motion within the computational vacuum domain. The initial distribution is a function of the ion number density determined by the EHD meniscus solver. The emission velocity is sampled from a biased Maxwellian based on the propellant temperature. From there, macroscopic plume properties that contribute to single emitter failure mechanisms can be calculated and simulations can be designed to study configurations that minimize these mechanisms. For example, the primary failure mode of electrosprays is overspray of propellant at the site of emission, resulting in impingement of the electrodes that ultimately contribute to shorting and power processing unit failure [2]. By conducting a sensitivity analysis, the proposed model may be able to elucidate what elements of the parameter space contribute most to the plume divergence angle, minimizing the probability of electrode impingement.

A complete schematic of the computational domain is presented in Fig. 2. Fig. 2a presents a macro-scale, two-dimensional domain of a single emitter tip below two extractor electrodes A voltage differential is applied between the emitter and electrodes to induce electric fields strengths on the order required for direct ion evaporation at the propellant free surface. Field emission at the interface is numerically treated within a separate sub-scale domain at the emitter apex and is coupled to the macro-scale domain via the Γ_{sub} intersection. Fig. 2b presents a sub-scale domain of an emission site at the emitter apex presented in Fig. 2a. Steady, open channel flow is assumed for the propellant in Ω_{liq}, where a fully developed velocity profile is imposed at the Γ_{inl} inlet boundary. Geometry of the EHD meniscus, Γ_{int}, is numerically perturbed to find configurations that satisfy mechanical equilibrium, a prerequisite to solve for steady-state emission characteristics.

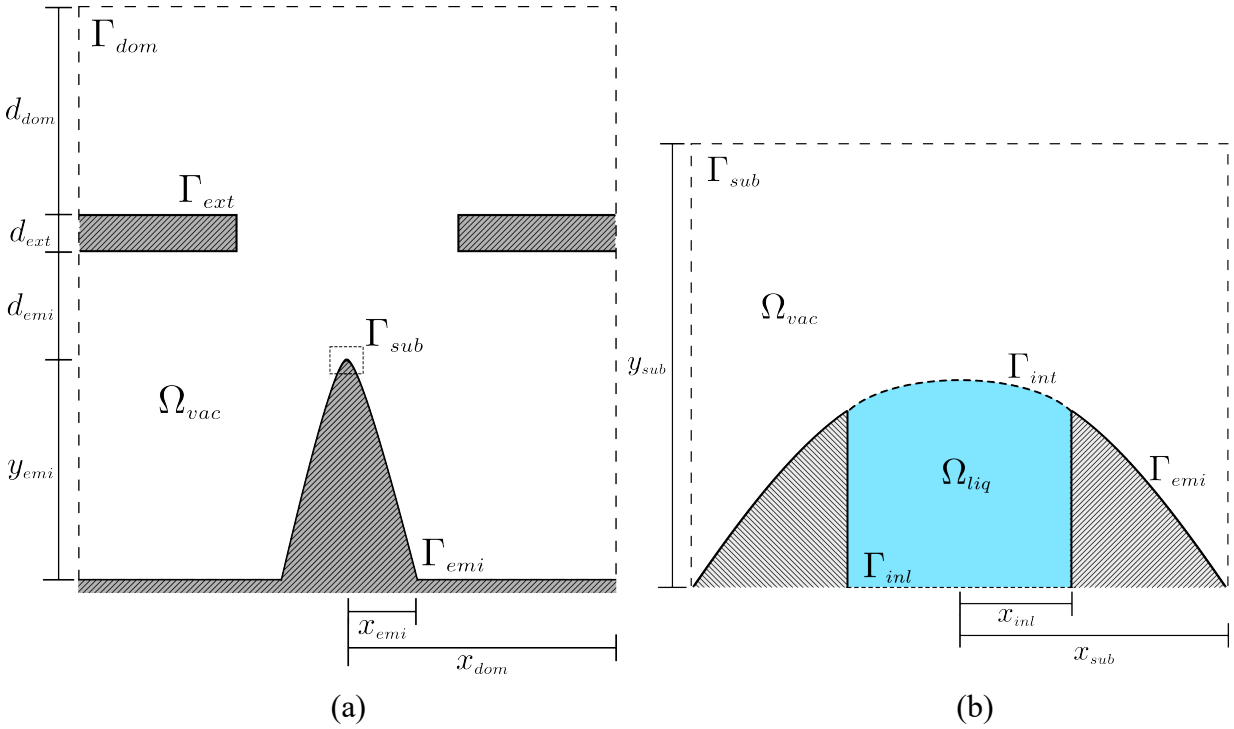


Figure 2. Computational domain.

DISTRIBUTION A: Distribution approved for public release.

2. Progress to Date

2.1 Numeric Implementation

The core developmental progress within the electrospray model has been within the Extraction Region. A finite element solver has been implemented using the Distributed and Unified Numerics Environment (DUNE), an open-source library for solving partial differential equations using grid-based methods. An algorithm has been developed that solves the coupled set of partial differential equations for a prescribed meniscus shape. The algorithm generally operates as follows:

The core Stokes and Laplace equations are solved in their respective domains. A multidomain module is configured to enforce boundary conditions that are dependent upon solutions across domains. An additional module is developed to enforce directionally dependent boundary conditions on the same interface. Consideration of electrostatic conditions, surface charge density transport, and stress balance at the free surface act as these unique multidomain boundary conditions. An iterative routine first solves the electric potential system until convergence, at which a global algorithm is implemented that solves the Stokes system and couples the domain together. A flowchart of this global algorithm is presented in Fig. 3. The result is a converged nonequilibrium solution for a prescribed meniscus shape. The current stage of development is expanding this to equilibrium solutions by including meniscus geometry perturbations in the global algorithm.

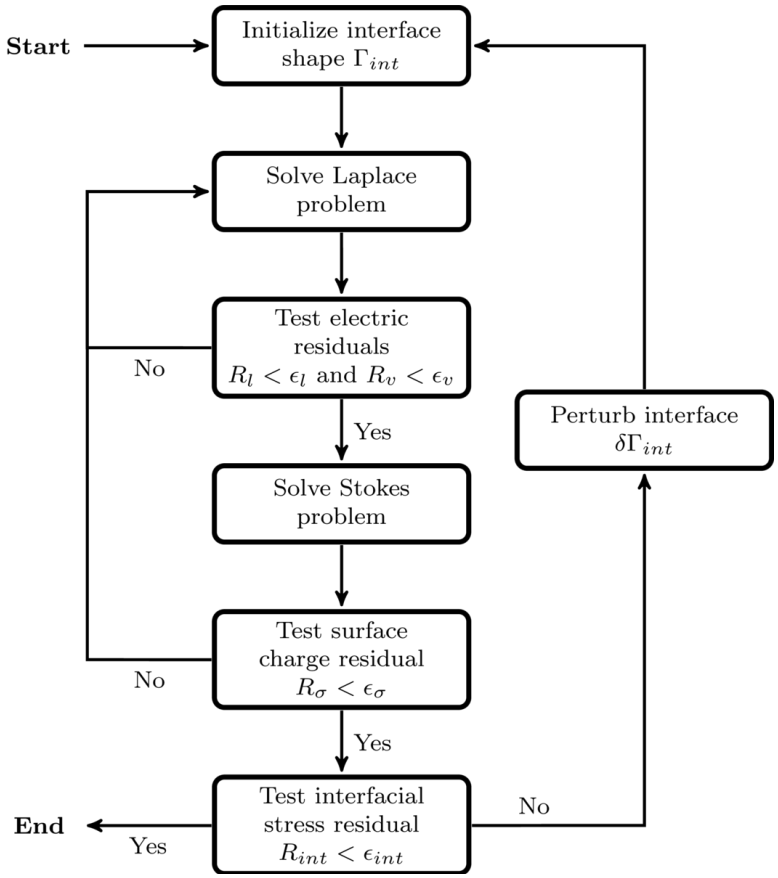


Figure 3. Algorithm to numerically solve for ion emission from the EHS meniscus within the Extraction Region.

DISTRIBUTION A: Distribution approved for public release.

2.2 Results

2.2.1 Simulation Parameters

Initial simulations within the Extraction and Plume region are conducted using similar operating parameters as those in [3]. Mapping of ion emission from the Extraction Region to the kinetic routine is not directly calculated. Experimental current values are used as input conditions into the kinetic routine via single cell injection at the emitter tip. The applied electric field condition within the EHD model is calibrated such that the integrated surface emission at the meniscus tip is of approximate order to the experimental current. Direct mapping of field emission from the EHD model within the Extraction Region to the kinetic model in the Plume Region is deferred to future work. A computational domain axial length of 0.1 μm and width of 0.1 μm is chosen for the Extraction Region, to emulate similar length scales of effective low paths within porous electrospray emitters. Meshes of the liquid and vacuum subdomains in the Extraction Region are shown in Fig. 3. A Taylor Cone angle of 49.29° is chosen for the emitter cone with a tip radius of 10 nm. Mesh elements at the emitter tip are refined in both subdomains to better resolve ion emission in this region. The computational domain of the Plume Region spans a radial distance of 500 μm and 1000 μm axially.

2.2.2 Electric Potentials

Electric potential distributions within the liquid and vacuum subdomains of the Extraction Region are presented in Fig. 4. A relatively linear progression is seen in the axial direction of both domains, with continuity between electric potentials at the interface. The potential within the liquid domain, Fig. 4a, can be seen enforced to zero where the fluid contacts the emitter electrode. A potential gradient tangential to the interface is also observed, suggesting a stronger electric field towards the meniscus center. This behavior is expected for a perturbed conductive fluid exposed to an external field, as the perturbation would result in a higher charge density at the tip and would result in a higher field strength. Continuity of electric potential across the liquid and vacuum domain interface is also observed. As the interfacial jump in electric displacement is innately enforced by the iteration scheme, all facets of the Laplace problem appear correctly represented within the semi-equilibrium potential distributions.

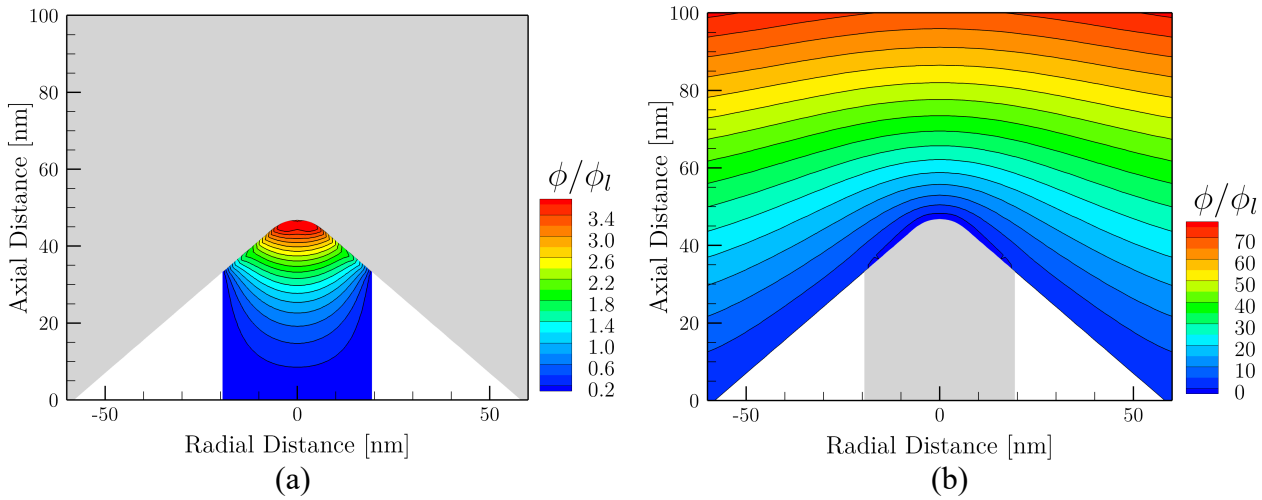


Figure 4. Electric potential distributions within the (a) liquid and (b) vacuum subdomains.

2.2.3 Stokes Flow and Ion Emission

Axial velocity contours within the liquid subdomain of the Extraction Region are presented in Fig. 5. Flow velocity of an ionic liquid meniscus operating in a purely ionic regime is known to scale with

$$v \sim \frac{I}{\pi\rho(q/m)(r^*)^2}, \tag{13}$$

where r^* is the characteristic length scale at the emitter tip and I is the emission current [4]. The Reynolds number scaling is then shown to be

$$Re \sim \frac{I}{\pi\mu(q/m)r^*} \sim 10^{-2}. \tag{14}$$

Using the single-emitter current for the -1562 V operational case ($I \approx 10^{-6}A$) in [3] and the fluid properties of EMI-BF_4 ($\mu \approx 10^{-2}$ Pa·s, $q/m \approx 10^6$ C/kg), the Reynolds number is shown to be significantly less than unity and thus Stokes flow is present. As mentioned, ion emission is only possible within a steady-state configuration if the normal fluid velocity at the intersection is nonzero. Field emission at the emitter tip is represented by arrows in the top-right plot of Fig. 5. It can be shown that the velocity at the emission tip is of approximate order to the emission velocity in the operational case, though it is important to note that the applied electric field, E_0, is adjusted in the Extraction Region to achieve this agreement.

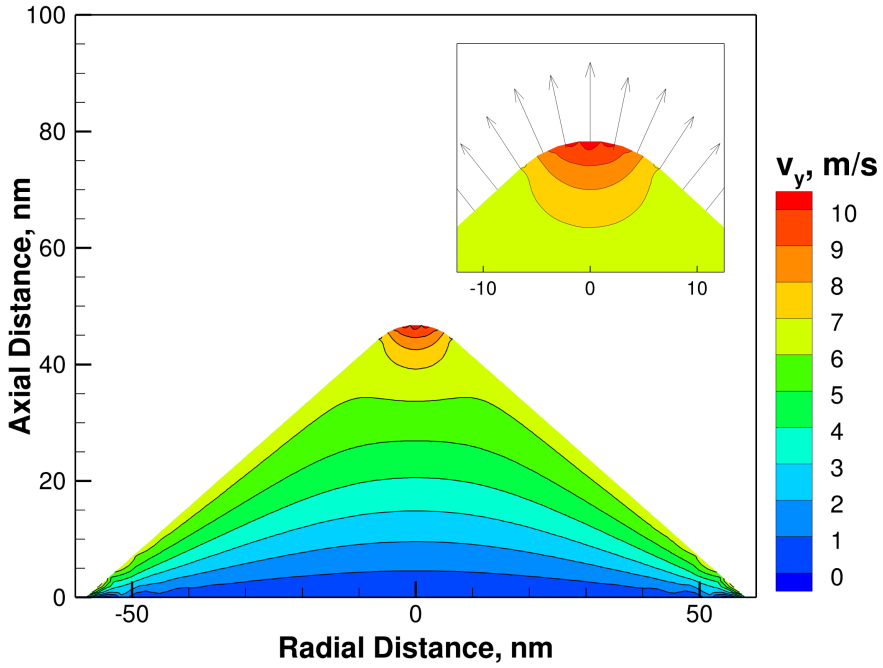


Figure 5. Axial velocity in the bulk fluid, with ion emission at the emitter tip shown in the inset.

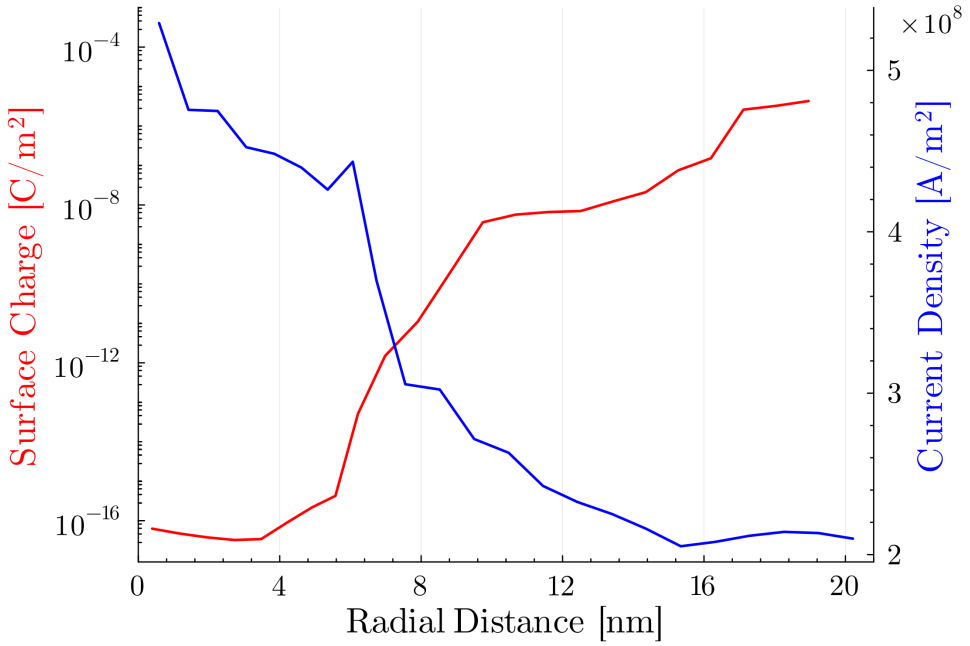


Figure 6. Interfacial surface charge and normal current density versus radial distance.

Characteristics of the Stokes problem can be observed through the interfacial current density, as it is linearly related to the normal fluid velocity at the meniscus. This current density in addition to the surface charge are plotted as a function of the radial distance in Fig. 6. As seen by the potential distribution, the emission centerline should correspond to the highest electric field, which in turn should result in the highest current density of emitted species. This is observed in Fig. 6, where the current density progressively declines with radial distance as the applied electric field weakens away from the centerline. The surface charge, on the other hand, appears to be inversely related to the current density with respect to radial distance. This is due to the continuity law of Eqn. (7), stating the surface charge represents the balance of current conducted to the interface and current evaporating from the interface. This balance is depicted in Fig. 6, where the surface charge is minimum at the interfacial locations corresponding to the highest ion emission, and vice versa. Additional quantitative validation of the EHD solver with occur once the interfacial perturbation scheme is implemented.

2.2.4 Plume Simulations

Independent simulations of the DSMC–PIC solver were conducted as well. As the coupling with the EHD meniscus solver has yet to be implemented, the simulations were initialized using experimental data of Natisin et al. [3]. Similarly, EMI-BF4 is chosen as the propellant. Within the simulation, the plume is assumed to consist of a 1:1 mixture of single-charged EMI^+ ions and EMI-BF4 neutrals. Ions colliding with any solid surfaces are reflected as neutral molecules. Emission current and thrust are calculated about the plane approximately 1000 μm away from the emitter base and are linearly scaled to match the experimental configuration where 576 emitters were operated in parallel. Within the plume, EMI^+ ion speeds (m/s) were calculated and are presented in Fig. 7, while comparisons of the numerical and measured values for emission current

and thrust are presented in Fig. 8. Agreement is shown between the numerical and experimental data across a range of extractor voltages, suggesting that downstream characteristics of the plume can be accurately simulated given sufficient initial conditions.

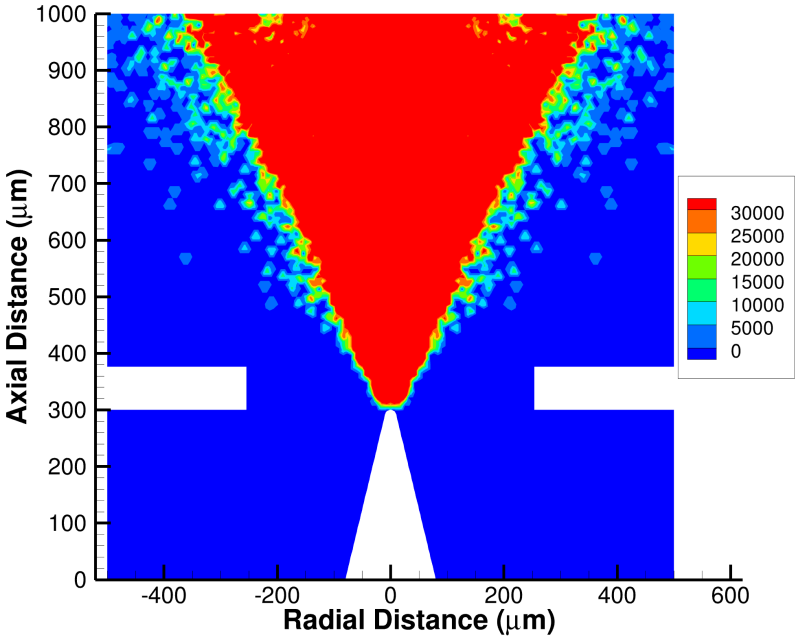


Figure 7. EMI+ ion speeds (m/s)

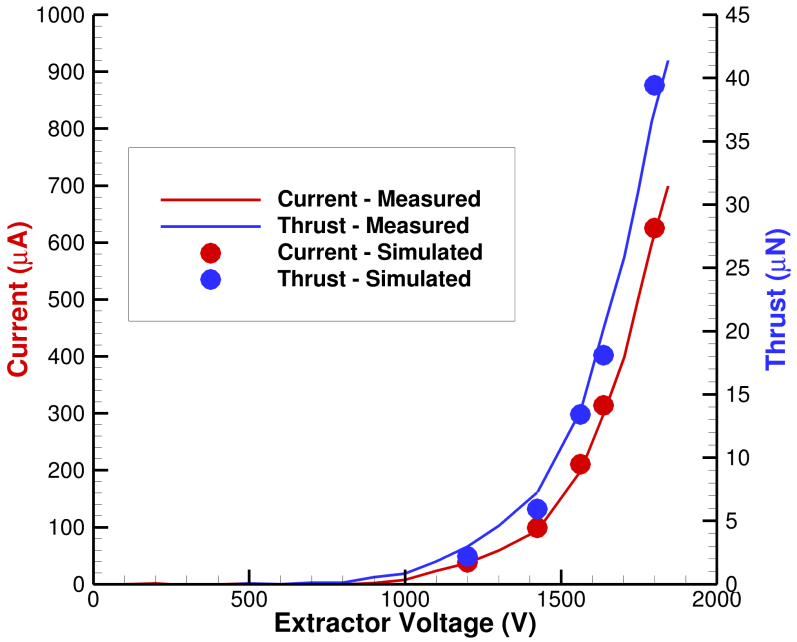


Figure 8. Comparison of emission current and thrust between experimental measurements by Natisin et al. [3] and DSMC–PIC simulation output.

3. Future Objectives

The majority of model development thus far has been within the Extraction Region. Implementing a normal stress balance routine at the interface, Eqn. (10), is the final module required for completion of the field emission model. This stress is a function of the surface tension, and thus the geometry of the meniscus. To complete this, a meniscus perturbation module must be developed that evolves the shape into one that satisfies equilibrium. Currently, the solver determines a nonequilibrium solution for a prescribed meniscus shape. With the addition of the meniscus perturbation module, the final equation of the field emission model is resolved, completing the Extraction Region component of the model. Development time for this module is estimated to take 1-2 months.

The kinetic model within the Plume Region is solved using an in-house direct simulation Monte-Carlo and particle-in-cell solver, and thus no core development is required. As such, the final task for the single emitter electrospray model is coupling the subscale routine in the Extraction Regime with the macroscale kinetic routine in the plume. To achieve a two-way coupling, the output of each submodel must be fed as boundary conditions to the other. Development time for this coupling module is estimated to take an additional month.

When the high-fidelity electrospray model is complete, its applications can be explored in parallel. First, the model must be benchmarked by comparing simulations with experimental measurements. Experimental measurements are nominally taken for electrosprays operating in arrays in the order of 100-1000, challenging validation of single emitter models as coupling effects cannot be accounted for. To overcome this, the Air Force Research Laboratory (AFRL) is conducting a Single Emitter Air Force Electrospray Thruster (SEAFET) program, providing data that can be directly used as validation for the single emitter model. The program has conducted a preliminary qualitative analysis of select emitters [5], with additional data to be made available in the coming months.

Further collaboration with the SEAFET program can allow exploration of the dependencies certain operating conditions have in life-limiting mechanisms. Once an initial benchmarking has been conducted, simulations spanning large parameter sweeps can be conducted to better quantify how perturbations in operations conditions such as geometry, voltage and material selection affect emission characteristics that directly contribute to failure modes. Experimental data could be taken for select configurations for calibration and further validation of the single emitter model. As the primary mechanism contributing to electrospray failure is emission impingement at the electrodes, exploring which facets of electrospray design and operation that directly contribute to overspraying at the grid will be the initial focus of the study.

The availability of both single emitter and multiplexed emitter data also allow for study of coupling effects within these systems. Experiments have demonstrated that emission characteristics of multiplexed arrays are not linear extrapolations of single emitter characteristics, alluding to possible inter-emitter dependencies. Once a single emitter model is validated, simulations can be configured to explore possible macroscopic effects that may occur from operating emitters in parallel. Again, these simulations may help elucidate what components of design and operation are contributing to this phenomenon by conducting parameter sweeps that are otherwise infeasible to perform experimentally. The results of which may then support select configurations of interest where experimentation can be conducted, optimizing the iterative routine towards building electrosprays whose mission capabilities vastly expand beyond those that are available today.

References

[1] C. Cai, "Theoretical and numerical studies of plume flows in vacuum chambers.," Ph.D. Dissertation, University of Michigan, Ann Arbor, 2005.

[2] A. Thuppul, P. L. Wright, A. L. Collins, J. K. Ziemer, and R. E. Wirz, "Lifetime Considerations for Electrospray Thrusters," *Aerospace*, vol. 7, no. 8, p. 108, Aug. 2020.

[3] M. Natisin, H. Zamora, W. McGehee, N. Arnold, Z. Holley, M. Holmes, and D. Eckhardt, "Fabrication and characterization of a fully conventionally machined, high-performance porous-media electrospray thruster," *Journal of Micromechanics and Microengineering*, vol. 30, no. 11, p. 115021, 2020.

[4] C. S. Coffman, "Electrically-assisted evaporation of charged fluids: Fundamental modeling and studies on ionic liquids," Ph.D. dissertation, Massachusetts Institute of Technology, 2016.

[5] W. A. McGehee, N. Arnold, M. R. Natisin, Z. A. Holley, and D. Eckhardt, "The single emitter air force electrospray thruster (SEAFET) Program: Goals and initial results," in *37th International Electric Propulsion Conference*, Massachusetts Institute of Technology, Cambridge, MA USA, Jun. 2022.

Final Technical Report

Prediction of Basic Operation of Electrospray Thrusters
Using High-Fidelity Modeling

AFOSR Grant FA9550-21-1-0045

Monitored by Mitat Birkan

Iain D. Boyd (PI), University of Colorado

Abstract

Electro-spray (ES) thrusters for in-space propulsion operate using ionic liquids that may be colloidal or metal as propellant. Individual ES devices generate very small thrust and impulse bits that are ideal for fine pointing missions. The Air Force has a more significant need for large-scale thrust levels required for station keeping, orbit raising, and orbit transfer. ES systems are of interest because they provide a specific impulse that may be tailored by the propellant, high thrust through the application of many devices in parallel, and all achieved at potentially high efficiencies of about 80%. There are significant fundamental challenges for the integration of the large numbers of devices needed for Air Force missions including: (1) failure modes of ES thrusters; (2) determining the lifetime of ES thrusters; and (3) understanding any crosstalk between adjacent thrusters. We are pursuing a comprehensive research project to address these gaps:

- Model Development: The key developments needed to model electro-spray systems are treatment of ionic-liquid physics, consideration of multiple emission sites, and extension to three dimensions.
- Model Benchmarking: Integration of high-fidelity modeling with empirical data is necessary to characterize life-limiting mechanisms and extrapolate performance in space environments. Direct comparisons will be made of model predictions with detailed plume measurements of AFRL porous-media flow emitters that are under way at the University of Michigan. Comparisons will also be made with all relevant data sets generated at the Air Force Research Laboratory in their current ES activities.
- Use the high-fidelity simulations to provide fundamental data needed for application of low-fidelity analysis of ES thrusters. For example, understanding the process and conditions for mode switching to the pure ionic regime is essential to meeting the USAF requirements for this technology.
- Analyses: Use the high-fidelity model for large arrays including assessment of coupling effects between multiple electro-spray emitters and prediction of primary failure modes.

This final report summarizes the progress made during the first and second years of the grant in terms of source and plume modeling.

DISTRIBUTION A: Distribution approved for public release.

1. Electrospray Model Description

A single porous electrospray emitter operating in a purely ionic emission regime is considered. The domain of interest spans from the emission site on the tip to the downstream plume between the extractor and accelerator electrodes. Computationally, this domain is partitioned into two two-dimensional subdomains: an Extraction Region where field emission from the electrohydrodynamic (EHD) meniscus is considered, and a Plume Region where the ion dynamics of the extracted species are considered. The Extraction Region is further decomposed into a vacuum and bulk liquid domain, Ω_{vac} and Ω_{liq} respectively, where Γ_{lv} denotes the intersection between them. A schematic of the global domain is presented in Fig. 1.

Within the bulk liquid, mass and momentum conservation are considered using the Navier-Stokes equations are the low Reynolds number limit, otherwise known as the Stokes equations,

$$\mu\nabla^2 v - \nabla \mathrm{p} = 0, \tag{1}$$
$$\nabla \cdot v = 0, \tag{2}$$

where μ is fluid viscosity, v is bulk fluid velocity, and p is pressure. Given the propellant is conductive, charge transport is considered as well. Convective charge transport is neglected and an Ohmic conduction model is chosen,

$$j = -K\nabla\phi_l, \tag{3}$$

where j is the current density, K is the electrical conductivity and ϕ_l is the electric potential in the bulk fluid. When charge conservation, $\nabla \cdot j = 0$, is considered with Eqn. (3) the electric potential can be shown to satisfy Laplace's equation,

$$\nabla^2\phi_l = 0. \tag{4}$$

Within the vacuum, space charge effects are negligible, and Laplace's equation is again used to determine the potential,

$$\nabla^2\phi_v = 0, \tag{5}$$

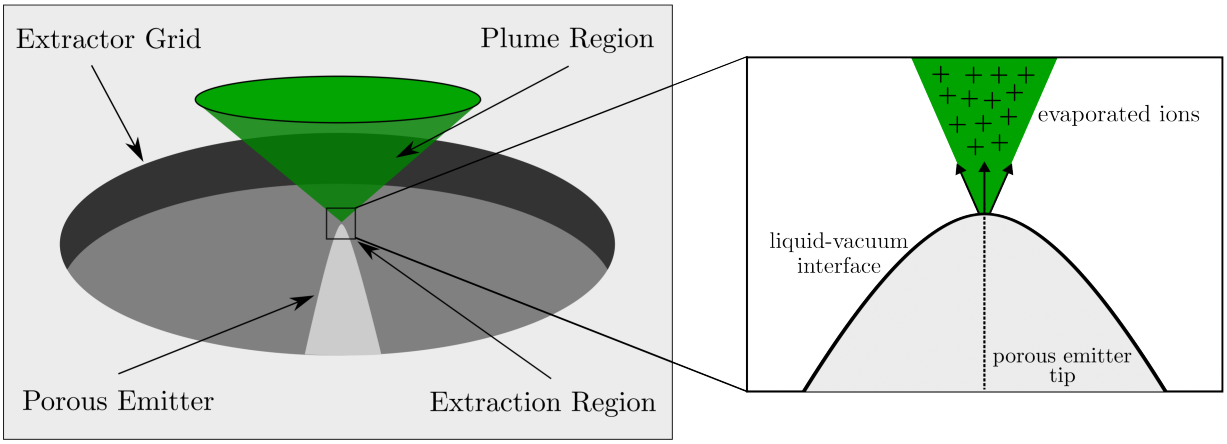


Figure 1. Domains of interest within a porous electrospray emitter.

DISTRIBUTION A: Distribution approved for public release.

where ϕ_v is the electric potential within the vacuum. At the liquid-vacuum interface, the free surface charge density is considered using the electrostatic condition,

$$(-\nabla\phi_v + \epsilon\nabla\phi_l)\cdot\hat{n} = \frac{\sigma}{\epsilon_0}, \tag{6}$$

where $\hat{n}$ is the unit vector normal to the interface, σ is the free surface charge density, ϵ is the relative permittivity, and ϵ_0 is the vacuum permittivity. Additionally, the free surface charge density satisfies the following steady-state transport equation,

$$v\cdot\nabla\sigma = \sigma\hat{n}\cdot\nabla v\cdot\hat{n} - K\nabla\phi_l\cdot\hat{n} - j\cdot\hat{n}. \tag{7}$$

Equation (7) states that the charge advected by the fluid flow is balanced by surface strain, the charge conducted to the surface, and the charge lost due to ion evaporation. Field emission of ions is described by the kinetic law,

$$j\cdot\hat{n} = \frac{k_b T}{h_c}\sigma\exp\left(\frac{-1}{k_b T}\left[\Delta G - \sqrt{\frac{\nabla\phi_v\cdot\hat{n}}{4\pi\epsilon_0/q^3}}\right]\right), \tag{8}$$

where k_b is the Boltzmann constant, h_c is the Planck constant, T is the temperature, q is the elementary charge and ΔG is the solvation energy of the ions. Additionally, force balance between the applied electric traction, viscous stresses, and surface tension is enforced at the liquid-vacuum interface,

$$\hat{t}\cdot(\tau_l - \tau_e)\cdot\hat{n} = 0, \tag{9}$$
$$\hat{n}\cdot(\tau_l - \tau_e)\cdot\hat{n} = -\gamma\nabla\cdot\hat{n}, \tag{10}$$

where $\hat{\boldsymbol{t}}$ is the unit vector tangent to the interface, τ_l is the viscous stress tensor, τ_e is the electrostatic Maxwell stress tensor, and γ is the surface tension. The normal and tangential projections of the Maxwell stress tensor on the interface satisfy the equations

$$\hat{t}\cdot\tau_e\cdot\hat{n} = -\sigma\nabla\phi_v\cdot\hat{t}, \tag{11}$$
$$\hat{n}\cdot\tau_e\cdot\hat{n} = \frac{1}{2}\epsilon_0((\nabla\phi_v\cdot\hat{n})^2 - \epsilon(\nabla\phi_l\cdot\hat{n})^2) + \frac{1}{2}\epsilon_0\big((\epsilon-1)(\nabla\phi_v\cdot\hat{t})^2\big). \tag{12}$$

A hybrid direct simulation Monte Carlo and particle-in-cell (DSMC–PIC) solver is implemented to simulate the downstream rarefied plume, of which a complete description of the solver can be found by Cai [1]. In summary, DSMC is a widely implemented particle method used to calculate collisional dynamics within dilute gases. Analogously for plasmas, PIC is a kinetic method used to simulate the dynamics of charged particles under the influence of external and self–induced electromagnetic fields. Simultaneous implementation of both methods within a

DISTRIBUTION A: Distribution approved for public release.

unified kinetic solver allows the study of gases characterized by both material and Coulombic interactions.

Within the multiscale model, the DSMC–PIC solver is used to initialize a distribution of charged macroparticles at the liquid–vacuum interface as well as simulate their motion within the computational vacuum domain. The initial distribution is a function of the ion number density determined by the EHD meniscus solver. The emission velocity is sampled from a biased Maxwellian based on the propellant temperature. From there, macroscopic plume properties that contribute to single emitter failure mechanisms can be calculated and simulations can be designed to study configurations that minimize these mechanisms. For example, the primary failure mode of electrosprays is overspray of propellant at the site of emission, resulting in impingement of the electrodes that ultimately contribute to shorting and power processing unit failure [2]. By conducting a sensitivity analysis, the proposed model may be able to elucidate what elements of the parameter space contribute most to the plume divergence angle, minimizing the probability of electrode impingement.

A complete schematic of the computational domain is presented in Fig. 2. Fig. 2a presents a macro-scale, two-dimensional domain of a single emitter tip below two extractor electrodes A voltage differential is applied between the emitter and electrodes to induce electric fields strengths on the order required for direct ion evaporation at the propellant free surface. Field emission at the interface is numerically treated within a separate sub-scale domain at the emitter apex and is coupled to the macro-scale domain via the Γ_{sub} intersection. Fig. 2b presents a sub-scale domain of an emission site at the emitter apex presented in Fig. 2a. Steady, open channel flow is assumed for the propellant in Ω_{liq}, where a fully developed velocity profile is imposed at the Γ_{inl} inlet boundary. Geometry of the EHD meniscus, Γ_{int}, is numerically perturbed to find configurations that satisfy mechanical equilibrium, a prerequisite to solve for steady-state emission characteristics.

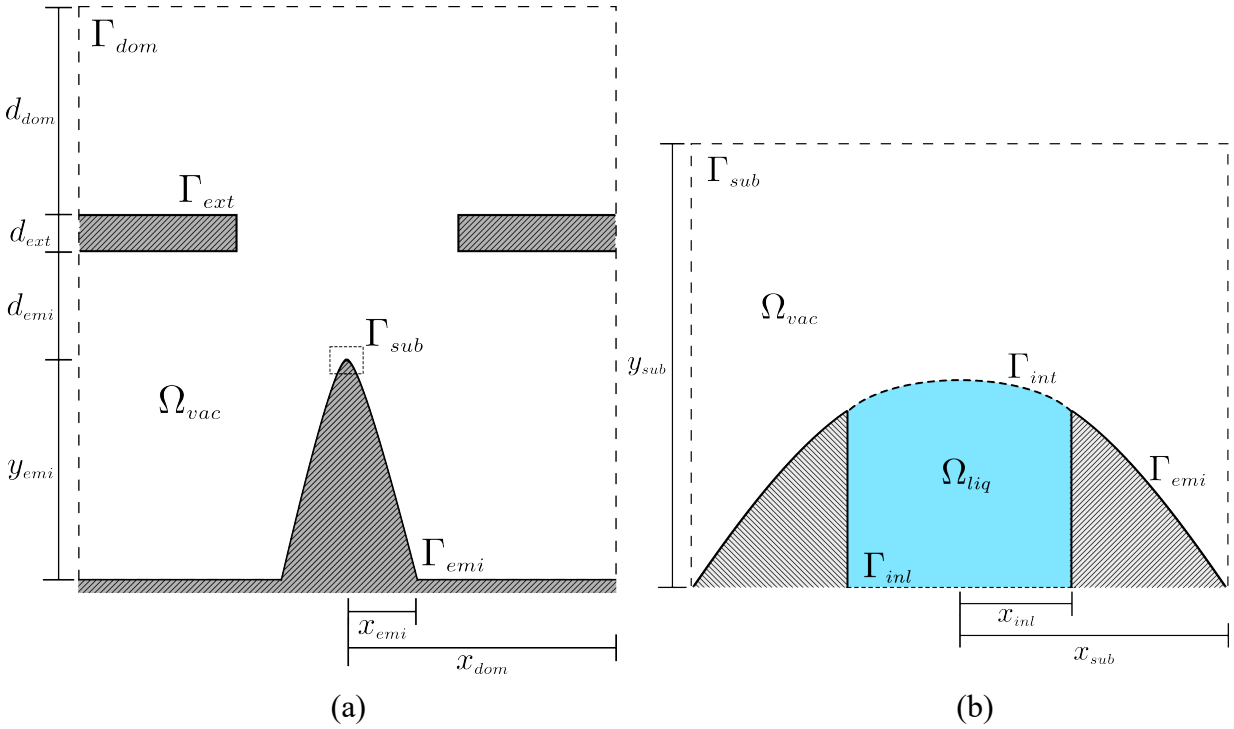


Figure 2. Computational domain.

DISTRIBUTION A: Distribution approved for public release.

2. Progress to Date

2.1 Numeric Implementation

The core developmental progress within the electrospray model has been within the Extraction Region. A finite element solver has been implemented using the Distributed and Unified Numerics Environment (DUNE), an open-source library for solving partial differential equations using grid-based methods. An algorithm has been developed that solves the coupled set of partial differential equations for a prescribed meniscus shape. The algorithm generally operates as follows:

The core Stokes and Laplace equations are solved in their respective domains. A multidomain module is configured to enforce boundary conditions that are dependent upon solutions across domains. An additional module is developed to enforce directionally dependent boundary conditions on the same interface. Consideration of electrostatic conditions, surface charge density transport, and stress balance at the free surface act as these unique multidomain boundary conditions. An iterative routine first solves the electric potential system until convergence, at which a global algorithm is implemented that solves the Stokes system and couples the domain together. A flowchart of this global algorithm is presented in Fig. 3. The result is a converged nonequilibrium solution for a prescribed meniscus shape. The current stage of development is expanding this to equilibrium solutions by including meniscus geometry perturbations in the global algorithm.

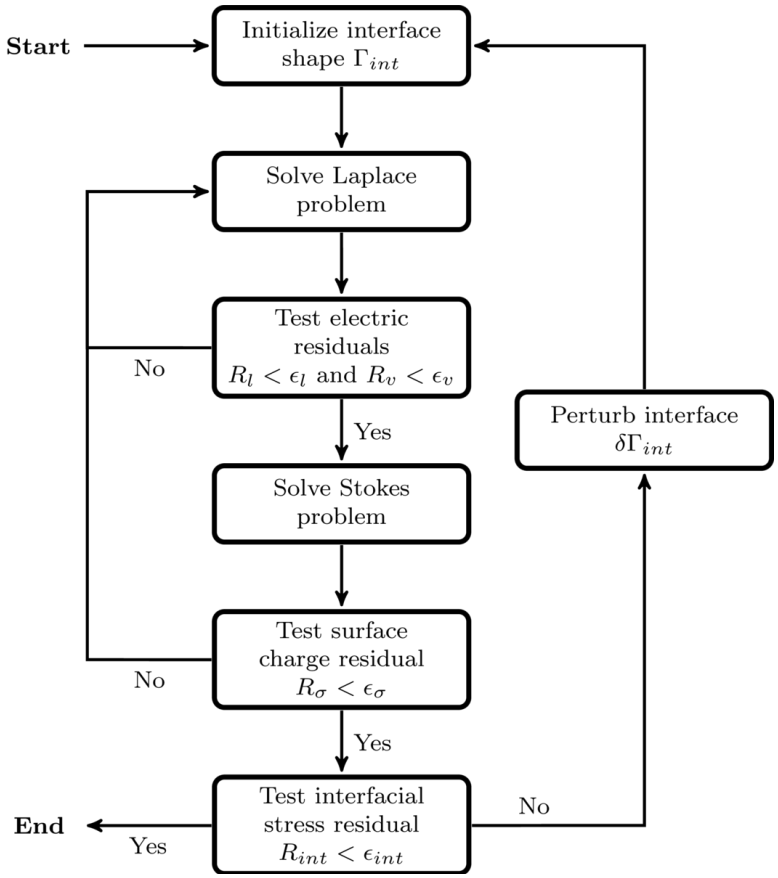


Figure 3. Algorithm to numerically solve for ion emission from the EHS meniscus within the Extraction Region.

DISTRIBUTION A: Distribution approved for public release.

2.2 Results

2.2.1 Simulation Parameters

Initial simulations within the Extraction and Plume region are conducted using similar operating parameters as those in [3]. Mapping of ion emission from the Extraction Region to the kinetic routine is not directly calculated. Experimental current values are used as input conditions into the kinetic routine via single cell injection at the emitter tip. The applied electric field condition within the EHD model is calibrated such that the integrated surface emission at the meniscus tip is of approximate order to the experimental current. Direct mapping of field emission from the EHD model within the Extraction Region to the kinetic model in the Plume Region is deferred to future work. A computational domain axial length of 0.1 μm and width of 0.1 μm is chosen for the Extraction Region, to emulate similar length scales of effective low paths within porous electrospray emitters. Meshes of the liquid and vacuum subdomains in the Extraction Region are shown in Fig. 3. A Taylor Cone angle of 49.29° is chosen for the emitter cone with a tip radius of 10 nm. Mesh elements at the emitter tip are refined in both subdomains to better resolve ion emission in this region. The computational domain of the Plume Region spans a radial distance of 500 μm and 1000 μm axially.

2.2.2 Electric Potentials

Electric potential distributions within the liquid and vacuum subdomains of the Extraction Region are presented in Fig. 4. A relatively linear progression is seen in the axial direction of both domains, with continuity between electric potentials at the interface. The potential within the liquid domain, Fig. 4a, can be seen enforced to zero where the fluid contacts the emitter electrode. A potential gradient tangential to the interface is also observed, suggesting a stronger electric field towards the meniscus center. This behavior is expected for a perturbed conductive fluid exposed to an external field, as the perturbation would result in a higher charge density at the tip and would result in a higher field strength. Continuity of electric potential across the liquid and vacuum domain interface is also observed. As the interfacial jump in electric displacement is innately enforced by the iteration scheme, all facets of the Laplace problem appear correctly represented within the semi-equilibrium potential distributions.

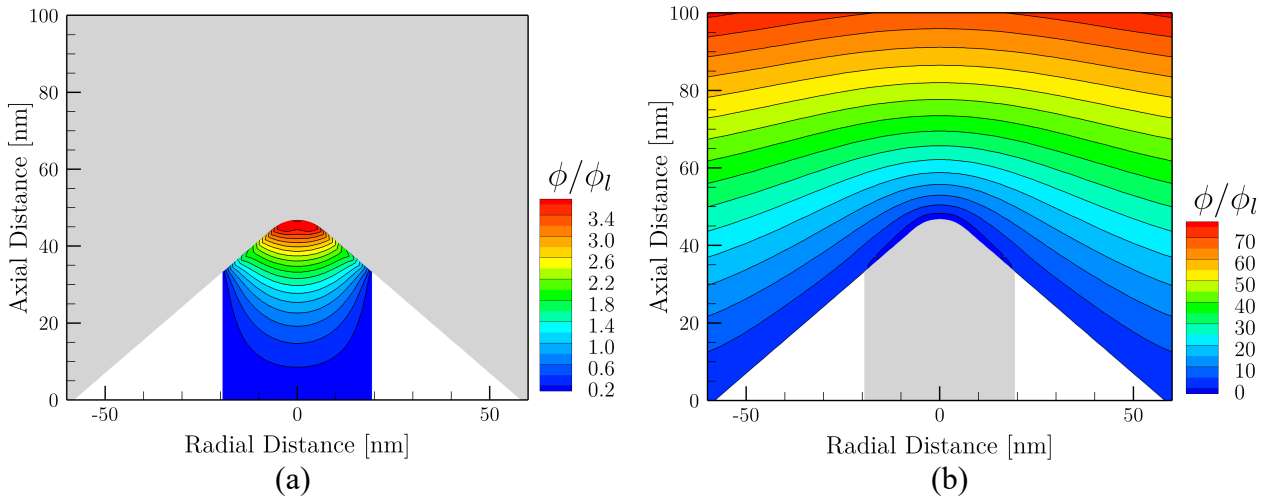


Figure 4. Electric potential distributions within the (a) liquid and (b) vacuum subdomains.

DISTRIBUTION A: Distribution approved for public release.

2.2.3 Stokes Flow and Ion Emission

Axial velocity contours within the liquid subdomain of the Extraction Region are presented in Fig. 5. Flow velocity of an ionic liquid meniscus operating in a purely ionic regime is known to scale with

$$v \sim \frac{I}{\pi\rho(q/m)(r^*)^2}, \tag{13}$$

where r^* is the characteristic length scale at the emitter tip and I is the emission current [4]. The Reynolds number scaling is then shown to be

$$Re \sim \frac{I}{\pi\mu(q/m)r^*} \sim 10^{-2}. \tag{14}$$

Using the single-emitter current for the -1562 V operational case ($I \approx 10^{-6}A$) in [3] and the fluid properties of EMI-BF_4 ($\mu \approx 10^{-2}$ Pa·s, $q/m \approx 10^6$ C/kg), the Reynolds number is shown to be significantly less than unity and thus Stokes flow is present. As mentioned, ion emission is only possible within a steady-state configuration if the normal fluid velocity at the intersection is nonzero. Field emission at the emitter tip is represented by arrows in the top-right plot of Fig. 5. It can be shown that the velocity at the emission tip is of approximate order to the emission velocity in the operational case, though it is important to note that the applied electric field, E_0, is adjusted in the Extraction Region to achieve this agreement.

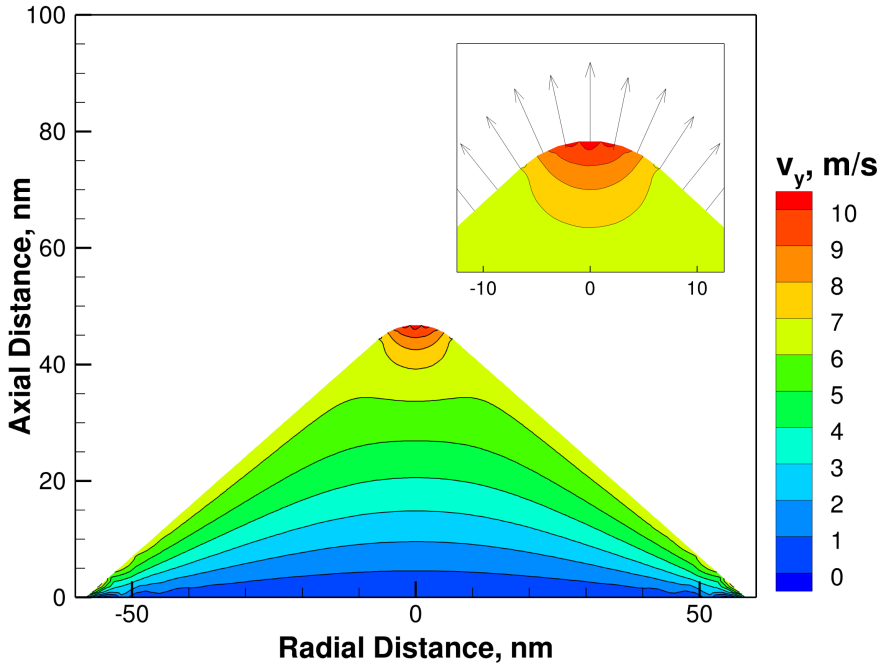


Figure 5. Axial velocity in the bulk fluid, with ion emission at the emitter tip shown in the inset.

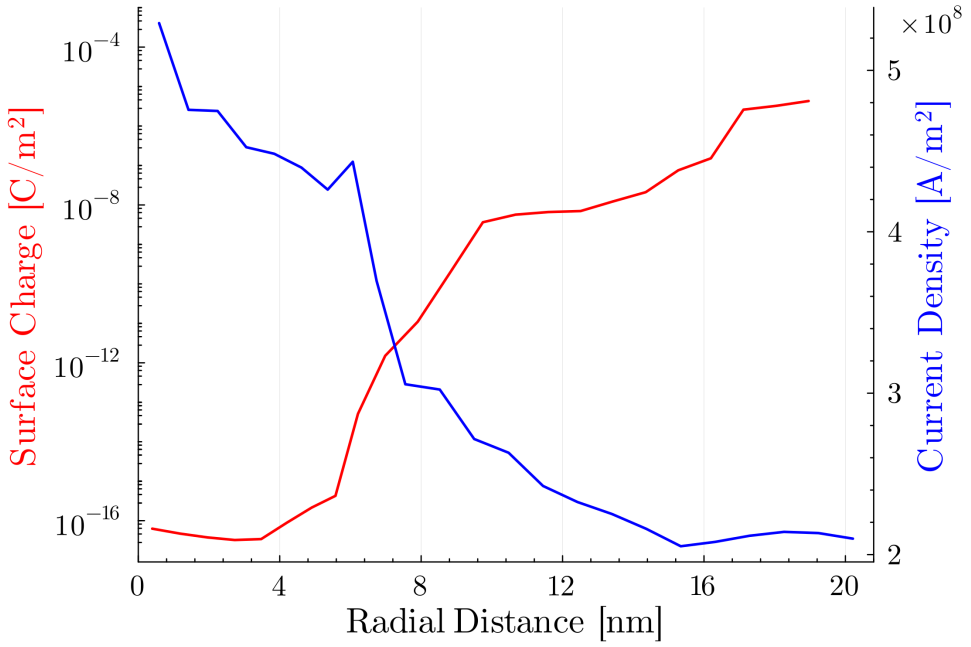


Figure 6. Interfacial surface charge and normal current density versus radial distance.

Characteristics of the Stokes problem can be observed through the interfacial current density, as it is linearly related to the normal fluid velocity at the meniscus. This current density in addition to the surface charge are plotted as a function of the radial distance in Fig. 6. As seen by the potential distribution, the emission centerline should correspond to the highest electric field, which in turn should result in the highest current density of emitted species. This is observed in Fig. 6, where the current density progressively declines with radial distance as the applied electric field weakens away from the centerline. The surface charge, on the other hand, appears to be inversely related to the current density with respect to radial distance. This is due to the continuity law of Eqn. (7), stating the surface charge represents the balance of current conducted to the interface and current evaporating from the interface. This balance is depicted in Fig. 6, where the surface charge is minimum at the interfacial locations corresponding to the highest ion emission, and vice versa. Additional quantitative validation of the EHD solver with occur once the interfacial perturbation scheme is implemented.

2.2.4 Plume Simulations

Independent simulations of the DSMC–PIC solver were conducted as well. As the coupling with the EHD meniscus solver has yet to be implemented, the simulations were initialized using experimental data of Natisin et al. [3]. Similarly, EMI-BF4 is chosen as the propellant. Within the simulation, the plume is assumed to consist of a 1:1 mixture of single-charged EMI^+ ions and EMI-BF4 neutrals. Ions colliding with any solid surfaces are reflected as neutral molecules. Emission current and thrust are calculated about the plane approximately 1000 μm away from the emitter base and are linearly scaled to match the experimental configuration where 576 emitters were operated in parallel. Within the plume, EMI^+ ion speeds (m/s) were calculated and are presented in Fig. 7, while comparisons of the numerical and measured values for emission current

and thrust are presented in Fig. 8. Agreement is shown between the numerical and experimental data across a range of extractor voltages, suggesting that downstream characteristics of the plume can be accurately simulated given sufficient initial conditions.

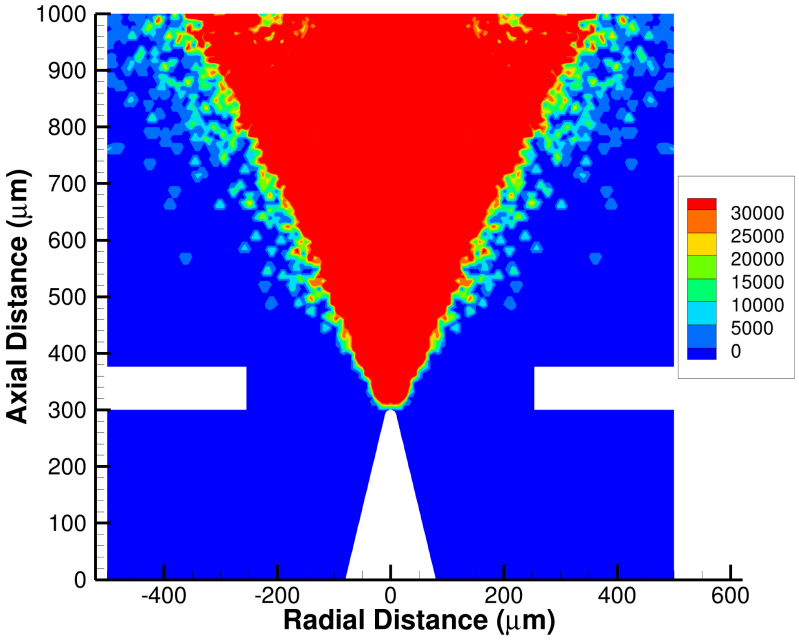


Figure 7. EMI+ ion speeds (m/s)

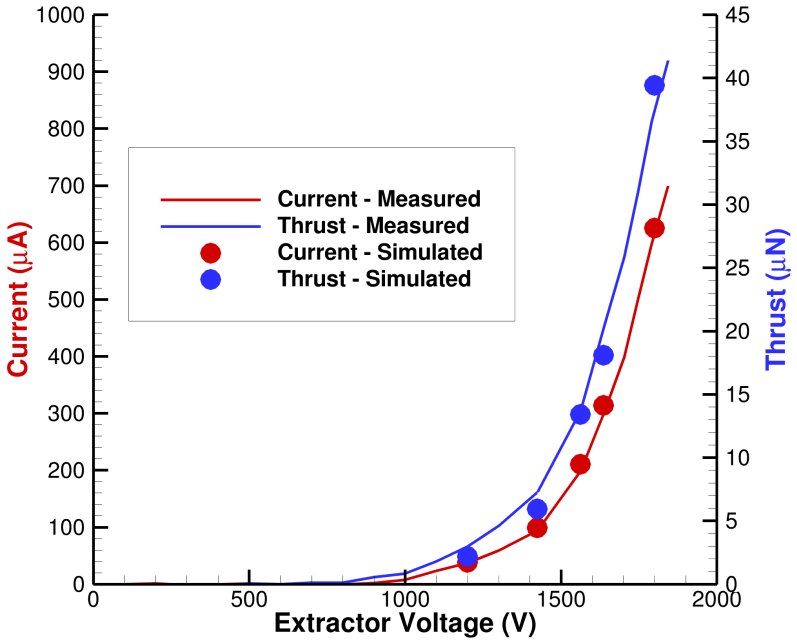


Figure 8. Comparison of emission current and thrust between experimental measurements by Natisin et al. [3] and DSMC–PIC simulation output.

3. Future Objectives

The majority of model development thus far has been within the Extraction Region. Implementing a normal stress balance routine at the interface, Eqn. (10), is the final module required for completion of the field emission model. This stress is a function of the surface tension, and thus the geometry of the meniscus. To complete this, a meniscus perturbation module must be developed that evolves the shape into one that satisfies equilibrium. Currently, the solver determines a nonequilibrium solution for a prescribed meniscus shape. With the addition of the meniscus perturbation module, the final equation of the field emission model is resolved, completing the Extraction Region component of the model. Development time for this module is estimated to take 1-2 months.

The kinetic model within the Plume Region is solved using an in-house direct simulation Monte-Carlo and particle-in-cell solver, and thus no core development is required. As such, the final task for the single emitter electrospray model is coupling the subscale routine in the Extraction Regime with the macroscale kinetic routine in the plume. To achieve a two-way coupling, the output of each submodel must be fed as boundary conditions to the other. Development time for this coupling module is estimated to take an additional month.

When the high-fidelity electrospray model is complete, its applications can be explored in parallel. First, the model must be benchmarked by comparing simulations with experimental measurements. Experimental measurements are nominally taken for electrosprays operating in arrays in the order of 100-1000, challenging validation of single emitter models as coupling effects cannot be accounted for. To overcome this, the Air Force Research Laboratory (AFRL) is conducting a Single Emitter Air Force Electrospray Thruster (SEAFET) program, providing data that can be directly used as validation for the single emitter model. The program has conducted a preliminary qualitative analysis of select emitters [5], with additional data to be made available in the coming months.

Further collaboration with the SEAFET program can allow exploration of the dependencies certain operating conditions have in life-limiting mechanisms. Once an initial benchmarking has been conducted, simulations spanning large parameter sweeps can be conducted to better quantify how perturbations in operations conditions such as geometry, voltage and material selection affect emission characteristics that directly contribute to failure modes. Experimental data could be taken for select configurations for calibration and further validation of the single emitter model. As the primary mechanism contributing to electrospray failure is emission impingement at the electrodes, exploring which facets of electrospray design and operation that directly contribute to overspraying at the grid will be the initial focus of the study.

The availability of both single emitter and multiplexed emitter data also allow for study of coupling effects within these systems. Experiments have demonstrated that emission characteristics of multiplexed arrays are not linear extrapolations of single emitter characteristics, alluding to possible inter-emitter dependencies. Once a single emitter model is validated, simulations can be configured to explore possible macroscopic effects that may occur from operating emitters in parallel. Again, these simulations may help elucidate what components of design and operation are contributing to this phenomenon by conducting parameter sweeps that are otherwise infeasible to perform experimentally. The results of which may then support select configurations of interest where experimentation can be conducted, optimizing the iterative routine towards building electrosprays whose mission capabilities vastly expand beyond those that are available today.

References

[1] C. Cai, "Theoretical and numerical studies of plume flows in vacuum chambers.," Ph.D. Dissertation, University of Michigan, Ann Arbor, 2005.

[2] A. Thuppul, P. L. Wright, A. L. Collins, J. K. Ziemer, and R. E. Wirz, "Lifetime Considerations for Electrospray Thrusters," *Aerospace*, vol. 7, no. 8, p. 108, Aug. 2020.

[3] M. Natisin, H. Zamora, W. McGehee, N. Arnold, Z. Holley, M. Holmes, and D. Eckhardt, "Fabrication and characterization of a fully conventionally machined, high-performance porous-media electrospray thruster," *Journal of Micromechanics and Microengineering*, vol. 30, no. 11, p. 115021, 2020.

[4] C. S. Coffman, "Electrically-assisted evaporation of charged fluids: Fundamental modeling and studies on ionic liquids," Ph.D. dissertation, Massachusetts Institute of Technology, 2016.

[5] W. A. McGehee, N. Arnold, M. R. Natisin, Z. A. Holley, and D. Eckhardt, "The single emitter air force electrospray thruster (SEAFET) Program: Goals and initial results," in *37th International Electric Propulsion Conference*, Massachusetts Institute of Technology, Cambridge, MA USA, Jun. 2022.

Final Technical Report

Prediction of Basic Operation of Electrospray Thrusters
Using High-Fidelity Modeling

AFOSR Grant FA9550-21-1-0045

Monitored by Mitat Birkan

Iain D. Boyd (PI), University of Colorado

Abstract

Electro-spray (ES) thrusters for in-space propulsion operate using ionic liquids that may be colloidal or metal as propellant. Individual ES devices generate very small thrust and impulse bits that are ideal for fine pointing missions. The Air Force has a more significant need for large-scale thrust levels required for station keeping, orbit raising, and orbit transfer. ES systems are of interest because they provide a specific impulse that may be tailored by the propellant, high thrust through the application of many devices in parallel, and all achieved at potentially high efficiencies of about 80%. There are significant fundamental challenges for the integration of the large numbers of devices needed for Air Force missions including: (1) failure modes of ES thrusters; (2) determining the lifetime of ES thrusters; and (3) understanding any crosstalk between adjacent thrusters. We are pursuing a comprehensive research project to address these gaps:

- Model Development: The key developments needed to model electro-spray systems are treatment of ionic-liquid physics, consideration of multiple emission sites, and extension to three dimensions.
- Model Benchmarking: Integration of high-fidelity modeling with empirical data is necessary to characterize life-limiting mechanisms and extrapolate performance in space environments. Direct comparisons will be made of model predictions with detailed plume measurements of AFRL porous-media flow emitters that are under way at the University of Michigan. Comparisons will also be made with all relevant data sets generated at the Air Force Research Laboratory in their current ES activities.
- Use the high-fidelity simulations to provide fundamental data needed for application of low-fidelity analysis of ES thrusters. For example, understanding the process and conditions for mode switching to the pure ionic regime is essential to meeting the USAF requirements for this technology.
- Analyses: Use the high-fidelity model for large arrays including assessment of coupling effects between multiple electro-spray emitters and prediction of primary failure modes.

This final report summarizes the progress made during the first and second years of the grant in terms of source and plume modeling.

DISTRIBUTION A: Distribution approved for public release.

1. Electrospray Model Description

A single porous electrospray emitter operating in a purely ionic emission regime is considered. The domain of interest spans from the emission site on the tip to the downstream plume between the extractor and accelerator electrodes. Computationally, this domain is partitioned into two two-dimensional subdomains: an Extraction Region where field emission from the electrohydrodynamic (EHD) meniscus is considered, and a Plume Region where the ion dynamics of the extracted species are considered. The Extraction Region is further decomposed into a vacuum and bulk liquid domain, Ω_{vac} and Ω_{liq} respectively, where Γ_{lv} denotes the intersection between them. A schematic of the global domain is presented in Fig. 1.

Within the bulk liquid, mass and momentum conservation are considered using the Navier-Stokes equations are the low Reynolds number limit, otherwise known as the Stokes equations,

$$\mu\nabla^2 v - \nabla \mathrm{p} = 0, \tag{1}$$
$$\nabla \cdot v = 0, \tag{2}$$

where μ is fluid viscosity, v is bulk fluid velocity, and p is pressure. Given the propellant is conductive, charge transport is considered as well. Convective charge transport is neglected and an Ohmic conduction model is chosen,

$$j = -K\nabla\phi_l, \tag{3}$$

where j is the current density, K is the electrical conductivity and ϕ_l is the electric potential in the bulk fluid. When charge conservation, $\nabla \cdot j = 0$, is considered with Eqn. (3) the electric potential can be shown to satisfy Laplace's equation,

$$\nabla^2\phi_l = 0. \tag{4}$$

Within the vacuum, space charge effects are negligible, and Laplace's equation is again used to determine the potential,

$$\nabla^2\phi_v = 0, \tag{5}$$

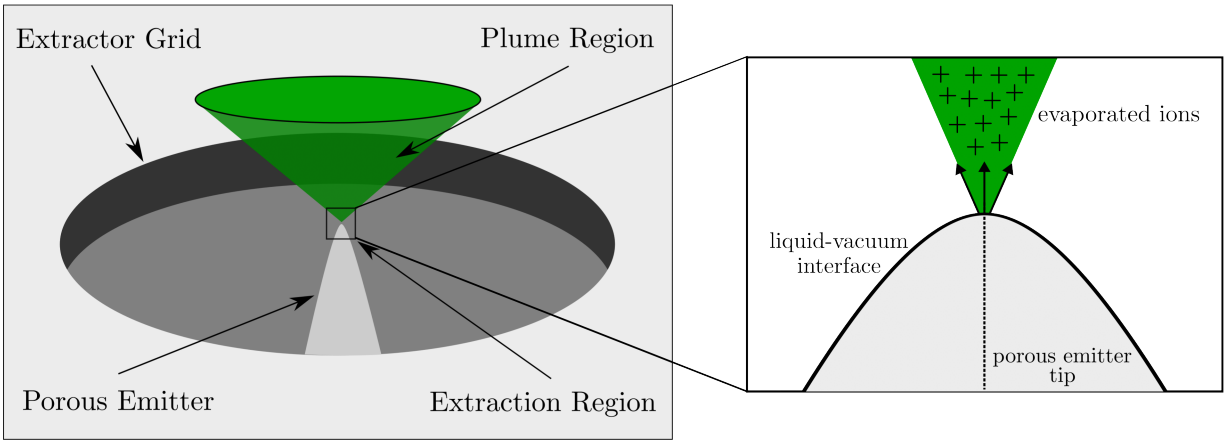


Figure 1. Domains of interest within a porous electrospray emitter.

DISTRIBUTION A: Distribution approved for public release.

where ϕ_v is the electric potential within the vacuum. At the liquid-vacuum interface, the free surface charge density is considered using the electrostatic condition,

$$(-\nabla\phi_v + \epsilon\nabla\phi_l)\cdot\hat{n} = \frac{\sigma}{\epsilon_0}, \tag{6}$$

where $\hat{n}$ is the unit vector normal to the interface, σ is the free surface charge density, ϵ is the relative permittivity, and ϵ_0 is the vacuum permittivity. Additionally, the free surface charge density satisfies the following steady-state transport equation,

$$v\cdot\nabla\sigma = \sigma\hat{n}\cdot\nabla v\cdot\hat{n} - K\nabla\phi_l\cdot\hat{n} - j\cdot\hat{n}. \tag{7}$$

Equation (7) states that the charge advected by the fluid flow is balanced by surface strain, the charge conducted to the surface, and the charge lost due to ion evaporation. Field emission of ions is described by the kinetic law,

$$j\cdot\hat{n} = \frac{k_b T}{h_c}\sigma\exp\left(\frac{-1}{k_b T}\left[\Delta G - \sqrt{\frac{\nabla\phi_v\cdot\hat{n}}{4\pi\epsilon_0/q^3}}\right]\right), \tag{8}$$

where k_b is the Boltzmann constant, h_c is the Planck constant, T is the temperature, q is the elementary charge and ΔG is the solvation energy of the ions. Additionally, force balance between the applied electric traction, viscous stresses, and surface tension is enforced at the liquid-vacuum interface,

$$\hat{t}\cdot(\tau_l - \tau_e)\cdot\hat{n} = 0, \tag{9}$$
$$\hat{n}\cdot(\tau_l - \tau_e)\cdot\hat{n} = -\gamma\nabla\cdot\hat{n}, \tag{10}$$

where $\hat{\boldsymbol{t}}$ is the unit vector tangent to the interface, τ_l is the viscous stress tensor, τ_e is the electrostatic Maxwell stress tensor, and γ is the surface tension. The normal and tangential projections of the Maxwell stress tensor on the interface satisfy the equations

$$\hat{t}\cdot\tau_e\cdot\hat{n} = -\sigma\nabla\phi_v\cdot\hat{t}, \tag{11}$$
$$\hat{n}\cdot\tau_e\cdot\hat{n} = \frac{1}{2}\epsilon_0((\nabla\phi_v\cdot\hat{n})^2 - \epsilon(\nabla\phi_l\cdot\hat{n})^2) + \frac{1}{2}\epsilon_0\big((\epsilon-1)(\nabla\phi_v\cdot\hat{t})^2\big). \tag{12}$$

A hybrid direct simulation Monte Carlo and particle-in-cell (DSMC–PIC) solver is implemented to simulate the downstream rarefied plume, of which a complete description of the solver can be found by Cai [1]. In summary, DSMC is a widely implemented particle method used to calculate collisional dynamics within dilute gases. Analogously for plasmas, PIC is a kinetic method used to simulate the dynamics of charged particles under the influence of external and self–induced electromagnetic fields. Simultaneous implementation of both methods within a

DISTRIBUTION A: Distribution approved for public release.

unified kinetic solver allows the study of gases characterized by both material and Coulombic interactions.

Within the multiscale model, the DSMC–PIC solver is used to initialize a distribution of charged macroparticles at the liquid–vacuum interface as well as simulate their motion within the computational vacuum domain. The initial distribution is a function of the ion number density determined by the EHD meniscus solver. The emission velocity is sampled from a biased Maxwellian based on the propellant temperature. From there, macroscopic plume properties that contribute to single emitter failure mechanisms can be calculated and simulations can be designed to study configurations that minimize these mechanisms. For example, the primary failure mode of electrosprays is overspray of propellant at the site of emission, resulting in impingement of the electrodes that ultimately contribute to shorting and power processing unit failure [2]. By conducting a sensitivity analysis, the proposed model may be able to elucidate what elements of the parameter space contribute most to the plume divergence angle, minimizing the probability of electrode impingement.

A complete schematic of the computational domain is presented in Fig. 2. Fig. 2a presents a macro-scale, two-dimensional domain of a single emitter tip below two extractor electrodes A voltage differential is applied between the emitter and electrodes to induce electric fields strengths on the order required for direct ion evaporation at the propellant free surface. Field emission at the interface is numerically treated within a separate sub-scale domain at the emitter apex and is coupled to the macro-scale domain via the Γ_{sub} intersection. Fig. 2b presents a sub-scale domain of an emission site at the emitter apex presented in Fig. 2a. Steady, open channel flow is assumed for the propellant in Ω_{liq}, where a fully developed velocity profile is imposed at the Γ_{inl} inlet boundary. Geometry of the EHD meniscus, Γ_{int}, is numerically perturbed to find configurations that satisfy mechanical equilibrium, a prerequisite to solve for steady-state emission characteristics.

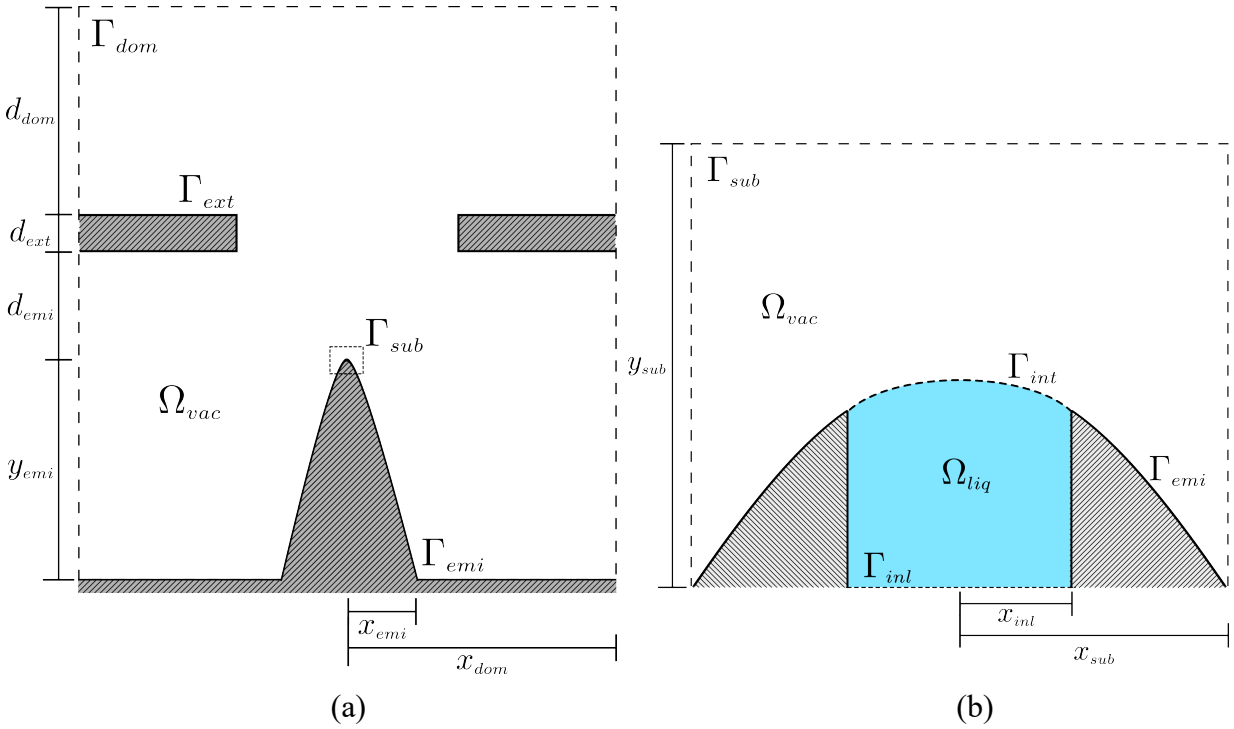


Figure 2. Computational domain.

DISTRIBUTION A: Distribution approved for public release.

2. Progress to Date

2.1 Numeric Implementation

The core developmental progress within the electrospray model has been within the Extraction Region. A finite element solver has been implemented using the Distributed and Unified Numerics Environment (DUNE), an open-source library for solving partial differential equations using grid-based methods. An algorithm has been developed that solves the coupled set of partial differential equations for a prescribed meniscus shape. The algorithm generally operates as follows:

The core Stokes and Laplace equations are solved in their respective domains. A multidomain module is configured to enforce boundary conditions that are dependent upon solutions across domains. An additional module is developed to enforce directionally dependent boundary conditions on the same interface. Consideration of electrostatic conditions, surface charge density transport, and stress balance at the free surface act as these unique multidomain boundary conditions. An iterative routine first solves the electric potential system until convergence, at which a global algorithm is implemented that solves the Stokes system and couples the domain together. A flowchart of this global algorithm is presented in Fig. 3. The result is a converged nonequilibrium solution for a prescribed meniscus shape. The current stage of development is expanding this to equilibrium solutions by including meniscus geometry perturbations in the global algorithm.

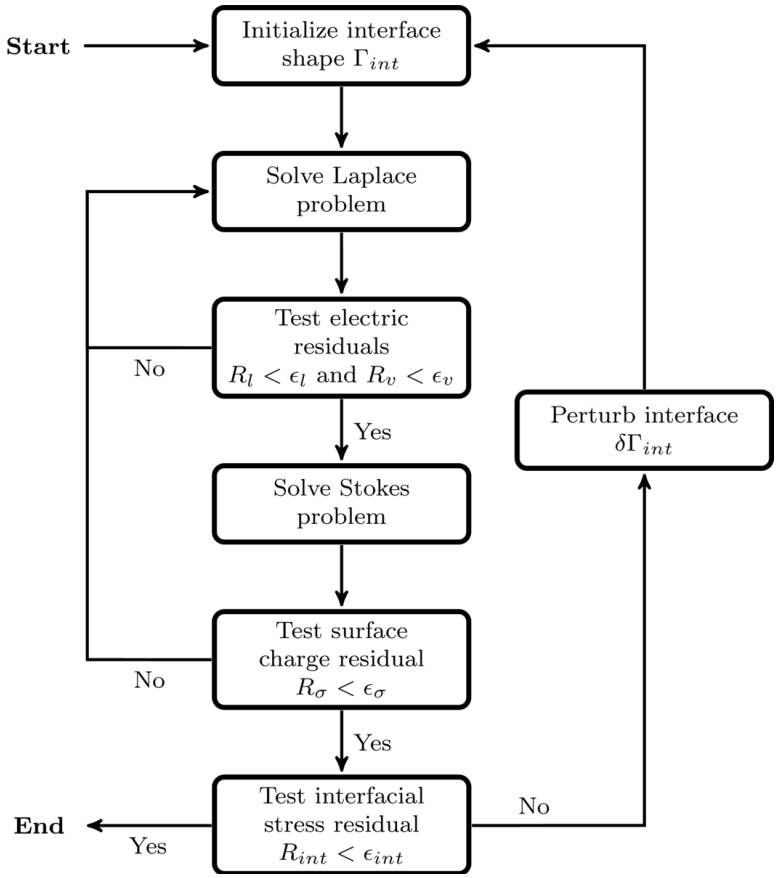


Figure 3. Algorithm to numerically solve for ion emission from the EHS meniscus within the Extraction Region.

DISTRIBUTION A: Distribution approved for public release.

2.2 Results

2.2.1 Simulation Parameters

Initial simulations within the Extraction and Plume region are conducted using similar operating parameters as those in [3]. Mapping of ion emission from the Extraction Region to the kinetic routine is not directly calculated. Experimental current values are used as input conditions into the kinetic routine via single cell injection at the emitter tip. The applied electric field condition within the EHD model is calibrated such that the integrated surface emission at the meniscus tip is of approximate order to the experimental current. Direct mapping of field emission from the EHD model within the Extraction Region to the kinetic model in the Plume Region is deferred to future work. A computational domain axial length of 0.1 μm and width of 0.1 μm is chosen for the Extraction Region, to emulate similar length scales of effective low paths within porous electrospray emitters. Meshes of the liquid and vacuum subdomains in the Extraction Region are shown in Fig. 3. A Taylor Cone angle of 49.29° is chosen for the emitter cone with a tip radius of 10 nm. Mesh elements at the emitter tip are refined in both subdomains to better resolve ion emission in this region. The computational domain of the Plume Region spans a radial distance of 500 μm and 1000 μm axially.

2.2.2 Electric Potentials

Electric potential distributions within the liquid and vacuum subdomains of the Extraction Region are presented in Fig. 4. A relatively linear progression is seen in the axial direction of both domains, with continuity between electric potentials at the interface. The potential within the liquid domain, Fig. 4a, can be seen enforced to zero where the fluid contacts the emitter electrode. A potential gradient tangential to the interface is also observed, suggesting a stronger electric field towards the meniscus center. This behavior is expected for a perturbed conductive fluid exposed to an external field, as the perturbation would result in a higher charge density at the tip and would result in a higher field strength. Continuity of electric potential across the liquid and vacuum domain interface is also observed. As the interfacial jump in electric displacement is innately enforced by the iteration scheme, all facets of the Laplace problem appear correctly represented within the semi-equilibrium potential distributions.

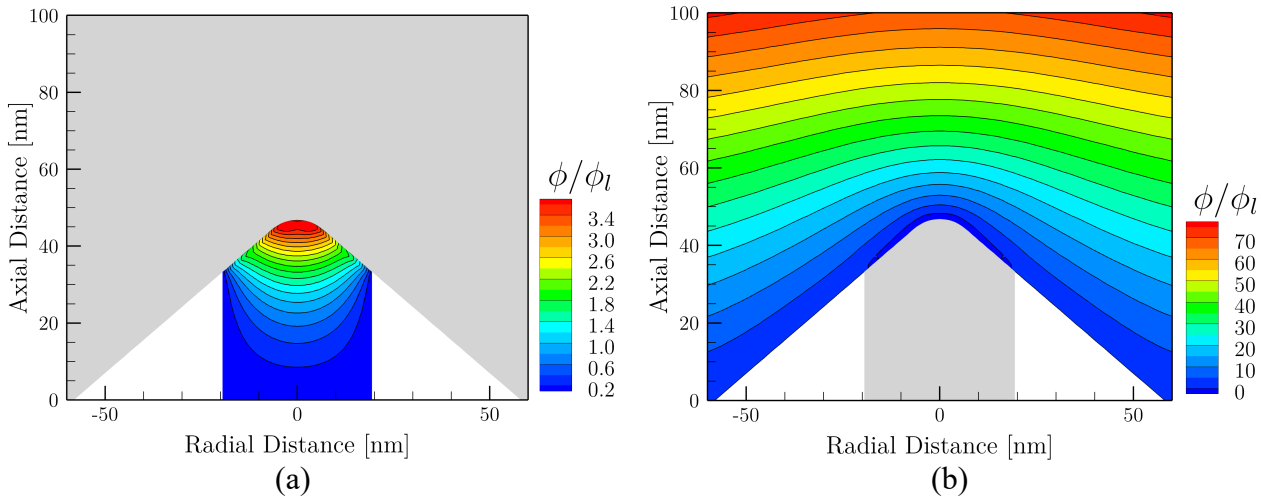


Figure 4. Electric potential distributions within the (a) liquid and (b) vacuum subdomains.

DISTRIBUTION A: Distribution approved for public release.

2.2.3 Stokes Flow and Ion Emission

Axial velocity contours within the liquid subdomain of the Extraction Region are presented in Fig. 5. Flow velocity of an ionic liquid meniscus operating in a purely ionic regime is known to scale with

$$v \sim \frac{I}{\pi\rho(q/m)(r^*)^2}, \tag{13}$$

where r^* is the characteristic length scale at the emitter tip and I is the emission current [4]. The Reynolds number scaling is then shown to be

$$Re \sim \frac{I}{\pi\mu(q/m)r^*} \sim 10^{-2}. \tag{14}$$

Using the single-emitter current for the -1562 V operational case ($I \approx 10^{-6}A$) in [3] and the fluid properties of EMI-BF_4 ($\mu \approx 10^{-2}$ Pa·s, $q/m \approx 10^6$ C/kg), the Reynolds number is shown to be significantly less than unity and thus Stokes flow is present. As mentioned, ion emission is only possible within a steady-state configuration if the normal fluid velocity at the intersection is nonzero. Field emission at the emitter tip is represented by arrows in the top-right plot of Fig. 5. It can be shown that the velocity at the emission tip is of approximate order to the emission velocity in the operational case, though it is important to note that the applied electric field, E_0, is adjusted in the Extraction Region to achieve this agreement.

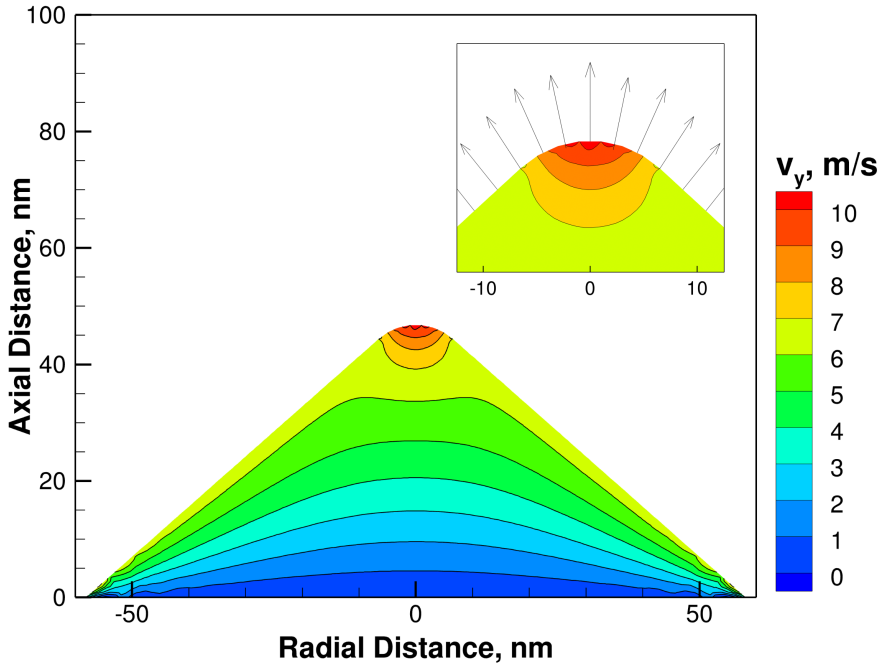


Figure 5. Axial velocity in the bulk fluid, with ion emission at the emitter tip shown in the inset.

DISTRIBUTION A: Distribution approved for public release.

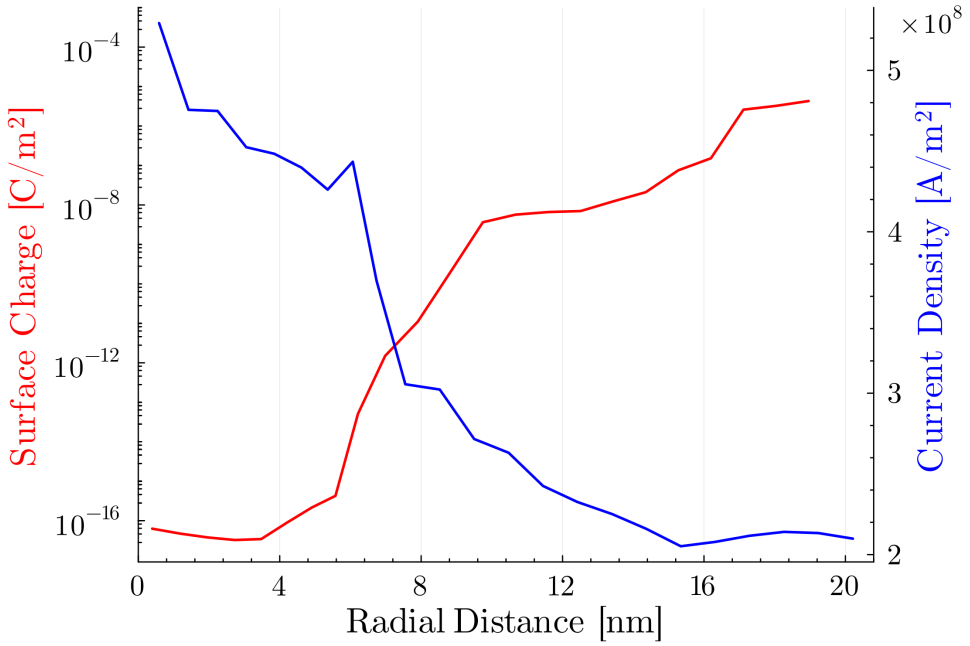


Figure 6. Interfacial surface charge and normal current density versus radial distance.

Characteristics of the Stokes problem can be observed through the interfacial current density, as it is linearly related to the normal fluid velocity at the meniscus. This current density in addition to the surface charge are plotted as a function of the radial distance in Fig. 6. As seen by the potential distribution, the emission centerline should correspond to the highest electric field, which in turn should result in the highest current density of emitted species. This is observed in Fig. 6, where the current density progressively declines with radial distance as the applied electric field weakens away from the centerline. The surface charge, on the other hand, appears to be inversely related to the current density with respect to radial distance. This is due to the continuity law of Eqn. (7), stating the surface charge represents the balance of current conducted to the interface and current evaporating from the interface. This balance is depicted in Fig. 6, where the surface charge is minimum at the interfacial locations corresponding to the highest ion emission, and vice versa. Additional quantitative validation of the EHD solver with occur once the interfacial perturbation scheme is implemented.

2.2.4 Plume Simulations

Independent simulations of the DSMC–PIC solver were conducted as well. As the coupling with the EHD meniscus solver has yet to be implemented, the simulations were initialized using experimental data of Natisin et al. [3]. Similarly, EMI-BF4 is chosen as the propellant. Within the simulation, the plume is assumed to consist of a 1:1 mixture of single-charged EMI^+ ions and EMI-BF4 neutrals. Ions colliding with any solid surfaces are reflected as neutral molecules. Emission current and thrust are calculated about the plane approximately 1000 μm away from the emitter base and are linearly scaled to match the experimental configuration where 576 emitters were operated in parallel. Within the plume, EMI^+ ion speeds (m/s) were calculated and are presented in Fig. 7, while comparisons of the numerical and measured values for emission current

and thrust are presented in Fig. 8. Agreement is shown between the numerical and experimental data across a range of extractor voltages, suggesting that downstream characteristics of the plume can be accurately simulated given sufficient initial conditions.

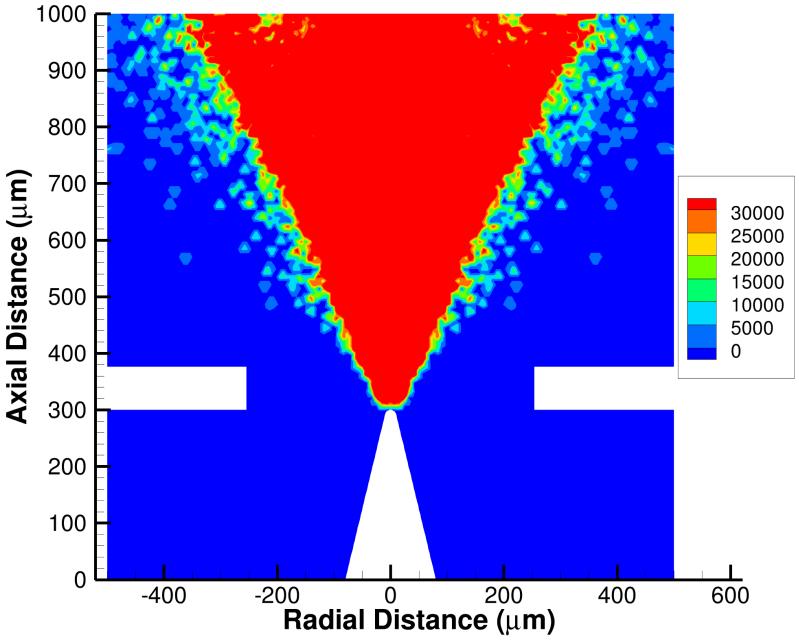


Figure 7. EMI+ ion speeds (m/s)

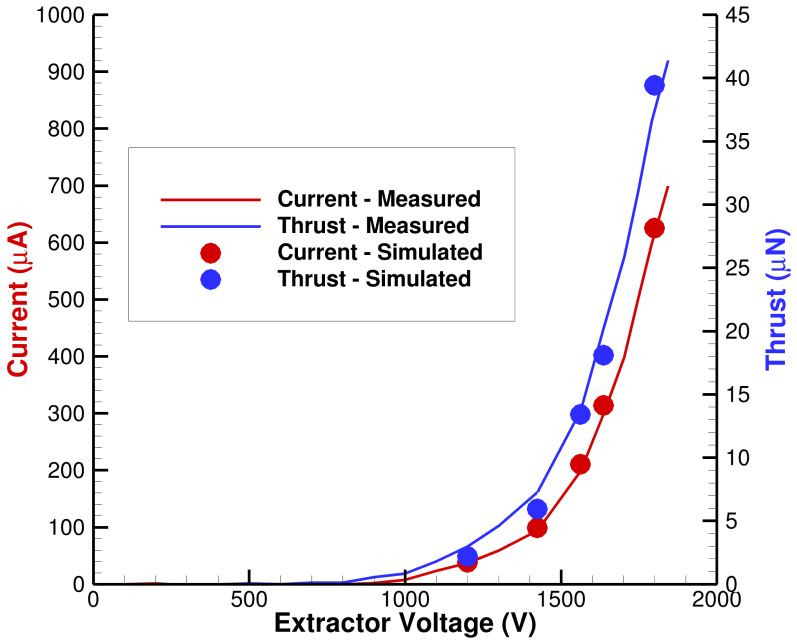


Figure 8. Comparison of emission current and thrust between experimental measurements by Natisin et al. [3] and DSMC–PIC simulation output.

3. Future Objectives

The majority of model development thus far has been within the Extraction Region. Implementing a normal stress balance routine at the interface, Eqn. (10), is the final module required for completion of the field emission model. This stress is a function of the surface tension, and thus the geometry of the meniscus. To complete this, a meniscus perturbation module must be developed that evolves the shape into one that satisfies equilibrium. Currently, the solver determines a nonequilibrium solution for a prescribed meniscus shape. With the addition of the meniscus perturbation module, the final equation of the field emission model is resolved, completing the Extraction Region component of the model. Development time for this module is estimated to take 1-2 months.

The kinetic model within the Plume Region is solved using an in-house direct simulation Monte-Carlo and particle-in-cell solver, and thus no core development is required. As such, the final task for the single emitter electrospray model is coupling the subscale routine in the Extraction Regime with the macroscale kinetic routine in the plume. To achieve a two-way coupling, the output of each submodel must be fed as boundary conditions to the other. Development time for this coupling module is estimated to take an additional month.

When the high-fidelity electrospray model is complete, its applications can be explored in parallel. First, the model must be benchmarked by comparing simulations with experimental measurements. Experimental measurements are nominally taken for electrosprays operating in arrays in the order of 100-1000, challenging validation of single emitter models as coupling effects cannot be accounted for. To overcome this, the Air Force Research Laboratory (AFRL) is conducting a Single Emitter Air Force Electrospray Thruster (SEAFET) program, providing data that can be directly used as validation for the single emitter model. The program has conducted a preliminary qualitative analysis of select emitters [5], with additional data to be made available in the coming months.

Further collaboration with the SEAFET program can allow exploration of the dependencies certain operating conditions have in life-limiting mechanisms. Once an initial benchmarking has been conducted, simulations spanning large parameter sweeps can be conducted to better quantify how perturbations in operations conditions such as geometry, voltage and material selection affect emission characteristics that directly contribute to failure modes. Experimental data could be taken for select configurations for calibration and further validation of the single emitter model. As the primary mechanism contributing to electrospray failure is emission impingement at the electrodes, exploring which facets of electrospray design and operation that directly contribute to overspraying at the grid will be the initial focus of the study.

The availability of both single emitter and multiplexed emitter data also allow for study of coupling effects within these systems. Experiments have demonstrated that emission characteristics of multiplexed arrays are not linear extrapolations of single emitter characteristics, alluding to possible inter-emitter dependencies. Once a single emitter model is validated, simulations can be configured to explore possible macroscopic effects that may occur from operating emitters in parallel. Again, these simulations may help elucidate what components of design and operation are contributing to this phenomenon by conducting parameter sweeps that are otherwise infeasible to perform experimentally. The results of which may then support select configurations of interest where experimentation can be conducted, optimizing the iterative routine towards building electrosprays whose mission capabilities vastly expand beyond those that are available today.

References

[1] C. Cai, "Theoretical and numerical studies of plume flows in vacuum chambers.," Ph.D. Dissertation, University of Michigan, Ann Arbor, 2005.

[2] A. Thuppul, P. L. Wright, A. L. Collins, J. K. Ziemer, and R. E. Wirz, "Lifetime Considerations for Electrospray Thrusters," *Aerospace*, vol. 7, no. 8, p. 108, Aug. 2020.

[3] M. Natisin, H. Zamora, W. McGehee, N. Arnold, Z. Holley, M. Holmes, and D. Eckhardt, "Fabrication and characterization of a fully conventionally machined, high-performance porous-media electrospray thruster," *Journal of Micromechanics and Microengineering*, vol. 30, no. 11, p. 115021, 2020.

[4] C. S. Coffman, "Electrically-assisted evaporation of charged fluids: Fundamental modeling and studies on ionic liquids," Ph.D. dissertation, Massachusetts Institute of Technology, 2016.

[5] W. A. McGehee, N. Arnold, M. R. Natisin, Z. A. Holley, and D. Eckhardt, "The single emitter air force electrospray thruster (SEAFET) Program: Goals and initial results," in *37th International Electric Propulsion Conference*, Massachusetts Institute of Technology, Cambridge, MA USA, Jun. 2022.

Final Technical Report

Prediction of Basic Operation of Electrospray Thrusters
Using High-Fidelity Modeling

AFOSR Grant FA9550-21-1-0045

Monitored by Mitat Birkan

Iain D. Boyd (PI), University of Colorado

Abstract

Electro-spray (ES) thrusters for in-space propulsion operate using ionic liquids that may be colloidal or metal as propellant. Individual ES devices generate very small thrust and impulse bits that are ideal for fine pointing missions. The Air Force has a more significant need for large-scale thrust levels required for station keeping, orbit raising, and orbit transfer. ES systems are of interest because they provide a specific impulse that may be tailored by the propellant, high thrust through the application of many devices in parallel, and all achieved at potentially high efficiencies of about 80%. There are significant fundamental challenges for the integration of the large numbers of devices needed for Air Force missions including: (1) failure modes of ES thrusters; (2) determining the lifetime of ES thrusters; and (3) understanding any crosstalk between adjacent thrusters. We are pursuing a comprehensive research project to address these gaps:

- Model Development: The key developments needed to model electro-spray systems are treatment of ionic-liquid physics, consideration of multiple emission sites, and extension to three dimensions.
- Model Benchmarking: Integration of high-fidelity modeling with empirical data is necessary to characterize life-limiting mechanisms and extrapolate performance in space environments. Direct comparisons will be made of model predictions with detailed plume measurements of AFRL porous-media flow emitters that are under way at the University of Michigan. Comparisons will also be made with all relevant data sets generated at the Air Force Research Laboratory in their current ES activities.
- Use the high-fidelity simulations to provide fundamental data needed for application of low-fidelity analysis of ES thrusters. For example, understanding the process and conditions for mode switching to the pure ionic regime is essential to meeting the USAF requirements for this technology.
- Analyses: Use the high-fidelity model for large arrays including assessment of coupling effects between multiple electro-spray emitters and prediction of primary failure modes.

This final report summarizes the progress made during the first and second years of the grant in terms of source and plume modeling.

DISTRIBUTION A: Distribution approved for public release.

1. Electrospray Model Description

A single porous electrospray emitter operating in a purely ionic emission regime is considered. The domain of interest spans from the emission site on the tip to the downstream plume between the extractor and accelerator electrodes. Computationally, this domain is partitioned into two two-dimensional subdomains: an Extraction Region where field emission from the electrohydrodynamic (EHD) meniscus is considered, and a Plume Region where the ion dynamics of the extracted species are considered. The Extraction Region is further decomposed into a vacuum and bulk liquid domain, Ω_{vac} and Ω_{liq} respectively, where Γ_{lv} denotes the intersection between them. A schematic of the global domain is presented in Fig. 1.

Within the bulk liquid, mass and momentum conservation are considered using the Navier-Stokes equations are the low Reynolds number limit, otherwise known as the Stokes equations,

$$\mu\nabla^2 v - \nabla \mathrm{p} = 0, \tag{1}$$
$$\nabla \cdot v = 0, \tag{2}$$

where μ is fluid viscosity, v is bulk fluid velocity, and p is pressure. Given the propellant is conductive, charge transport is considered as well. Convective charge transport is neglected and an Ohmic conduction model is chosen,

$$j = -K\nabla\phi_l, \tag{3}$$

where j is the current density, K is the electrical conductivity and ϕ_l is the electric potential in the bulk fluid. When charge conservation, $\nabla \cdot j = 0$, is considered with Eqn. (3) the electric potential can be shown to satisfy Laplace's equation,

$$\nabla^2\phi_l = 0. \tag{4}$$

Within the vacuum, space charge effects are negligible, and Laplace's equation is again used to determine the potential,

$$\nabla^2\phi_v = 0, \tag{5}$$

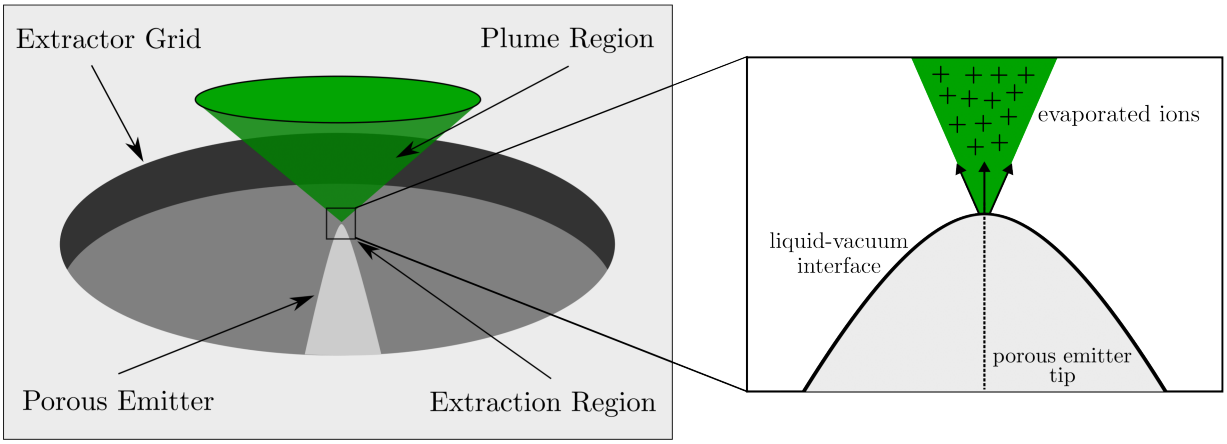


Figure 1. Domains of interest within a porous electrospray emitter.

DISTRIBUTION A: Distribution approved for public release.

where ϕ_v is the electric potential within the vacuum. At the liquid-vacuum interface, the free surface charge density is considered using the electrostatic condition,

$$(-\nabla\phi_v + \epsilon\nabla\phi_l)\cdot\hat{n} = \frac{\sigma}{\epsilon_0}, \tag{6}$$

where $\hat{n}$ is the unit vector normal to the interface, σ is the free surface charge density, ϵ is the relative permittivity, and ϵ_0 is the vacuum permittivity. Additionally, the free surface charge density satisfies the following steady-state transport equation,

$$v\cdot\nabla\sigma = \sigma\hat{n}\cdot\nabla v\cdot\hat{n} - K\nabla\phi_l\cdot\hat{n} - j\cdot\hat{n}. \tag{7}$$

Equation (7) states that the charge advected by the fluid flow is balanced by surface strain, the charge conducted to the surface, and the charge lost due to ion evaporation. Field emission of ions is described by the kinetic law,

$$j\cdot\hat{n} = \frac{k_b T}{h_c}\sigma\exp\left(\frac{-1}{k_b T}\left[\Delta G - \sqrt{\frac{\nabla\phi_v\cdot\hat{n}}{4\pi\epsilon_0/q^3}}\right]\right), \tag{8}$$

where k_b is the Boltzmann constant, h_c is the Planck constant, T is the temperature, q is the elementary charge and ΔG is the solvation energy of the ions. Additionally, force balance between the applied electric traction, viscous stresses, and surface tension is enforced at the liquid-vacuum interface,

$$\hat{t}\cdot(\tau_l - \tau_e)\cdot\hat{n} = 0, \tag{9}$$
$$\hat{n}\cdot(\tau_l - \tau_e)\cdot\hat{n} = -\gamma\nabla\cdot\hat{n}, \tag{10}$$

where $\hat{\boldsymbol{t}}$ is the unit vector tangent to the interface, τ_l is the viscous stress tensor, τ_e is the electrostatic Maxwell stress tensor, and γ is the surface tension. The normal and tangential projections of the Maxwell stress tensor on the interface satisfy the equations

$$\hat{t}\cdot\tau_e\cdot\hat{n} = -\sigma\nabla\phi_v\cdot\hat{t}, \tag{11}$$
$$\hat{n}\cdot\tau_e\cdot\hat{n} = \frac{1}{2}\epsilon_0((\nabla\phi_v\cdot\hat{n})^2 - \epsilon(\nabla\phi_l\cdot\hat{n})^2) + \frac{1}{2}\epsilon_0\big((\epsilon-1)(\nabla\phi_v\cdot\hat{t})^2\big). \tag{12}$$

A hybrid direct simulation Monte Carlo and particle-in-cell (DSMC–PIC) solver is implemented to simulate the downstream rarefied plume, of which a complete description of the solver can be found by Cai [1]. In summary, DSMC is a widely implemented particle method used to calculate collisional dynamics within dilute gases. Analogously for plasmas, PIC is a kinetic method used to simulate the dynamics of charged particles under the influence of external and self–induced electromagnetic fields. Simultaneous implementation of both methods within a

DISTRIBUTION A: Distribution approved for public release.

unified kinetic solver allows the study of gases characterized by both material and Coulombic interactions.

Within the multiscale model, the DSMC–PIC solver is used to initialize a distribution of charged macroparticles at the liquid–vacuum interface as well as simulate their motion within the computational vacuum domain. The initial distribution is a function of the ion number density determined by the EHD meniscus solver. The emission velocity is sampled from a biased Maxwellian based on the propellant temperature. From there, macroscopic plume properties that contribute to single emitter failure mechanisms can be calculated and simulations can be designed to study configurations that minimize these mechanisms. For example, the primary failure mode of electrosprays is overspray of propellant at the site of emission, resulting in impingement of the electrodes that ultimately contribute to shorting and power processing unit failure [2]. By conducting a sensitivity analysis, the proposed model may be able to elucidate what elements of the parameter space contribute most to the plume divergence angle, minimizing the probability of electrode impingement.

A complete schematic of the computational domain is presented in Fig. 2. Fig. 2a presents a macro-scale, two-dimensional domain of a single emitter tip below two extractor electrodes A voltage differential is applied between the emitter and electrodes to induce electric fields strengths on the order required for direct ion evaporation at the propellant free surface. Field emission at the interface is numerically treated within a separate sub-scale domain at the emitter apex and is coupled to the macro-scale domain via the Γ_{sub} intersection. Fig. 2b presents a sub-scale domain of an emission site at the emitter apex presented in Fig. 2a. Steady, open channel flow is assumed for the propellant in Ω_{liq}, where a fully developed velocity profile is imposed at the Γ_{inl} inlet boundary. Geometry of the EHD meniscus, Γ_{int}, is numerically perturbed to find configurations that satisfy mechanical equilibrium, a prerequisite to solve for steady-state emission characteristics.

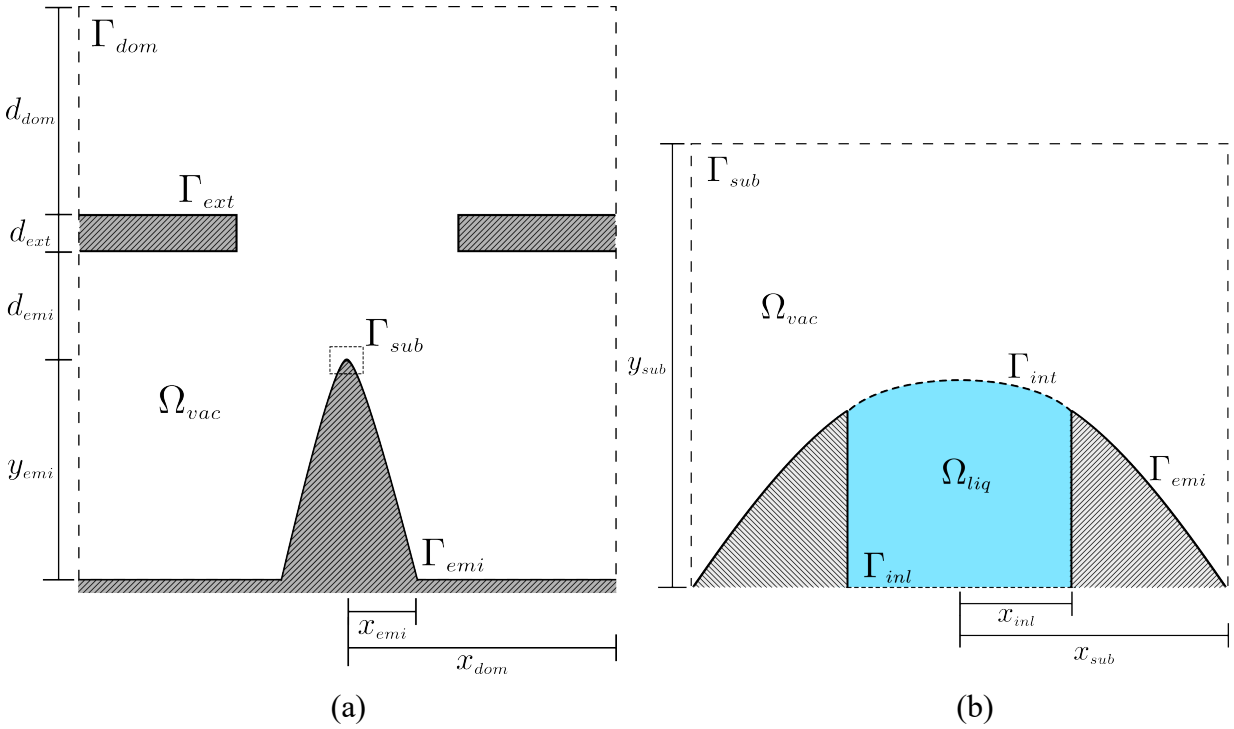


Figure 2. Computational domain.

DISTRIBUTION A: Distribution approved for public release.

2. Progress to Date

2.1 Numeric Implementation

The core developmental progress within the electrospray model has been within the Extraction Region. A finite element solver has been implemented using the Distributed and Unified Numerics Environment (DUNE), an open-source library for solving partial differential equations using grid-based methods. An algorithm has been developed that solves the coupled set of partial differential equations for a prescribed meniscus shape. The algorithm generally operates as follows:

The core Stokes and Laplace equations are solved in their respective domains. A multidomain module is configured to enforce boundary conditions that are dependent upon solutions across domains. An additional module is developed to enforce directionally dependent boundary conditions on the same interface. Consideration of electrostatic conditions, surface charge density transport, and stress balance at the free surface act as these unique multidomain boundary conditions. An iterative routine first solves the electric potential system until convergence, at which a global algorithm is implemented that solves the Stokes system and couples the domain together. A flowchart of this global algorithm is presented in Fig. 3. The result is a converged nonequilibrium solution for a prescribed meniscus shape. The current stage of development is expanding this to equilibrium solutions by including meniscus geometry perturbations in the global algorithm.

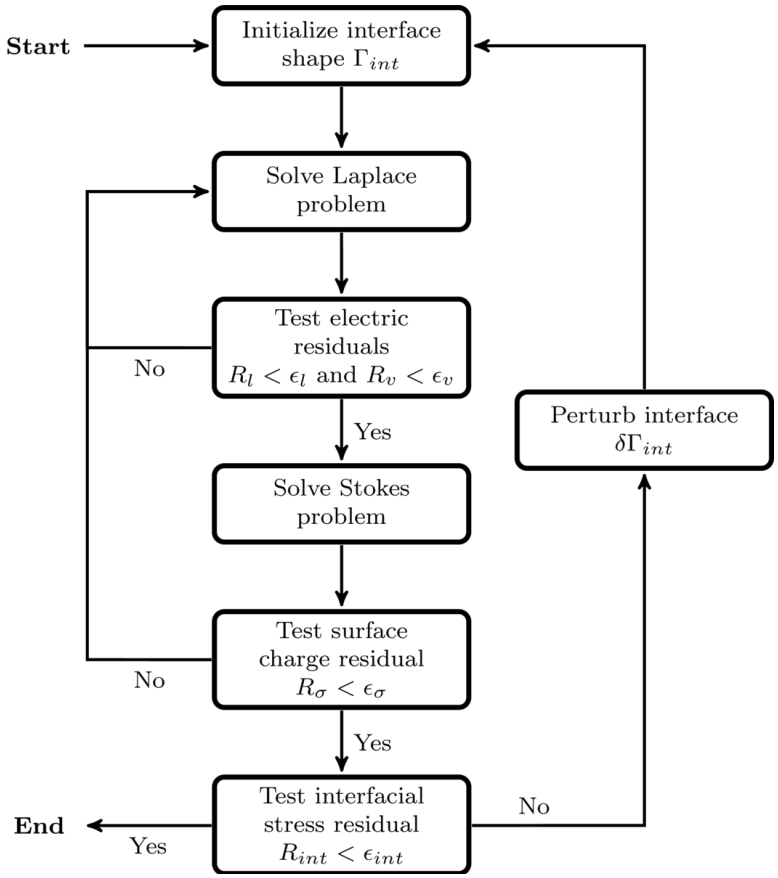


Figure 3. Algorithm to numerically solve for ion emission from the EHS meniscus within the Extraction Region.

DISTRIBUTION A: Distribution approved for public release.

2.2 Results

2.2.1 Simulation Parameters

Initial simulations within the Extraction and Plume region are conducted using similar operating parameters as those in [3]. Mapping of ion emission from the Extraction Region to the kinetic routine is not directly calculated. Experimental current values are used as input conditions into the kinetic routine via single cell injection at the emitter tip. The applied electric field condition within the EHD model is calibrated such that the integrated surface emission at the meniscus tip is of approximate order to the experimental current. Direct mapping of field emission from the EHD model within the Extraction Region to the kinetic model in the Plume Region is deferred to future work. A computational domain axial length of 0.1 μm and width of 0.1 μm is chosen for the Extraction Region, to emulate similar length scales of effective low paths within porous electrospray emitters. Meshes of the liquid and vacuum subdomains in the Extraction Region are shown in Fig. 3. A Taylor Cone angle of 49.29° is chosen for the emitter cone with a tip radius of 10 nm. Mesh elements at the emitter tip are refined in both subdomains to better resolve ion emission in this region. The computational domain of the Plume Region spans a radial distance of 500 μm and 1000 μm axially.

2.2.2 Electric Potentials

Electric potential distributions within the liquid and vacuum subdomains of the Extraction Region are presented in Fig. 4. A relatively linear progression is seen in the axial direction of both domains, with continuity between electric potentials at the interface. The potential within the liquid domain, Fig. 4a, can be seen enforced to zero where the fluid contacts the emitter electrode. A potential gradient tangential to the interface is also observed, suggesting a stronger electric field towards the meniscus center. This behavior is expected for a perturbed conductive fluid exposed to an external field, as the perturbation would result in a higher charge density at the tip and would result in a higher field strength. Continuity of electric potential across the liquid and vacuum domain interface is also observed. As the interfacial jump in electric displacement is innately enforced by the iteration scheme, all facets of the Laplace problem appear correctly represented within the semi-equilibrium potential distributions.

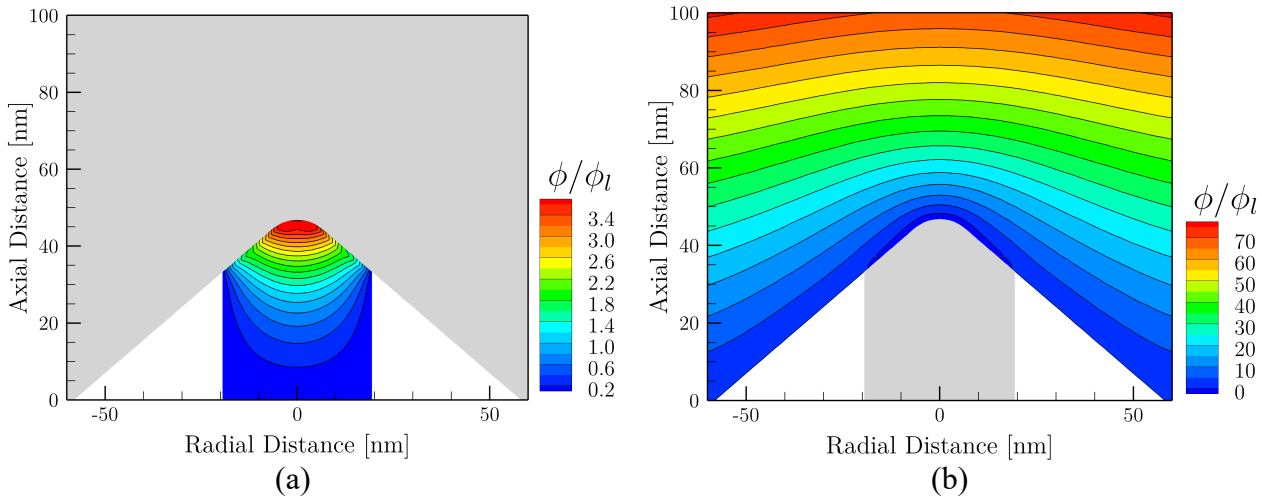


Figure 4. Electric potential distributions within the (a) liquid and (b) vacuum subdomains.

DISTRIBUTION A: Distribution approved for public release.

2.2.3 Stokes Flow and Ion Emission

Axial velocity contours within the liquid subdomain of the Extraction Region are presented in Fig. 5. Flow velocity of an ionic liquid meniscus operating in a purely ionic regime is known to scale with

$$v \sim \frac{I}{\pi\rho(q/m)(r^*)^2}, \tag{13}$$

where r^* is the characteristic length scale at the emitter tip and I is the emission current [4]. The Reynolds number scaling is then shown to be

$$Re \sim \frac{I}{\pi\mu(q/m)r^*} \sim 10^{-2}. \tag{14}$$

Using the single-emitter current for the -1562 V operational case ($I \approx 10^{-6}A$) in [3] and the fluid properties of EMI-BF_4 ($\mu \approx 10^{-2}$ Pa·s, $q/m \approx 10^6$ C/kg), the Reynolds number is shown to be significantly less than unity and thus Stokes flow is present. As mentioned, ion emission is only possible within a steady-state configuration if the normal fluid velocity at the intersection is nonzero. Field emission at the emitter tip is represented by arrows in the top-right plot of Fig. 5. It can be shown that the velocity at the emission tip is of approximate order to the emission velocity in the operational case, though it is important to note that the applied electric field, E_0, is adjusted in the Extraction Region to achieve this agreement.

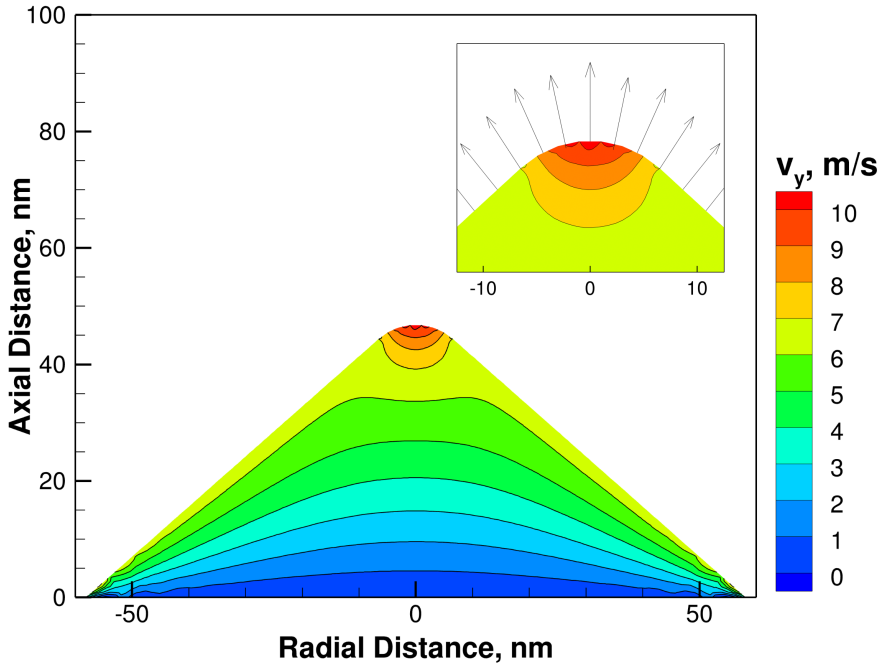


Figure 5. Axial velocity in the bulk fluid, with ion emission at the emitter tip shown in the inset.

DISTRIBUTION A: Distribution approved for public release.

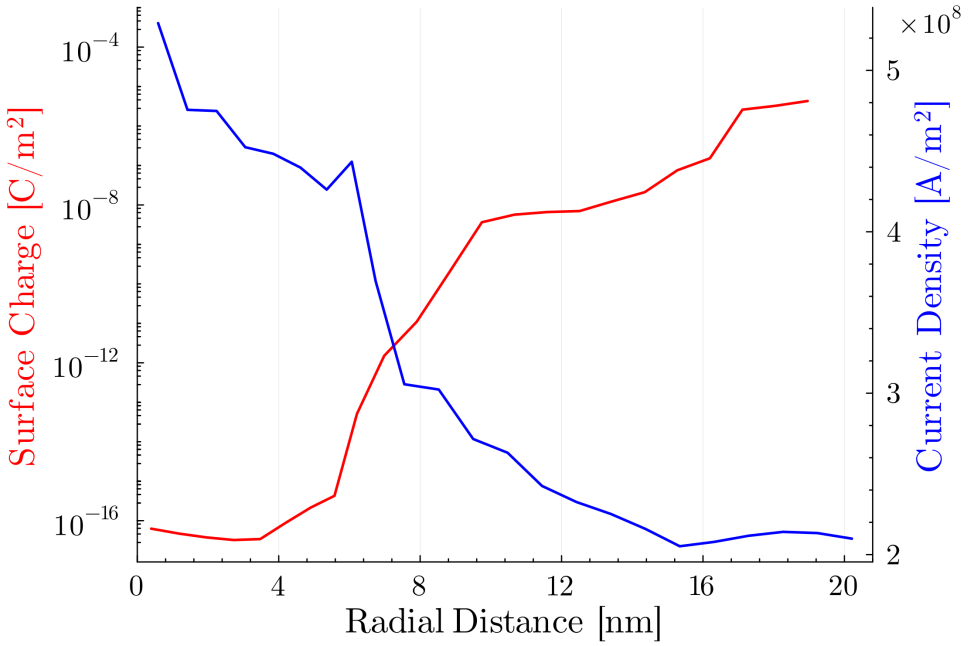


Figure 6. Interfacial surface charge and normal current density versus radial distance.

Characteristics of the Stokes problem can be observed through the interfacial current density, as it is linearly related to the normal fluid velocity at the meniscus. This current density in addition to the surface charge are plotted as a function of the radial distance in Fig. 6. As seen by the potential distribution, the emission centerline should correspond to the highest electric field, which in turn should result in the highest current density of emitted species. This is observed in Fig. 6, where the current density progressively declines with radial distance as the applied electric field weakens away from the centerline. The surface charge, on the other hand, appears to be inversely related to the current density with respect to radial distance. This is due to the continuity law of Eqn. (7), stating the surface charge represents the balance of current conducted to the interface and current evaporating from the interface. This balance is depicted in Fig. 6, where the surface charge is minimum at the interfacial locations corresponding to the highest ion emission, and vice versa. Additional quantitative validation of the EHD solver with occur once the interfacial perturbation scheme is implemented.

2.2.4 Plume Simulations

Independent simulations of the DSMC–PIC solver were conducted as well. As the coupling with the EHD meniscus solver has yet to be implemented, the simulations were initialized using experimental data of Natisin et al. [3]. Similarly, EMI-BF4 is chosen as the propellant. Within the simulation, the plume is assumed to consist of a 1:1 mixture of single-charged EMI^+ ions and EMI-BF4 neutrals. Ions colliding with any solid surfaces are reflected as neutral molecules. Emission current and thrust are calculated about the plane approximately 1000 μm away from the emitter base and are linearly scaled to match the experimental configuration where 576 emitters were operated in parallel. Within the plume, EMI^+ ion speeds (m/s) were calculated and are presented in Fig. 7, while comparisons of the numerical and measured values for emission current

DISTRIBUTION A: Distribution approved for public release.

and thrust are presented in Fig. 8. Agreement is shown between the numerical and experimental data across a range of extractor voltages, suggesting that downstream characteristics of the plume can be accurately simulated given sufficient initial conditions.

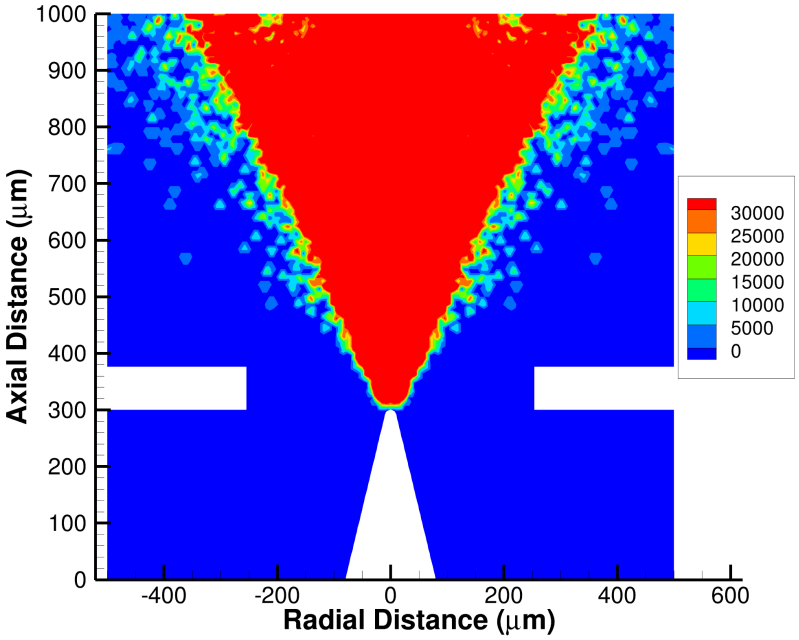


Figure 7. EMI+ ion speeds (m/s)

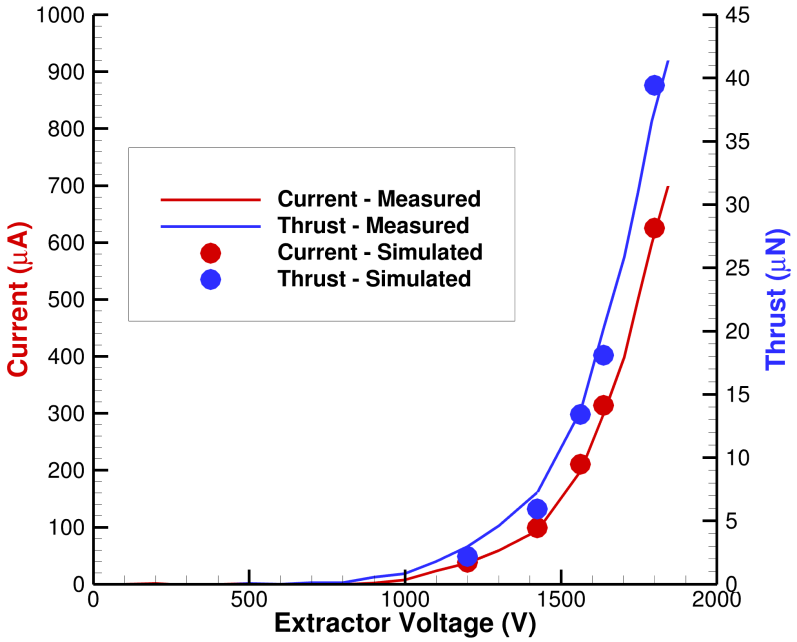


Figure 8. Comparison of emission current and thrust between experimental measurements by Natisin et al. [3] and DSMC–PIC simulation output.

3. Future Objectives

The majority of model development thus far has been within the Extraction Region. Implementing a normal stress balance routine at the interface, Eqn. (10), is the final module required for completion of the field emission model. This stress is a function of the surface tension, and thus the geometry of the meniscus. To complete this, a meniscus perturbation module must be developed that evolves the shape into one that satisfies equilibrium. Currently, the solver determines a nonequilibrium solution for a prescribed meniscus shape. With the addition of the meniscus perturbation module, the final equation of the field emission model is resolved, completing the Extraction Region component of the model. Development time for this module is estimated to take 1-2 months.

The kinetic model within the Plume Region is solved using an in-house direct simulation Monte-Carlo and particle-in-cell solver, and thus no core development is required. As such, the final task for the single emitter electrospray model is coupling the subscale routine in the Extraction Regime with the macroscale kinetic routine in the plume. To achieve a two-way coupling, the output of each submodel must be fed as boundary conditions to the other. Development time for this coupling module is estimated to take an additional month.

When the high-fidelity electrospray model is complete, its applications can be explored in parallel. First, the model must be benchmarked by comparing simulations with experimental measurements. Experimental measurements are nominally taken for electrosprays operating in arrays in the order of 100-1000, challenging validation of single emitter models as coupling effects cannot be accounted for. To overcome this, the Air Force Research Laboratory (AFRL) is conducting a Single Emitter Air Force Electrospray Thruster (SEAFET) program, providing data that can be directly used as validation for the single emitter model. The program has conducted a preliminary qualitative analysis of select emitters [5], with additional data to be made available in the coming months.

Further collaboration with the SEAFET program can allow exploration of the dependencies certain operating conditions have in life-limiting mechanisms. Once an initial benchmarking has been conducted, simulations spanning large parameter sweeps can be conducted to better quantify how perturbations in operations conditions such as geometry, voltage and material selection affect emission characteristics that directly contribute to failure modes. Experimental data could be taken for select configurations for calibration and further validation of the single emitter model. As the primary mechanism contributing to electrospray failure is emission impingement at the electrodes, exploring which facets of electrospray design and operation that directly contribute to overspraying at the grid will be the initial focus of the study.

The availability of both single emitter and multiplexed emitter data also allow for study of coupling effects within these systems. Experiments have demonstrated that emission characteristics of multiplexed arrays are not linear extrapolations of single emitter characteristics, alluding to possible inter-emitter dependencies. Once a single emitter model is validated, simulations can be configured to explore possible macroscopic effects that may occur from operating emitters in parallel. Again, these simulations may help elucidate what components of design and operation are contributing to this phenomenon by conducting parameter sweeps that are otherwise infeasible to perform experimentally. The results of which may then support select configurations of interest where experimentation can be conducted, optimizing the iterative routine towards building electrosprays whose mission capabilities vastly expand beyond those that are available today.

References

[1] C. Cai, "Theoretical and numerical studies of plume flows in vacuum chambers.," Ph.D. Dissertation, University of Michigan, Ann Arbor, 2005.

[2] A. Thuppul, P. L. Wright, A. L. Collins, J. K. Ziemer, and R. E. Wirz, "Lifetime Considerations for Electrospray Thrusters," *Aerospace*, vol. 7, no. 8, p. 108, Aug. 2020.

[3] M. Natisin, H. Zamora, W. McGehee, N. Arnold, Z. Holley, M. Holmes, and D. Eckhardt, "Fabrication and characterization of a fully conventionally machined, high-performance porous-media electrospray thruster," *Journal of Micromechanics and Microengineering*, vol. 30, no. 11, p. 115021, 2020.

[4] C. S. Coffman, "Electrically-assisted evaporation of charged fluids: Fundamental modeling and studies on ionic liquids," Ph.D. dissertation, Massachusetts Institute of Technology, 2016.

[5] W. A. McGehee, N. Arnold, M. R. Natisin, Z. A. Holley, and D. Eckhardt, "The single emitter air force electrospray thruster (SEAFET) Program: Goals and initial results," in *37th International Electric Propulsion Conference*, Massachusetts Institute of Technology, Cambridge, MA USA, Jun. 2022.

Final Technical Report

Prediction of Basic Operation of Electrospray Thrusters
Using High-Fidelity Modeling

AFOSR Grant FA9550-21-1-0045

Monitored by Mitat Birkan

Iain D. Boyd (PI), University of Colorado

Abstract

Electro-spray (ES) thrusters for in-space propulsion operate using ionic liquids that may be colloidal or metal as propellant. Individual ES devices generate very small thrust and impulse bits that are ideal for fine pointing missions. The Air Force has a more significant need for large-scale thrust levels required for station keeping, orbit raising, and orbit transfer. ES systems are of interest because they provide a specific impulse that may be tailored by the propellant, high thrust through the application of many devices in parallel, and all achieved at potentially high efficiencies of about 80%. There are significant fundamental challenges for the integration of the large numbers of devices needed for Air Force missions including: (1) failure modes of ES thrusters; (2) determining the lifetime of ES thrusters; and (3) understanding any crosstalk between adjacent thrusters. We are pursuing a comprehensive research project to address these gaps:

- Model Development: The key developments needed to model electro-spray systems are treatment of ionic-liquid physics, consideration of multiple emission sites, and extension to three dimensions.
- Model Benchmarking: Integration of high-fidelity modeling with empirical data is necessary to characterize life-limiting mechanisms and extrapolate performance in space environments. Direct comparisons will be made of model predictions with detailed plume measurements of AFRL porous-media flow emitters that are under way at the University of Michigan. Comparisons will also be made with all relevant data sets generated at the Air Force Research Laboratory in their current ES activities.
- Use the high-fidelity simulations to provide fundamental data needed for application of low-fidelity analysis of ES thrusters. For example, understanding the process and conditions for mode switching to the pure ionic regime is essential to meeting the USAF requirements for this technology.
- Analyses: Use the high-fidelity model for large arrays including assessment of coupling effects between multiple electro-spray emitters and prediction of primary failure modes.

This final report summarizes the progress made during the first and second years of the grant in terms of source and plume modeling.

DISTRIBUTION A: Distribution approved for public release.

1. Electrospray Model Description

A single porous electrospray emitter operating in a purely ionic emission regime is considered. The domain of interest spans from the emission site on the tip to the downstream plume between the extractor and accelerator electrodes. Computationally, this domain is partitioned into two two-dimensional subdomains: an Extraction Region where field emission from the electrohydrodynamic (EHD) meniscus is considered, and a Plume Region where the ion dynamics of the extracted species are considered. The Extraction Region is further decomposed into a vacuum and bulk liquid domain, Ω_{vac} and Ω_{liq} respectively, where Γ_{lv} denotes the intersection between them. A schematic of the global domain is presented in Fig. 1.

Within the bulk liquid, mass and momentum conservation are considered using the Navier-Stokes equations are the low Reynolds number limit, otherwise known as the Stokes equations,

$$\mu\nabla^2 v - \nabla \mathrm{p} = 0, \tag{1}$$
$$\nabla \cdot v = 0, \tag{2}$$

where μ is fluid viscosity, v is bulk fluid velocity, and p is pressure. Given the propellant is conductive, charge transport is considered as well. Convective charge transport is neglected and an Ohmic conduction model is chosen,

$$j = -K\nabla\phi_l, \tag{3}$$

where j is the current density, K is the electrical conductivity and ϕ_l is the electric potential in the bulk fluid. When charge conservation, $\nabla \cdot j = 0$, is considered with Eqn. (3) the electric potential can be shown to satisfy Laplace's equation,

$$\nabla^2\phi_l = 0. \tag{4}$$

Within the vacuum, space charge effects are negligible, and Laplace's equation is again used to determine the potential,

$$\nabla^2\phi_v = 0, \tag{5}$$

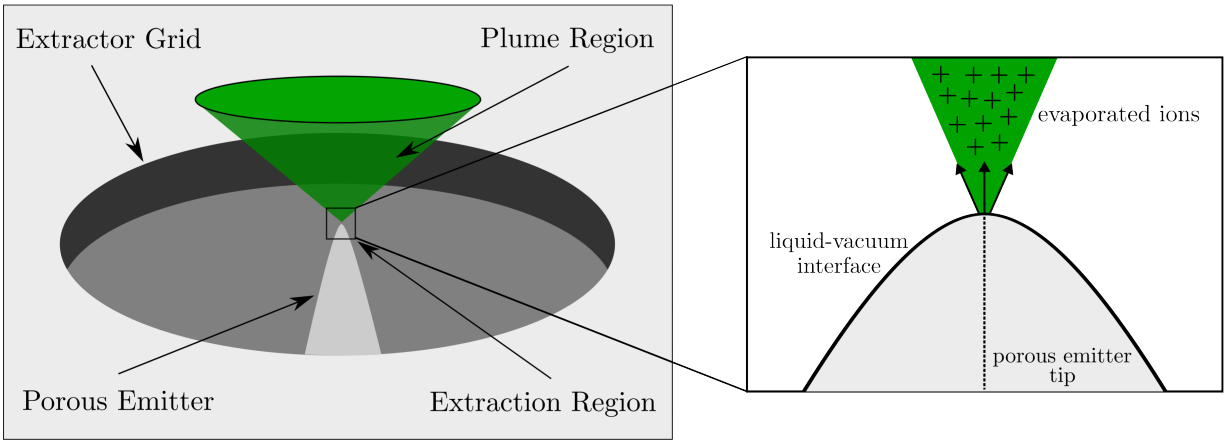


Figure 1. Domains of interest within a porous electrospray emitter.

DISTRIBUTION A: Distribution approved for public release.

where ϕ_v is the electric potential within the vacuum. At the liquid-vacuum interface, the free surface charge density is considered using the electrostatic condition,

$$(-\nabla\phi_v + \epsilon\nabla\phi_l)\cdot\hat{n} = \frac{\sigma}{\epsilon_0}, \tag{6}$$

where $\hat{n}$ is the unit vector normal to the interface, σ is the free surface charge density, ϵ is the relative permittivity, and ϵ_0 is the vacuum permittivity. Additionally, the free surface charge density satisfies the following steady-state transport equation,

$$v\cdot\nabla\sigma = \sigma\hat{n}\cdot\nabla v\cdot\hat{n} - K\nabla\phi_l\cdot\hat{n} - j\cdot\hat{n}. \tag{7}$$

Equation (7) states that the charge advected by the fluid flow is balanced by surface strain, the charge conducted to the surface, and the charge lost due to ion evaporation. Field emission of ions is described by the kinetic law,

$$j\cdot\hat{n} = \frac{k_b T}{h_c}\sigma\exp\left(\frac{-1}{k_b T}\left[\Delta G - \sqrt{\frac{\nabla\phi_v\cdot\hat{n}}{4\pi\epsilon_0/q^3}}\right]\right), \tag{8}$$

where k_b is the Boltzmann constant, h_c is the Planck constant, T is the temperature, q is the elementary charge and ΔG is the solvation energy of the ions. Additionally, force balance between the applied electric traction, viscous stresses, and surface tension is enforced at the liquid-vacuum interface,

$$\hat{t}\cdot(\tau_l - \tau_e)\cdot\hat{n} = 0, \tag{9}$$
$$\hat{n}\cdot(\tau_l - \tau_e)\cdot\hat{n} = -\gamma\nabla\cdot\hat{n}, \tag{10}$$

where $\hat{\boldsymbol{t}}$ is the unit vector tangent to the interface, τ_l is the viscous stress tensor, τ_e is the electrostatic Maxwell stress tensor, and γ is the surface tension. The normal and tangential projections of the Maxwell stress tensor on the interface satisfy the equations

$$\hat{t}\cdot\tau_e\cdot\hat{n} = -\sigma\nabla\phi_v\cdot\hat{t}, \tag{11}$$
$$\hat{n}\cdot\tau_e\cdot\hat{n} = \frac{1}{2}\epsilon_0((\nabla\phi_v\cdot\hat{n})^2 - \epsilon(\nabla\phi_l\cdot\hat{n})^2) + \frac{1}{2}\epsilon_0\big((\epsilon-1)(\nabla\phi_v\cdot\hat{t})^2\big). \tag{12}$$

A hybrid direct simulation Monte Carlo and particle-in-cell (DSMC–PIC) solver is implemented to simulate the downstream rarefied plume, of which a complete description of the solver can be found by Cai [1]. In summary, DSMC is a widely implemented particle method used to calculate collisional dynamics within dilute gases. Analogously for plasmas, PIC is a kinetic method used to simulate the dynamics of charged particles under the influence of external and self–induced electromagnetic fields. Simultaneous implementation of both methods within a

DISTRIBUTION A: Distribution approved for public release.

unified kinetic solver allows the study of gases characterized by both material and Coulombic interactions.

Within the multiscale model, the DSMC–PIC solver is used to initialize a distribution of charged macroparticles at the liquid–vacuum interface as well as simulate their motion within the computational vacuum domain. The initial distribution is a function of the ion number density determined by the EHD meniscus solver. The emission velocity is sampled from a biased Maxwellian based on the propellant temperature. From there, macroscopic plume properties that contribute to single emitter failure mechanisms can be calculated and simulations can be designed to study configurations that minimize these mechanisms. For example, the primary failure mode of electrosprays is overspray of propellant at the site of emission, resulting in impingement of the electrodes that ultimately contribute to shorting and power processing unit failure [2]. By conducting a sensitivity analysis, the proposed model may be able to elucidate what elements of the parameter space contribute most to the plume divergence angle, minimizing the probability of electrode impingement.

A complete schematic of the computational domain is presented in Fig. 2. Fig. 2a presents a macro-scale, two-dimensional domain of a single emitter tip below two extractor electrodes A voltage differential is applied between the emitter and electrodes to induce electric fields strengths on the order required for direct ion evaporation at the propellant free surface. Field emission at the interface is numerically treated within a separate sub-scale domain at the emitter apex and is coupled to the macro-scale domain via the Γ_{sub} intersection. Fig. 2b presents a sub-scale domain of an emission site at the emitter apex presented in Fig. 2a. Steady, open channel flow is assumed for the propellant in Ω_{liq}, where a fully developed velocity profile is imposed at the Γ_{inl} inlet boundary. Geometry of the EHD meniscus, Γ_{int}, is numerically perturbed to find configurations that satisfy mechanical equilibrium, a prerequisite to solve for steady-state emission characteristics.

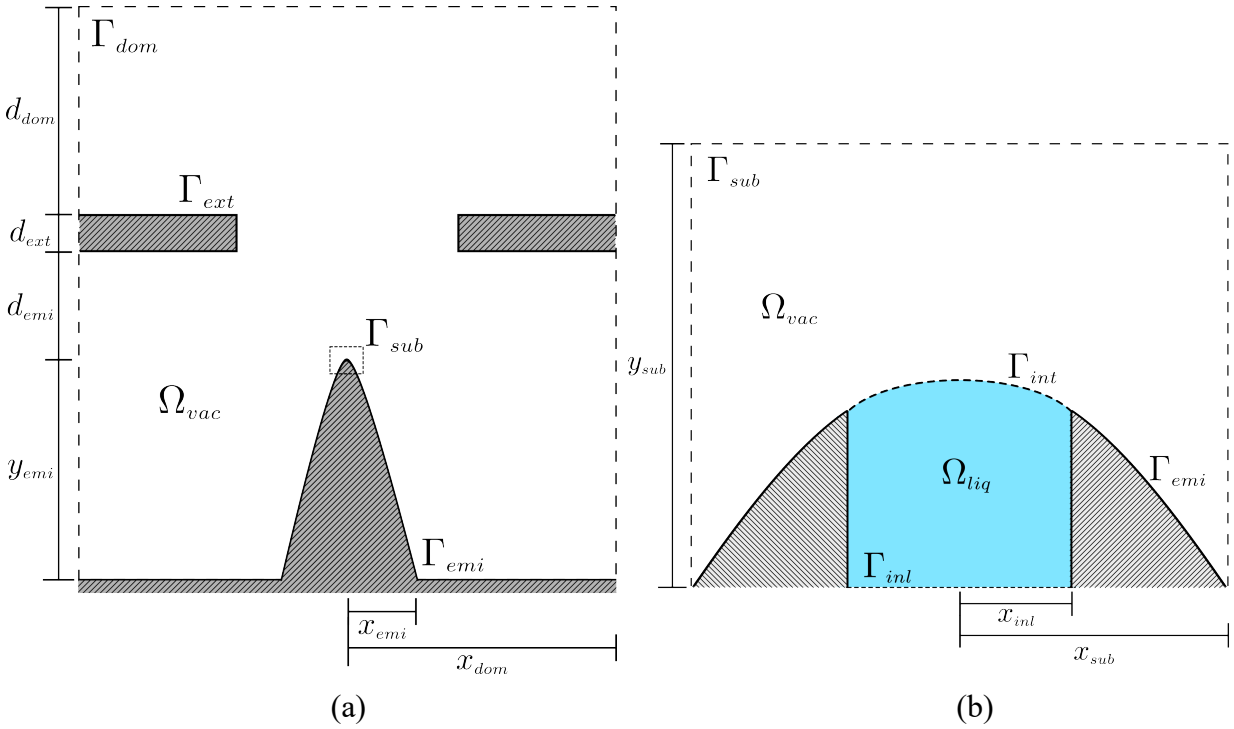


Figure 2. Computational domain.

DISTRIBUTION A: Distribution approved for public release.

2. Progress to Date

2.1 Numeric Implementation

The core developmental progress within the electrospray model has been within the Extraction Region. A finite element solver has been implemented using the Distributed and Unified Numerics Environment (DUNE), an open-source library for solving partial differential equations using grid-based methods. An algorithm has been developed that solves the coupled set of partial differential equations for a prescribed meniscus shape. The algorithm generally operates as follows:

The core Stokes and Laplace equations are solved in their respective domains. A multidomain module is configured to enforce boundary conditions that are dependent upon solutions across domains. An additional module is developed to enforce directionally dependent boundary conditions on the same interface. Consideration of electrostatic conditions, surface charge density transport, and stress balance at the free surface act as these unique multidomain boundary conditions. An iterative routine first solves the electric potential system until convergence, at which a global algorithm is implemented that solves the Stokes system and couples the domain together. A flowchart of this global algorithm is presented in Fig. 3. The result is a converged nonequilibrium solution for a prescribed meniscus shape. The current stage of development is expanding this to equilibrium solutions by including meniscus geometry perturbations in the global algorithm.

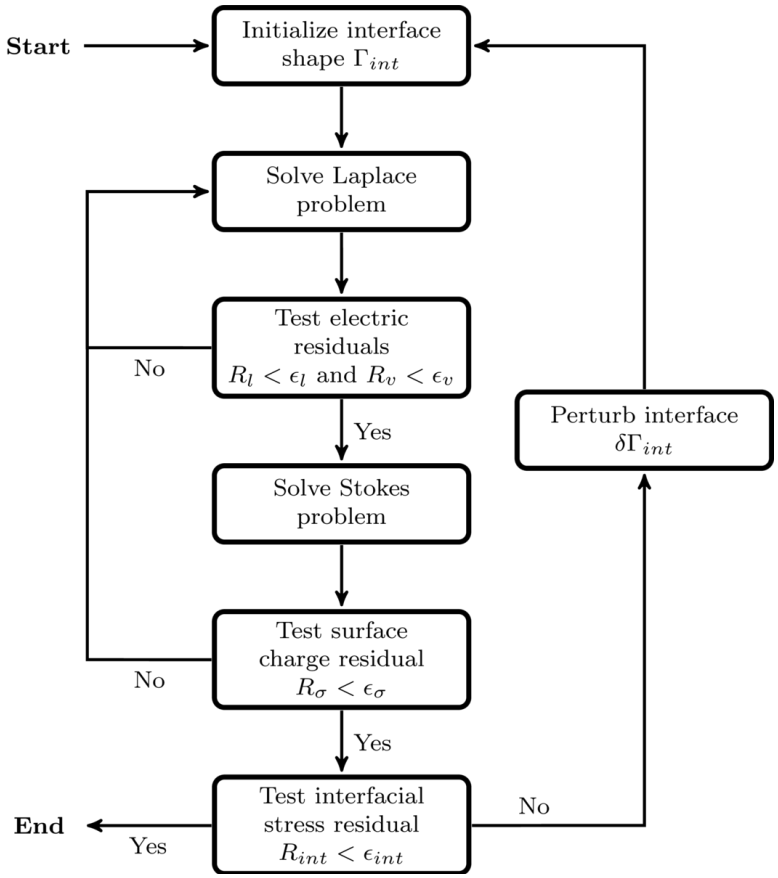


Figure 3. Algorithm to numerically solve for ion emission from the EHS meniscus within the Extraction Region.

DISTRIBUTION A: Distribution approved for public release.

2.2 Results

2.2.1 Simulation Parameters

Initial simulations within the Extraction and Plume region are conducted using similar operating parameters as those in [3]. Mapping of ion emission from the Extraction Region to the kinetic routine is not directly calculated. Experimental current values are used as input conditions into the kinetic routine via single cell injection at the emitter tip. The applied electric field condition within the EHD model is calibrated such that the integrated surface emission at the meniscus tip is of approximate order to the experimental current. Direct mapping of field emission from the EHD model within the Extraction Region to the kinetic model in the Plume Region is deferred to future work. A computational domain axial length of 0.1 μm and width of 0.1 μm is chosen for the Extraction Region, to emulate similar length scales of effective low paths within porous electrospray emitters. Meshes of the liquid and vacuum subdomains in the Extraction Region are shown in Fig. 3. A Taylor Cone angle of 49.29° is chosen for the emitter cone with a tip radius of 10 nm. Mesh elements at the emitter tip are refined in both subdomains to better resolve ion emission in this region. The computational domain of the Plume Region spans a radial distance of 500 μm and 1000 μm axially.

2.2.2 Electric Potentials

Electric potential distributions within the liquid and vacuum subdomains of the Extraction Region are presented in Fig. 4. A relatively linear progression is seen in the axial direction of both domains, with continuity between electric potentials at the interface. The potential within the liquid domain, Fig. 4a, can be seen enforced to zero where the fluid contacts the emitter electrode. A potential gradient tangential to the interface is also observed, suggesting a stronger electric field towards the meniscus center. This behavior is expected for a perturbed conductive fluid exposed to an external field, as the perturbation would result in a higher charge density at the tip and would result in a higher field strength. Continuity of electric potential across the liquid and vacuum domain interface is also observed. As the interfacial jump in electric displacement is innately enforced by the iteration scheme, all facets of the Laplace problem appear correctly represented within the semi-equilibrium potential distributions.

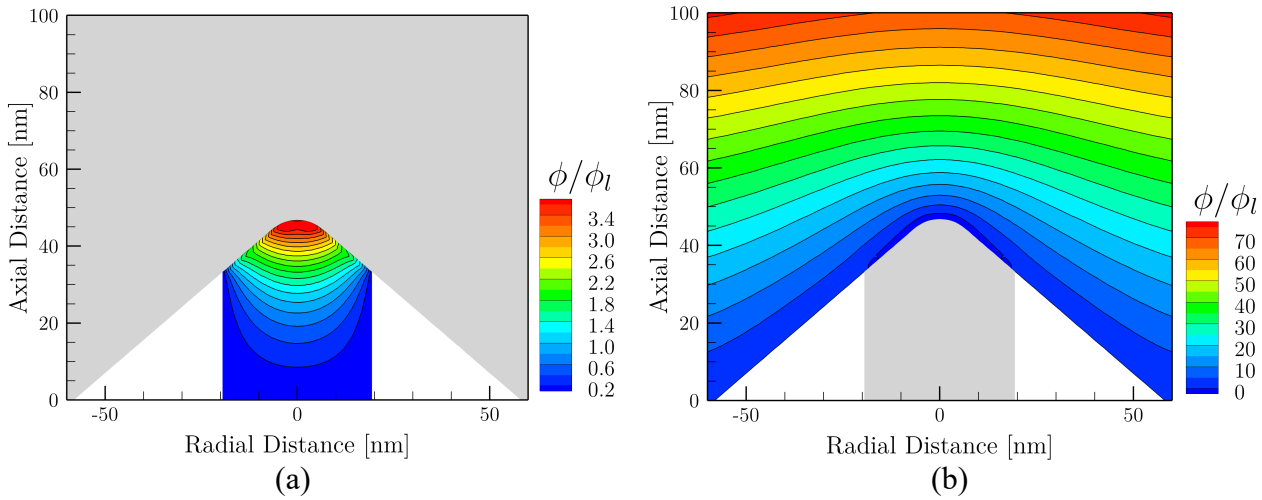


Figure 4. Electric potential distributions within the (a) liquid and (b) vacuum subdomains.

DISTRIBUTION A: Distribution approved for public release.

2.2.3 Stokes Flow and Ion Emission

Axial velocity contours within the liquid subdomain of the Extraction Region are presented in Fig. 5. Flow velocity of an ionic liquid meniscus operating in a purely ionic regime is known to scale with

$$v \sim \frac{I}{\pi\rho(q/m)(r^*)^2}, \tag{13}$$

where r^* is the characteristic length scale at the emitter tip and I is the emission current [4]. The Reynolds number scaling is then shown to be

$$Re \sim \frac{I}{\pi\mu(q/m)r^*} \sim 10^{-2}. \tag{14}$$

Using the single-emitter current for the -1562 V operational case ($I \approx 10^{-6}A$) in [3] and the fluid properties of EMI-BF_4 ($\mu \approx 10^{-2}$ Pa·s, $q/m \approx 10^6$ C/kg), the Reynolds number is shown to be significantly less than unity and thus Stokes flow is present. As mentioned, ion emission is only possible within a steady-state configuration if the normal fluid velocity at the intersection is nonzero. Field emission at the emitter tip is represented by arrows in the top-right plot of Fig. 5. It can be shown that the velocity at the emission tip is of approximate order to the emission velocity in the operational case, though it is important to note that the applied electric field, E_0, is adjusted in the Extraction Region to achieve this agreement.

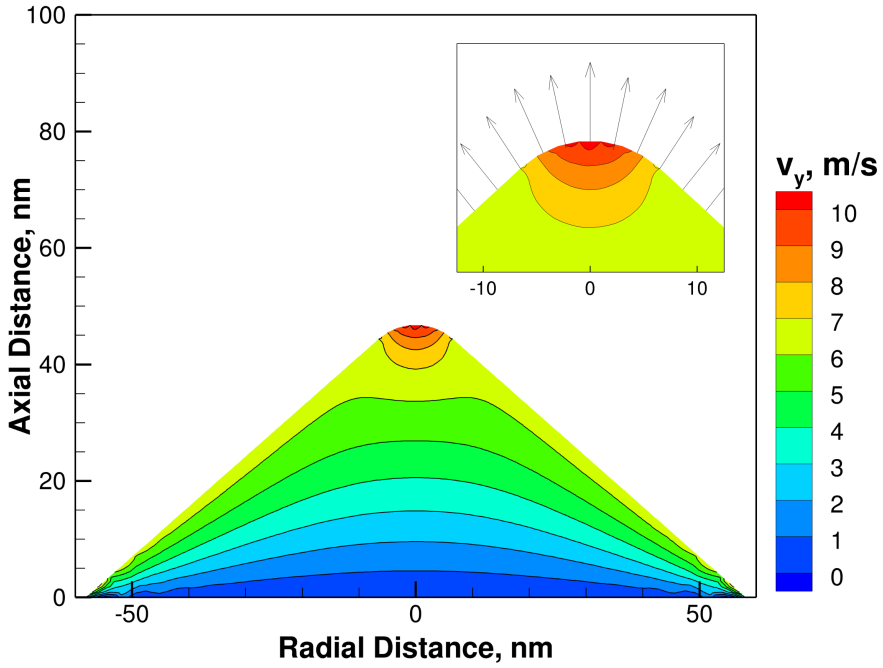


Figure 5. Axial velocity in the bulk fluid, with ion emission at the emitter tip shown in the inset.

DISTRIBUTION A: Distribution approved for public release.

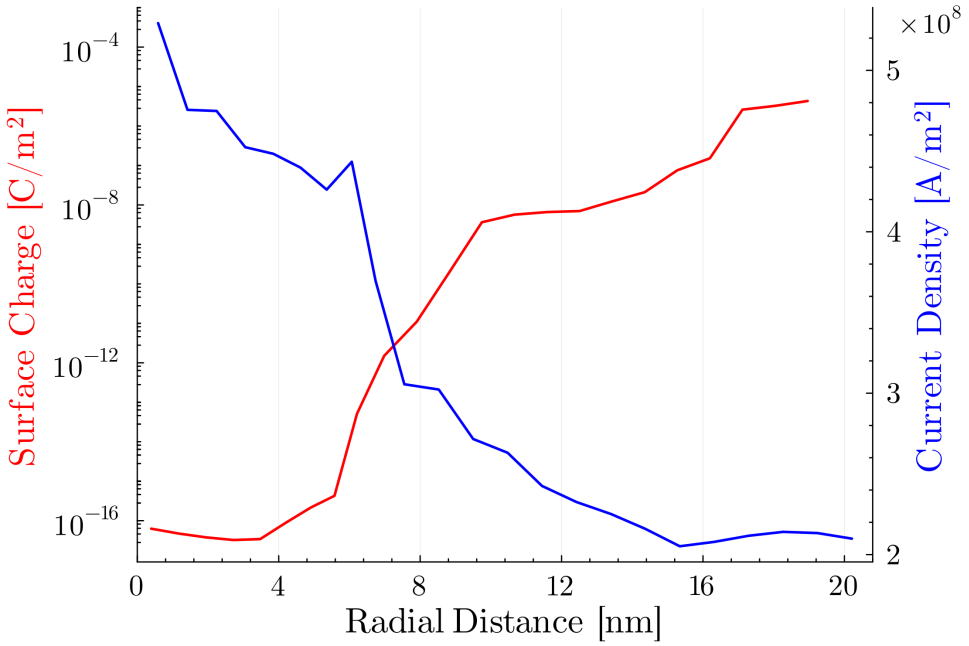


Figure 6. Interfacial surface charge and normal current density versus radial distance.

Characteristics of the Stokes problem can be observed through the interfacial current density, as it is linearly related to the normal fluid velocity at the meniscus. This current density in addition to the surface charge are plotted as a function of the radial distance in Fig. 6. As seen by the potential distribution, the emission centerline should correspond to the highest electric field, which in turn should result in the highest current density of emitted species. This is observed in Fig. 6, where the current density progressively declines with radial distance as the applied electric field weakens away from the centerline. The surface charge, on the other hand, appears to be inversely related to the current density with respect to radial distance. This is due to the continuity law of Eqn. (7), stating the surface charge represents the balance of current conducted to the interface and current evaporating from the interface. This balance is depicted in Fig. 6, where the surface charge is minimum at the interfacial locations corresponding to the highest ion emission, and vice versa. Additional quantitative validation of the EHD solver with occur once the interfacial perturbation scheme is implemented.

2.2.4 Plume Simulations

Independent simulations of the DSMC–PIC solver were conducted as well. As the coupling with the EHD meniscus solver has yet to be implemented, the simulations were initialized using experimental data of Natisin et al. [3]. Similarly, EMI-BF4 is chosen as the propellant. Within the simulation, the plume is assumed to consist of a 1:1 mixture of single-charged EMI^+ ions and EMI-BF4 neutrals. Ions colliding with any solid surfaces are reflected as neutral molecules. Emission current and thrust are calculated about the plane approximately 1000 μm away from the emitter base and are linearly scaled to match the experimental configuration where 576 emitters were operated in parallel. Within the plume, EMI^+ ion speeds (m/s) were calculated and are presented in Fig. 7, while comparisons of the numerical and measured values for emission current

DISTRIBUTION A: Distribution approved for public release.

and thrust are presented in Fig. 8. Agreement is shown between the numerical and experimental data across a range of extractor voltages, suggesting that downstream characteristics of the plume can be accurately simulated given sufficient initial conditions.

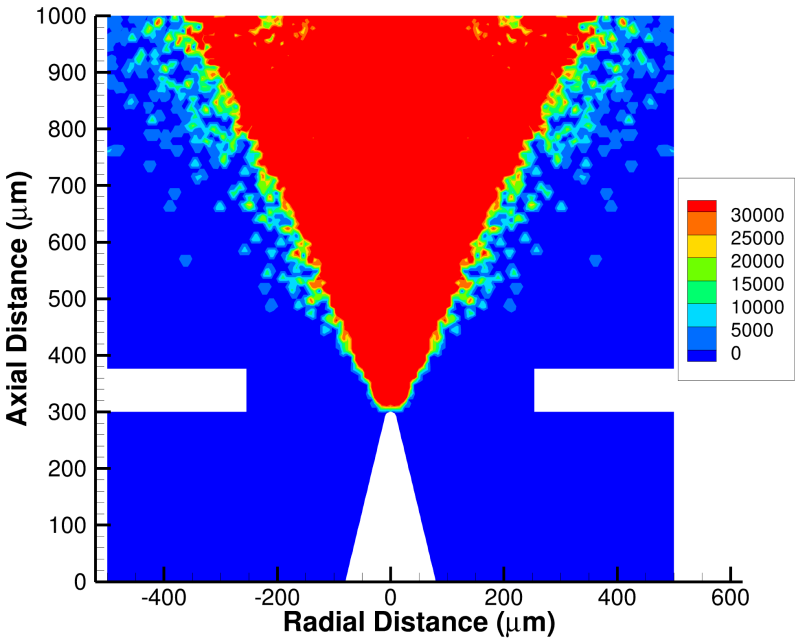


Figure 7. EMI+ ion speeds (m/s)

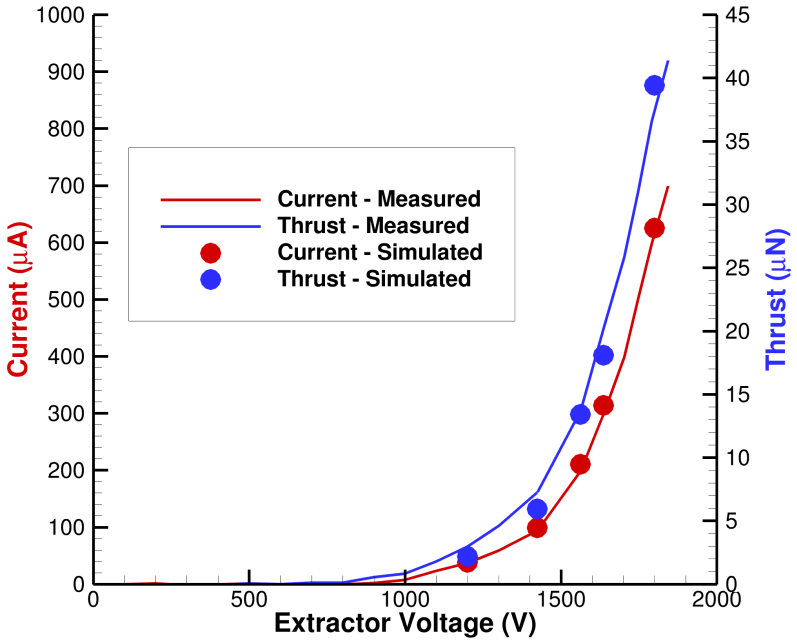


Figure 8. Comparison of emission current and thrust between experimental measurements by Natisin et al. [3] and DSMC–PIC simulation output.

DISTRIBUTION A: Distribution approved for public release.

3. Future Objectives

The majority of model development thus far has been within the Extraction Region. Implementing a normal stress balance routine at the interface, Eqn. (10), is the final module required for completion of the field emission model. This stress is a function of the surface tension, and thus the geometry of the meniscus. To complete this, a meniscus perturbation module must be developed that evolves the shape into one that satisfies equilibrium. Currently, the solver determines a nonequilibrium solution for a prescribed meniscus shape. With the addition of the meniscus perturbation module, the final equation of the field emission model is resolved, completing the Extraction Region component of the model. Development time for this module is estimated to take 1-2 months.

The kinetic model within the Plume Region is solved using an in-house direct simulation Monte-Carlo and particle-in-cell solver, and thus no core development is required. As such, the final task for the single emitter electrospray model is coupling the subscale routine in the Extraction Regime with the macroscale kinetic routine in the plume. To achieve a two-way coupling, the output of each submodel must be fed as boundary conditions to the other. Development time for this coupling module is estimated to take an additional month.

When the high-fidelity electrospray model is complete, its applications can be explored in parallel. First, the model must be benchmarked by comparing simulations with experimental measurements. Experimental measurements are nominally taken for electrosprays operating in arrays in the order of 100-1000, challenging validation of single emitter models as coupling effects cannot be accounted for. To overcome this, the Air Force Research Laboratory (AFRL) is conducting a Single Emitter Air Force Electrospray Thruster (SEAFET) program, providing data that can be directly used as validation for the single emitter model. The program has conducted a preliminary qualitative analysis of select emitters [5], with additional data to be made available in the coming months.

Further collaboration with the SEAFET program can allow exploration of the dependencies certain operating conditions have in life-limiting mechanisms. Once an initial benchmarking has been conducted, simulations spanning large parameter sweeps can be conducted to better quantify how perturbations in operations conditions such as geometry, voltage and material selection affect emission characteristics that directly contribute to failure modes. Experimental data could be taken for select configurations for calibration and further validation of the single emitter model. As the primary mechanism contributing to electrospray failure is emission impingement at the electrodes, exploring which facets of electrospray design and operation that directly contribute to overspraying at the grid will be the initial focus of the study.

The availability of both single emitter and multiplexed emitter data also allow for study of coupling effects within these systems. Experiments have demonstrated that emission characteristics of multiplexed arrays are not linear extrapolations of single emitter characteristics, alluding to possible inter-emitter dependencies. Once a single emitter model is validated, simulations can be configured to explore possible macroscopic effects that may occur from operating emitters in parallel. Again, these simulations may help elucidate what components of design and operation are contributing to this phenomenon by conducting parameter sweeps that are otherwise infeasible to perform experimentally. The results of which may then support select configurations of interest where experimentation can be conducted, optimizing the iterative routine towards building electrosprays whose mission capabilities vastly expand beyond those that are available today.

References

[1] C. Cai, "Theoretical and numerical studies of plume flows in vacuum chambers.," Ph.D. Dissertation, University of Michigan, Ann Arbor, 2005.

[2] A. Thuppul, P. L. Wright, A. L. Collins, J. K. Ziemer, and R. E. Wirz, "Lifetime Considerations for Electrospray Thrusters," *Aerospace*, vol. 7, no. 8, p. 108, Aug. 2020.

[3] M. Natisin, H. Zamora, W. McGehee, N. Arnold, Z. Holley, M. Holmes, and D. Eckhardt, "Fabrication and characterization of a fully conventionally machined, high-performance porous-media electrospray thruster," *Journal of Micromechanics and Microengineering*, vol. 30, no. 11, p. 115021, 2020.

[4] C. S. Coffman, "Electrically-assisted evaporation of charged fluids: Fundamental modeling and studies on ionic liquids," Ph.D. dissertation, Massachusetts Institute of Technology, 2016.

[5] W. A. McGehee, N. Arnold, M. R. Natisin, Z. A. Holley, and D. Eckhardt, "The single emitter air force electrospray thruster (SEAFET) Program: Goals and initial results," in *37th International Electric Propulsion Conference*, Massachusetts Institute of Technology, Cambridge, MA USA, Jun. 2022.

Final Technical Report

Prediction of Basic Operation of Electrospray Thrusters
Using High-Fidelity Modeling

AFOSR Grant FA9550-21-1-0045

Monitored by Mitat Birkan

Iain D. Boyd (PI), University of Colorado

Abstract

Electro-spray (ES) thrusters for in-space propulsion operate using ionic liquids that may be colloidal or metal as propellant. Individual ES devices generate very small thrust and impulse bits that are ideal for fine pointing missions. The Air Force has a more significant need for large-scale thrust levels required for station keeping, orbit raising, and orbit transfer. ES systems are of interest because they provide a specific impulse that may be tailored by the propellant, high thrust through the application of many devices in parallel, and all achieved at potentially high efficiencies of about 80%. There are significant fundamental challenges for the integration of the large numbers of devices needed for Air Force missions including: (1) failure modes of ES thrusters; (2) determining the lifetime of ES thrusters; and (3) understanding any crosstalk between adjacent thrusters. We are pursuing a comprehensive research project to address these gaps:

- Model Development: The key developments needed to model electro-spray systems are treatment of ionic-liquid physics, consideration of multiple emission sites, and extension to three dimensions.
- Model Benchmarking: Integration of high-fidelity modeling with empirical data is necessary to characterize life-limiting mechanisms and extrapolate performance in space environments. Direct comparisons will be made of model predictions with detailed plume measurements of AFRL porous-media flow emitters that are under way at the University of Michigan. Comparisons will also be made with all relevant data sets generated at the Air Force Research Laboratory in their current ES activities.
- Use the high-fidelity simulations to provide fundamental data needed for application of low-fidelity analysis of ES thrusters. For example, understanding the process and conditions for mode switching to the pure ionic regime is essential to meeting the USAF requirements for this technology.
- Analyses: Use the high-fidelity model for large arrays including assessment of coupling effects between multiple electro-spray emitters and prediction of primary failure modes.

This final report summarizes the progress made during the first and second years of the grant in terms of source and plume modeling.

DISTRIBUTION A: Distribution approved for public release.

1. Electrospray Model Description

A single porous electrospray emitter operating in a purely ionic emission regime is considered. The domain of interest spans from the emission site on the tip to the downstream plume between the extractor and accelerator electrodes. Computationally, this domain is partitioned into two two-dimensional subdomains: an Extraction Region where field emission from the electrohydrodynamic (EHD) meniscus is considered, and a Plume Region where the ion dynamics of the extracted species are considered. The Extraction Region is further decomposed into a vacuum and bulk liquid domain, Ω_{vac} and Ω_{liq} respectively, where Γ_{lv} denotes the intersection between them. A schematic of the global domain is presented in Fig. 1.

Within the bulk liquid, mass and momentum conservation are considered using the Navier-Stokes equations are the low Reynolds number limit, otherwise known as the Stokes equations,

$$\mu\nabla^2 v - \nabla \mathrm{p} = 0, \tag{1}$$
$$\nabla \cdot v = 0, \tag{2}$$

where μ is fluid viscosity, v is bulk fluid velocity, and p is pressure. Given the propellant is conductive, charge transport is considered as well. Convective charge transport is neglected and an Ohmic conduction model is chosen,

$$j = -K\nabla\phi_l, \tag{3}$$

where j is the current density, K is the electrical conductivity and ϕ_l is the electric potential in the bulk fluid. When charge conservation, $\nabla \cdot j = 0$, is considered with Eqn. (3) the electric potential can be shown to satisfy Laplace's equation,

$$\nabla^2\phi_l = 0. \tag{4}$$

Within the vacuum, space charge effects are negligible, and Laplace's equation is again used to determine the potential,

$$\nabla^2\phi_v = 0, \tag{5}$$

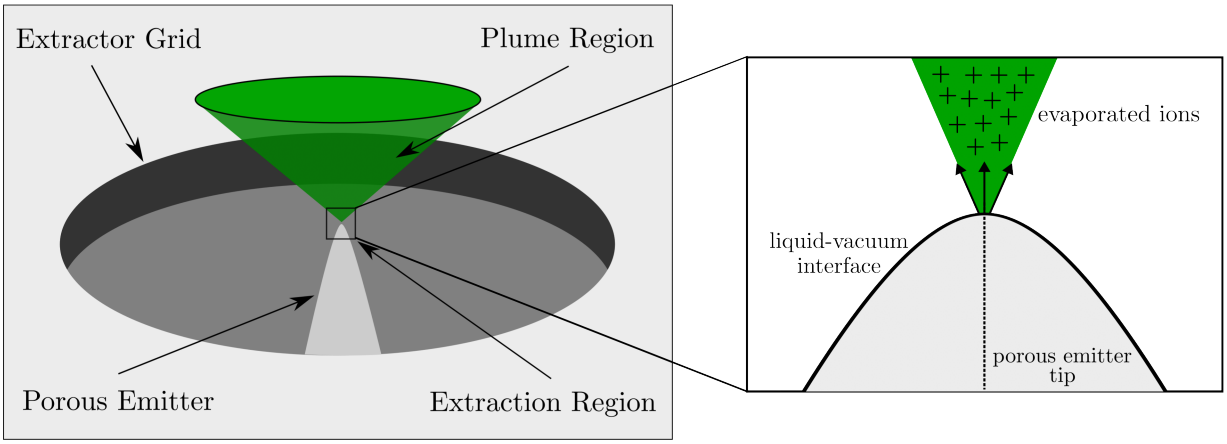


Figure 1. Domains of interest within a porous electrospray emitter.

DISTRIBUTION A: Distribution approved for public release.

where ϕ_v is the electric potential within the vacuum. At the liquid-vacuum interface, the free surface charge density is considered using the electrostatic condition,

$$(-\nabla\phi_v + \epsilon\nabla\phi_l)\cdot\hat{n} = \frac{\sigma}{\epsilon_0}, \tag{6}$$

where $\hat{n}$ is the unit vector normal to the interface, σ is the free surface charge density, ϵ is the relative permittivity, and ϵ_0 is the vacuum permittivity. Additionally, the free surface charge density satisfies the following steady-state transport equation,

$$v\cdot\nabla\sigma = \sigma\hat{n}\cdot\nabla v\cdot\hat{n} - K\nabla\phi_l\cdot\hat{n} - j\cdot\hat{n}. \tag{7}$$

Equation (7) states that the charge advected by the fluid flow is balanced by surface strain, the charge conducted to the surface, and the charge lost due to ion evaporation. Field emission of ions is described by the kinetic law,

$$j\cdot\hat{n} = \frac{k_b T}{h_c}\sigma\exp\left(\frac{-1}{k_b T}\left[\Delta G - \sqrt{\frac{\nabla\phi_v\cdot\hat{n}}{4\pi\epsilon_0/q^3}}\right]\right), \tag{8}$$

where k_b is the Boltzmann constant, h_c is the Planck constant, T is the temperature, q is the elementary charge and ΔG is the solvation energy of the ions. Additionally, force balance between the applied electric traction, viscous stresses, and surface tension is enforced at the liquid-vacuum interface,

$$\hat{t}\cdot(\tau_l - \tau_e)\cdot\hat{n} = 0, \tag{9}$$
$$\hat{n}\cdot(\tau_l - \tau_e)\cdot\hat{n} = -\gamma\nabla\cdot\hat{n}, \tag{10}$$

where $\hat{\boldsymbol{t}}$ is the unit vector tangent to the interface, τ_l is the viscous stress tensor, τ_e is the electrostatic Maxwell stress tensor, and γ is the surface tension. The normal and tangential projections of the Maxwell stress tensor on the interface satisfy the equations

$$\hat{t}\cdot\tau_e\cdot\hat{n} = -\sigma\nabla\phi_v\cdot\hat{t}, \tag{11}$$
$$\hat{n}\cdot\tau_e\cdot\hat{n} = \frac{1}{2}\epsilon_0((\nabla\phi_v\cdot\hat{n})^2 - \epsilon(\nabla\phi_l\cdot\hat{n})^2) + \frac{1}{2}\epsilon_0\big((\epsilon-1)(\nabla\phi_v\cdot\hat{t})^2\big). \tag{12}$$

A hybrid direct simulation Monte Carlo and particle-in-cell (DSMC–PIC) solver is implemented to simulate the downstream rarefied plume, of which a complete description of the solver can be found by Cai [1]. In summary, DSMC is a widely implemented particle method used to calculate collisional dynamics within dilute gases. Analogously for plasmas, PIC is a kinetic method used to simulate the dynamics of charged particles under the influence of external and self–induced electromagnetic fields. Simultaneous implementation of both methods within a

DISTRIBUTION A: Distribution approved for public release.

unified kinetic solver allows the study of gases characterized by both material and Coulombic interactions.

Within the multiscale model, the DSMC–PIC solver is used to initialize a distribution of charged macroparticles at the liquid–vacuum interface as well as simulate their motion within the computational vacuum domain. The initial distribution is a function of the ion number density determined by the EHD meniscus solver. The emission velocity is sampled from a biased Maxwellian based on the propellant temperature. From there, macroscopic plume properties that contribute to single emitter failure mechanisms can be calculated and simulations can be designed to study configurations that minimize these mechanisms. For example, the primary failure mode of electrosprays is overspray of propellant at the site of emission, resulting in impingement of the electrodes that ultimately contribute to shorting and power processing unit failure [2]. By conducting a sensitivity analysis, the proposed model may be able to elucidate what elements of the parameter space contribute most to the plume divergence angle, minimizing the probability of electrode impingement.

A complete schematic of the computational domain is presented in Fig. 2. Fig. 2a presents a macro-scale, two-dimensional domain of a single emitter tip below two extractor electrodes A voltage differential is applied between the emitter and electrodes to induce electric fields strengths on the order required for direct ion evaporation at the propellant free surface. Field emission at the interface is numerically treated within a separate sub-scale domain at the emitter apex and is coupled to the macro-scale domain via the Γ_{sub} intersection. Fig. 2b presents a sub-scale domain of an emission site at the emitter apex presented in Fig. 2a. Steady, open channel flow is assumed for the propellant in Ω_{liq}, where a fully developed velocity profile is imposed at the Γ_{inl} inlet boundary. Geometry of the EHD meniscus, Γ_{int}, is numerically perturbed to find configurations that satisfy mechanical equilibrium, a prerequisite to solve for steady-state emission characteristics.

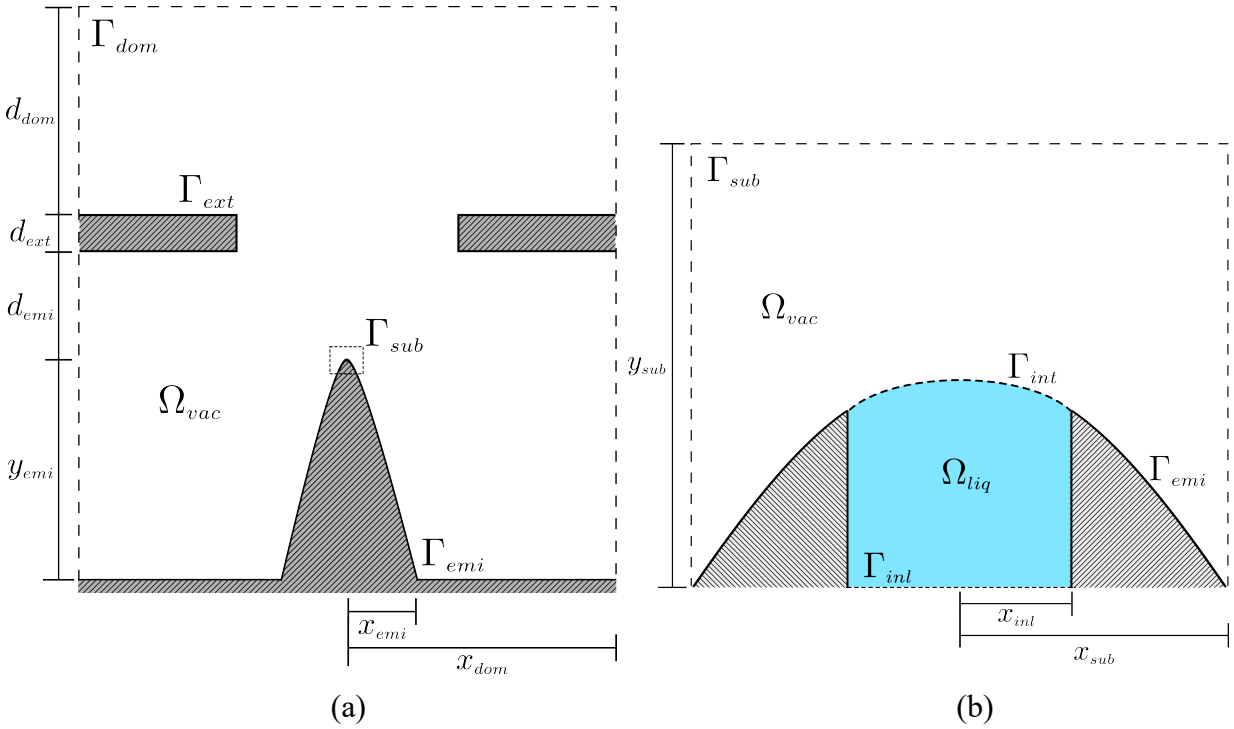


Figure 2. Computational domain.

DISTRIBUTION A: Distribution approved for public release.

2. Progress to Date

2.1 Numeric Implementation

The core developmental progress within the electrospray model has been within the Extraction Region. A finite element solver has been implemented using the Distributed and Unified Numerics Environment (DUNE), an open-source library for solving partial differential equations using grid-based methods. An algorithm has been developed that solves the coupled set of partial differential equations for a prescribed meniscus shape. The algorithm generally operates as follows:

The core Stokes and Laplace equations are solved in their respective domains. A multidomain module is configured to enforce boundary conditions that are dependent upon solutions across domains. An additional module is developed to enforce directionally dependent boundary conditions on the same interface. Consideration of electrostatic conditions, surface charge density transport, and stress balance at the free surface act as these unique multidomain boundary conditions. An iterative routine first solves the electric potential system until convergence, at which a global algorithm is implemented that solves the Stokes system and couples the domain together. A flowchart of this global algorithm is presented in Fig. 3. The result is a converged nonequilibrium solution for a prescribed meniscus shape. The current stage of development is expanding this to equilibrium solutions by including meniscus geometry perturbations in the global algorithm.

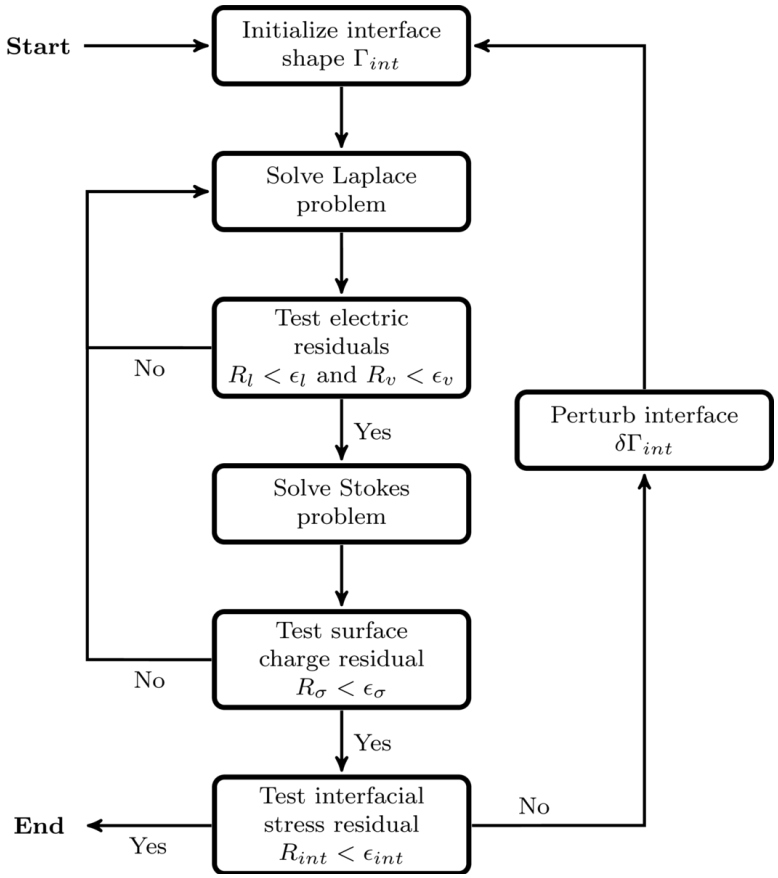


Figure 3. Algorithm to numerically solve for ion emission from the EHS meniscus within the Extraction Region.

DISTRIBUTION A: Distribution approved for public release.

2.2 Results

2.2.1 Simulation Parameters

Initial simulations within the Extraction and Plume region are conducted using similar operating parameters as those in [3]. Mapping of ion emission from the Extraction Region to the kinetic routine is not directly calculated. Experimental current values are used as input conditions into the kinetic routine via single cell injection at the emitter tip. The applied electric field condition within the EHD model is calibrated such that the integrated surface emission at the meniscus tip is of approximate order to the experimental current. Direct mapping of field emission from the EHD model within the Extraction Region to the kinetic model in the Plume Region is deferred to future work. A computational domain axial length of 0.1 μm and width of 0.1 μm is chosen for the Extraction Region, to emulate similar length scales of effective low paths within porous electrospray emitters. Meshes of the liquid and vacuum subdomains in the Extraction Region are shown in Fig. 3. A Taylor Cone angle of 49.29° is chosen for the emitter cone with a tip radius of 10 nm. Mesh elements at the emitter tip are refined in both subdomains to better resolve ion emission in this region. The computational domain of the Plume Region spans a radial distance of 500 μm and 1000 μm axially.

2.2.2 Electric Potentials

Electric potential distributions within the liquid and vacuum subdomains of the Extraction Region are presented in Fig. 4. A relatively linear progression is seen in the axial direction of both domains, with continuity between electric potentials at the interface. The potential within the liquid domain, Fig. 4a, can be seen enforced to zero where the fluid contacts the emitter electrode. A potential gradient tangential to the interface is also observed, suggesting a stronger electric field towards the meniscus center. This behavior is expected for a perturbed conductive fluid exposed to an external field, as the perturbation would result in a higher charge density at the tip and would result in a higher field strength. Continuity of electric potential across the liquid and vacuum domain interface is also observed. As the interfacial jump in electric displacement is innately enforced by the iteration scheme, all facets of the Laplace problem appear correctly represented within the semi-equilibrium potential distributions.

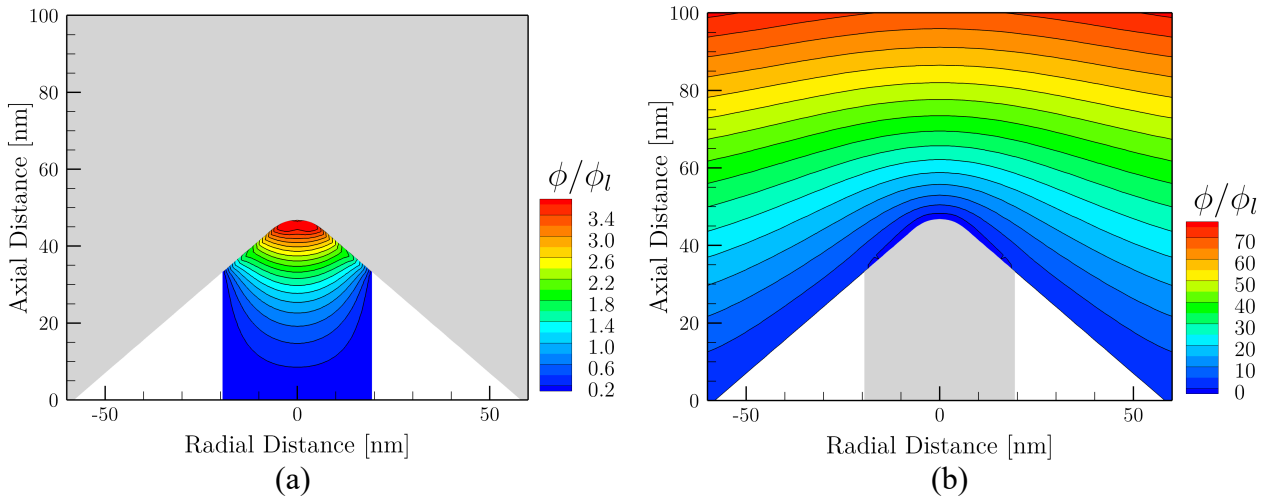


Figure 4. Electric potential distributions within the (a) liquid and (b) vacuum subdomains.

DISTRIBUTION A: Distribution approved for public release.

2.2.3 Stokes Flow and Ion Emission

Axial velocity contours within the liquid subdomain of the Extraction Region are presented in Fig. 5. Flow velocity of an ionic liquid meniscus operating in a purely ionic regime is known to scale with

$$v \sim \frac{I}{\pi\rho(q/m)(r^*)^2}, \tag{13}$$

where r^* is the characteristic length scale at the emitter tip and I is the emission current [4]. The Reynolds number scaling is then shown to be

$$Re \sim \frac{I}{\pi\mu(q/m)r^*} \sim 10^{-2}. \tag{14}$$

Using the single-emitter current for the -1562 V operational case ($I \approx 10^{-6}A$) in [3] and the fluid properties of EMI-BF_4 ($\mu \approx 10^{-2}$ Pa·s, $q/m \approx 10^6$ C/kg), the Reynolds number is shown to be significantly less than unity and thus Stokes flow is present. As mentioned, ion emission is only possible within a steady-state configuration if the normal fluid velocity at the intersection is nonzero. Field emission at the emitter tip is represented by arrows in the top-right plot of Fig. 5. It can be shown that the velocity at the emission tip is of approximate order to the emission velocity in the operational case, though it is important to note that the applied electric field, E_0, is adjusted in the Extraction Region to achieve this agreement.

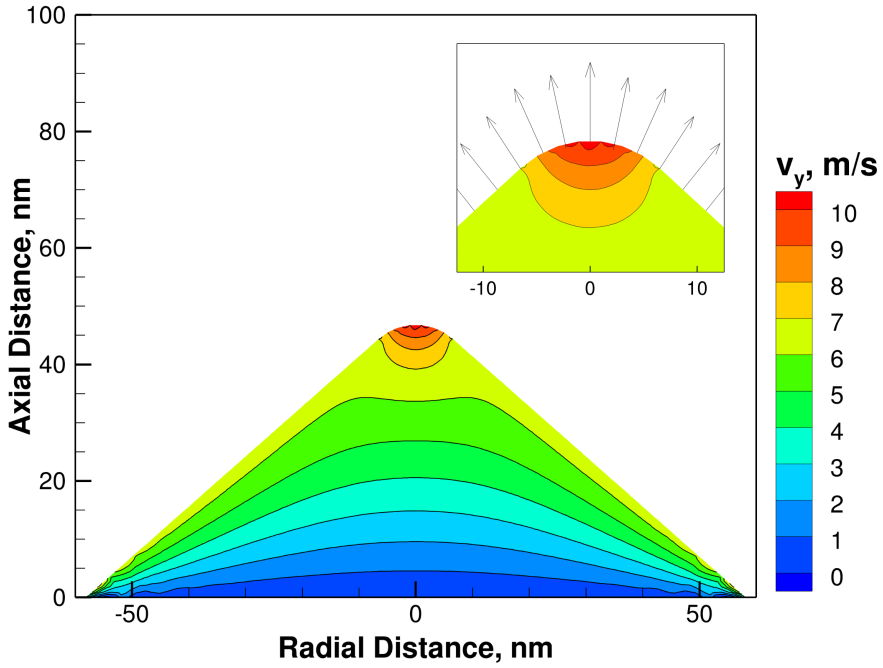


Figure 5. Axial velocity in the bulk fluid, with ion emission at the emitter tip shown in the inset.

DISTRIBUTION A: Distribution approved for public release.

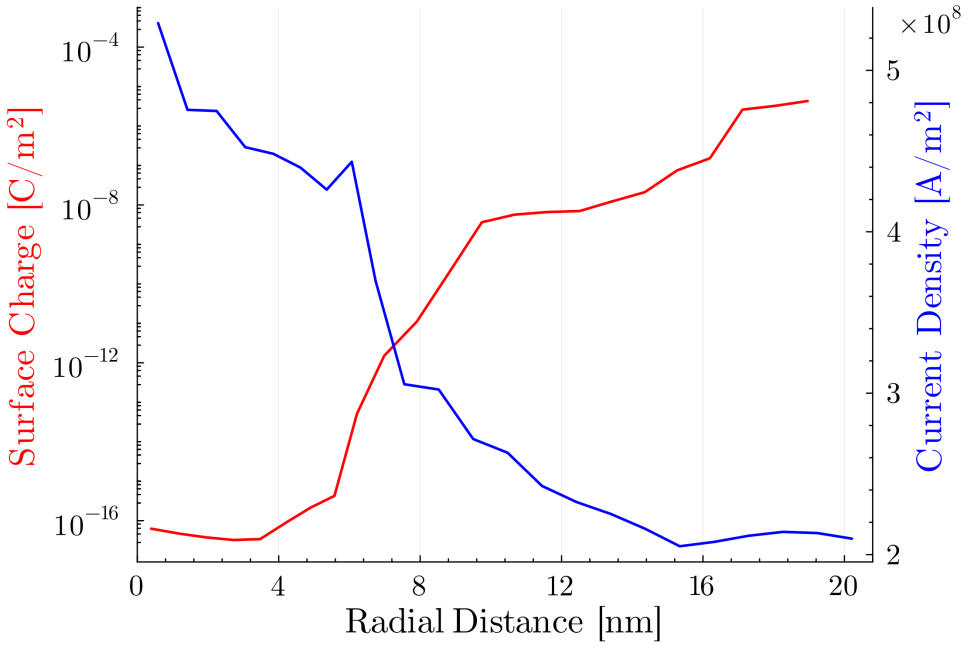


Figure 6. Interfacial surface charge and normal current density versus radial distance.

Characteristics of the Stokes problem can be observed through the interfacial current density, as it is linearly related to the normal fluid velocity at the meniscus. This current density in addition to the surface charge are plotted as a function of the radial distance in Fig. 6. As seen by the potential distribution, the emission centerline should correspond to the highest electric field, which in turn should result in the highest current density of emitted species. This is observed in Fig. 6, where the current density progressively declines with radial distance as the applied electric field weakens away from the centerline. The surface charge, on the other hand, appears to be inversely related to the current density with respect to radial distance. This is due to the continuity law of Eqn. (7), stating the surface charge represents the balance of current conducted to the interface and current evaporating from the interface. This balance is depicted in Fig. 6, where the surface charge is minimum at the interfacial locations corresponding to the highest ion emission, and vice versa. Additional quantitative validation of the EHD solver with occur once the interfacial perturbation scheme is implemented.

2.2.4 Plume Simulations

Independent simulations of the DSMC–PIC solver were conducted as well. As the coupling with the EHD meniscus solver has yet to be implemented, the simulations were initialized using experimental data of Natisin et al. [3]. Similarly, EMI-BF4 is chosen as the propellant. Within the simulation, the plume is assumed to consist of a 1:1 mixture of single-charged EMI^+ ions and EMI-BF4 neutrals. Ions colliding with any solid surfaces are reflected as neutral molecules. Emission current and thrust are calculated about the plane approximately 1000 μm away from the emitter base and are linearly scaled to match the experimental configuration where 576 emitters were operated in parallel. Within the plume, EMI^+ ion speeds (m/s) were calculated and are presented in Fig. 7, while comparisons of the numerical and measured values for emission current

DISTRIBUTION A: Distribution approved for public release.

and thrust are presented in Fig. 8. Agreement is shown between the numerical and experimental data across a range of extractor voltages, suggesting that downstream characteristics of the plume can be accurately simulated given sufficient initial conditions.

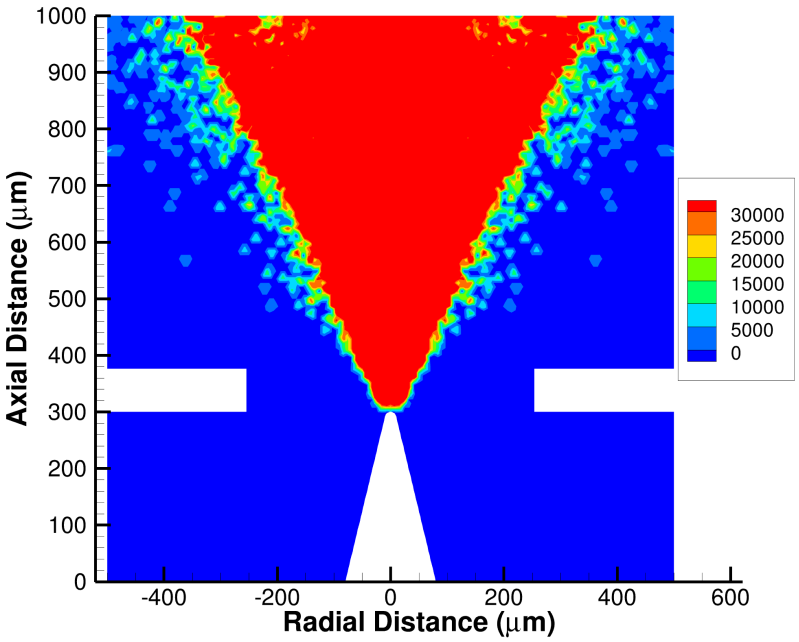


Figure 7. EMI+ ion speeds (m/s)

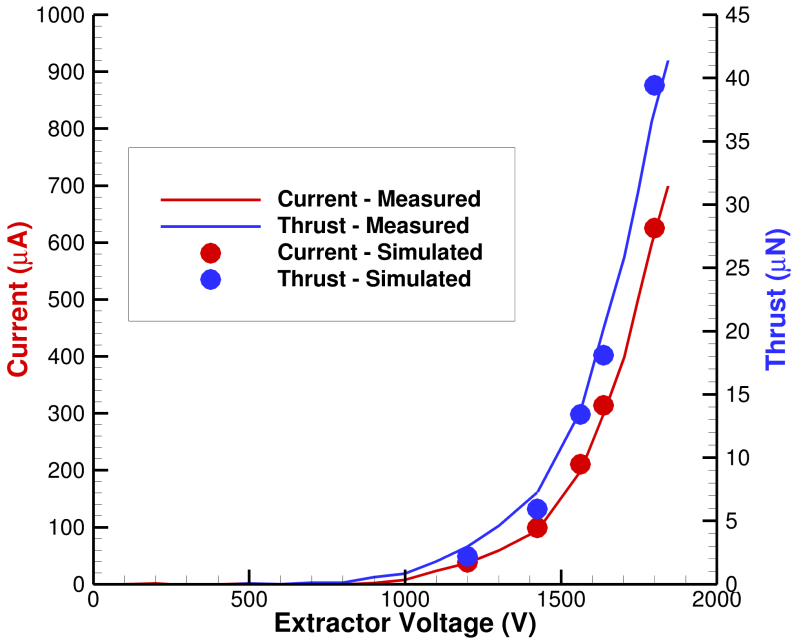


Figure 8. Comparison of emission current and thrust between experimental measurements by Natisin et al. [3] and DSMC–PIC simulation output.

DISTRIBUTION A: Distribution approved for public release.

3. Future Objectives

The majority of model development thus far has been within the Extraction Region. Implementing a normal stress balance routine at the interface, Eqn. (10), is the final module required for completion of the field emission model. This stress is a function of the surface tension, and thus the geometry of the meniscus. To complete this, a meniscus perturbation module must be developed that evolves the shape into one that satisfies equilibrium. Currently, the solver determines a nonequilibrium solution for a prescribed meniscus shape. With the addition of the meniscus perturbation module, the final equation of the field emission model is resolved, completing the Extraction Region component of the model. Development time for this module is estimated to take 1-2 months.

The kinetic model within the Plume Region is solved using an in-house direct simulation Monte-Carlo and particle-in-cell solver, and thus no core development is required. As such, the final task for the single emitter electrospray model is coupling the subscale routine in the Extraction Regime with the macroscale kinetic routine in the plume. To achieve a two-way coupling, the output of each submodel must be fed as boundary conditions to the other. Development time for this coupling module is estimated to take an additional month.

When the high-fidelity electrospray model is complete, its applications can be explored in parallel. First, the model must be benchmarked by comparing simulations with experimental measurements. Experimental measurements are nominally taken for electrosprays operating in arrays in the order of 100-1000, challenging validation of single emitter models as coupling effects cannot be accounted for. To overcome this, the Air Force Research Laboratory (AFRL) is conducting a Single Emitter Air Force Electrospray Thruster (SEAFET) program, providing data that can be directly used as validation for the single emitter model. The program has conducted a preliminary qualitative analysis of select emitters [5], with additional data to be made available in the coming months.

Further collaboration with the SEAFET program can allow exploration of the dependencies certain operating conditions have in life-limiting mechanisms. Once an initial benchmarking has been conducted, simulations spanning large parameter sweeps can be conducted to better quantify how perturbations in operations conditions such as geometry, voltage and material selection affect emission characteristics that directly contribute to failure modes. Experimental data could be taken for select configurations for calibration and further validation of the single emitter model. As the primary mechanism contributing to electrospray failure is emission impingement at the electrodes, exploring which facets of electrospray design and operation that directly contribute to overspraying at the grid will be the initial focus of the study.

The availability of both single emitter and multiplexed emitter data also allow for study of coupling effects within these systems. Experiments have demonstrated that emission characteristics of multiplexed arrays are not linear extrapolations of single emitter characteristics, alluding to possible inter-emitter dependencies. Once a single emitter model is validated, simulations can be configured to explore possible macroscopic effects that may occur from operating emitters in parallel. Again, these simulations may help elucidate what components of design and operation are contributing to this phenomenon by conducting parameter sweeps that are otherwise infeasible to perform experimentally. The results of which may then support select configurations of interest where experimentation can be conducted, optimizing the iterative routine towards building electrosprays whose mission capabilities vastly expand beyond those that are available today.

DISTRIBUTION A: Distribution approved for public release.

References

[1] C. Cai, "Theoretical and numerical studies of plume flows in vacuum chambers.," Ph.D. Dissertation, University of Michigan, Ann Arbor, 2005.

[2] A. Thuppul, P. L. Wright, A. L. Collins, J. K. Ziemer, and R. E. Wirz, "Lifetime Considerations for Electrospray Thrusters," *Aerospace*, vol. 7, no. 8, p. 108, Aug. 2020.

[3] M. Natisin, H. Zamora, W. McGehee, N. Arnold, Z. Holley, M. Holmes, and D. Eckhardt, "Fabrication and characterization of a fully conventionally machined, high-performance porous-media electrospray thruster," *Journal of Micromechanics and Microengineering*, vol. 30, no. 11, p. 115021, 2020.

[4] C. S. Coffman, "Electrically-assisted evaporation of charged fluids: Fundamental modeling and studies on ionic liquids," Ph.D. dissertation, Massachusetts Institute of Technology, 2016.

[5] W. A. McGehee, N. Arnold, M. R. Natisin, Z. A. Holley, and D. Eckhardt, "The single emitter air force electrospray thruster (SEAFET) Program: Goals and initial results," in *37th International Electric Propulsion Conference*, Massachusetts Institute of Technology, Cambridge, MA USA, Jun. 2022.

Final Technical Report

Prediction of Basic Operation of Electrospray Thrusters
Using High-Fidelity Modeling

AFOSR Grant FA9550-21-1-0045

Monitored by Mitat Birkan

Iain D. Boyd (PI), University of Colorado

Abstract

Electro-spray (ES) thrusters for in-space propulsion operate using ionic liquids that may be colloidal or metal as propellant. Individual ES devices generate very small thrust and impulse bits that are ideal for fine pointing missions. The Air Force has a more significant need for large-scale thrust levels required for station keeping, orbit raising, and orbit transfer. ES systems are of interest because they provide a specific impulse that may be tailored by the propellant, high thrust through the application of many devices in parallel, and all achieved at potentially high efficiencies of about 80%. There are significant fundamental challenges for the integration of the large numbers of devices needed for Air Force missions including: (1) failure modes of ES thrusters; (2) determining the lifetime of ES thrusters; and (3) understanding any crosstalk between adjacent thrusters. We are pursuing a comprehensive research project to address these gaps:

- Model Development: The key developments needed to model electro-spray systems are treatment of ionic-liquid physics, consideration of multiple emission sites, and extension to three dimensions.
- Model Benchmarking: Integration of high-fidelity modeling with empirical data is necessary to characterize life-limiting mechanisms and extrapolate performance in space environments. Direct comparisons will be made of model predictions with detailed plume measurements of AFRL porous-media flow emitters that are under way at the University of Michigan. Comparisons will also be made with all relevant data sets generated at the Air Force Research Laboratory in their current ES activities.
- Use the high-fidelity simulations to provide fundamental data needed for application of low-fidelity analysis of ES thrusters. For example, understanding the process and conditions for mode switching to the pure ionic regime is essential to meeting the USAF requirements for this technology.
- Analyses: Use the high-fidelity model for large arrays including assessment of coupling effects between multiple electro-spray emitters and prediction of primary failure modes.

This final report summarizes the progress made during the first and second years of the grant in terms of source and plume modeling.

DISTRIBUTION A: Distribution approved for public release.

1. Electrospray Model Description

A single porous electrospray emitter operating in a purely ionic emission regime is considered. The domain of interest spans from the emission site on the tip to the downstream plume between the extractor and accelerator electrodes. Computationally, this domain is partitioned into two two-dimensional subdomains: an Extraction Region where field emission from the electrohydrodynamic (EHD) meniscus is considered, and a Plume Region where the ion dynamics of the extracted species are considered. The Extraction Region is further decomposed into a vacuum and bulk liquid domain, Ω_{vac} and Ω_{liq} respectively, where Γ_{lv} denotes the intersection between them. A schematic of the global domain is presented in Fig. 1.

Within the bulk liquid, mass and momentum conservation are considered using the Navier-Stokes equations are the low Reynolds number limit, otherwise known as the Stokes equations,

$$\mu\nabla^2 v - \nabla \mathrm{p} = 0, \tag{1}$$
$$\nabla \cdot v = 0, \tag{2}$$

where μ is fluid viscosity, v is bulk fluid velocity, and p is pressure. Given the propellant is conductive, charge transport is considered as well. Convective charge transport is neglected and an Ohmic conduction model is chosen,

$$j = -K\nabla\phi_l, \tag{3}$$

where j is the current density, K is the electrical conductivity and ϕ_l is the electric potential in the bulk fluid. When charge conservation, $\nabla \cdot j = 0$, is considered with Eqn. (3) the electric potential can be shown to satisfy Laplace's equation,

$$\nabla^2\phi_l = 0. \tag{4}$$

Within the vacuum, space charge effects are negligible, and Laplace's equation is again used to determine the potential,

$$\nabla^2\phi_v = 0, \tag{5}$$

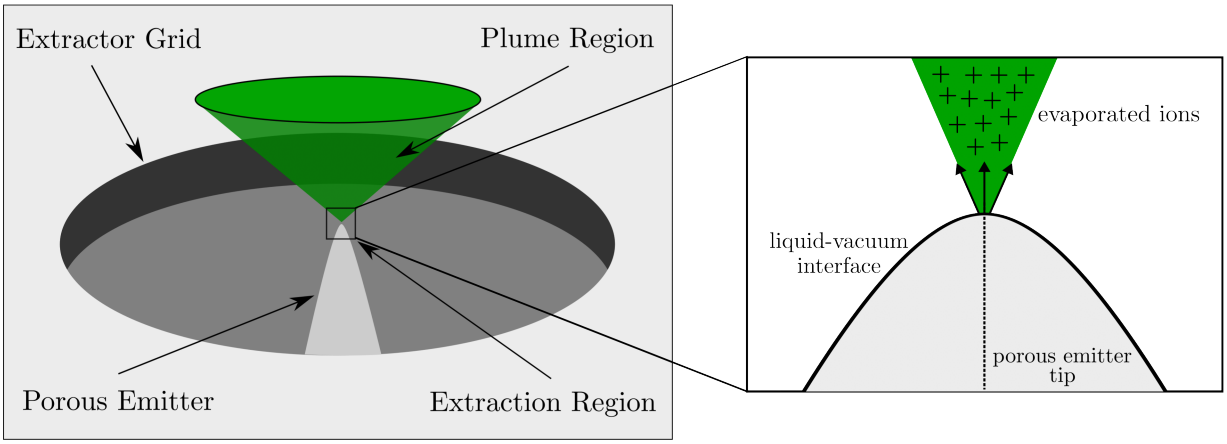


Figure 1. Domains of interest within a porous electrospray emitter.

DISTRIBUTION A: Distribution approved for public release.

where ϕ_v is the electric potential within the vacuum. At the liquid-vacuum interface, the free surface charge density is considered using the electrostatic condition,

$$(-\nabla\phi_v + \epsilon\nabla\phi_l)\cdot\hat{n} = \frac{\sigma}{\epsilon_0}, \tag{6}$$

where $\hat{n}$ is the unit vector normal to the interface, σ is the free surface charge density, ϵ is the relative permittivity, and ϵ_0 is the vacuum permittivity. Additionally, the free surface charge density satisfies the following steady-state transport equation,

$$v\cdot\nabla\sigma = \sigma\hat{n}\cdot\nabla v\cdot\hat{n} - K\nabla\phi_l\cdot\hat{n} - j\cdot\hat{n}. \tag{7}$$

Equation (7) states that the charge advected by the fluid flow is balanced by surface strain, the charge conducted to the surface, and the charge lost due to ion evaporation. Field emission of ions is described by the kinetic law,

$$j\cdot\hat{n} = \frac{k_b T}{h_c}\sigma\exp\left(\frac{-1}{k_b T}\left[\Delta G - \sqrt{\frac{\nabla\phi_v\cdot\hat{n}}{4\pi\epsilon_0/q^3}}\right]\right), \tag{8}$$

where k_b is the Boltzmann constant, h_c is the Planck constant, T is the temperature, q is the elementary charge and ΔG is the solvation energy of the ions. Additionally, force balance between the applied electric traction, viscous stresses, and surface tension is enforced at the liquid-vacuum interface,

$$\hat{t}\cdot(\tau_l - \tau_e)\cdot\hat{n} = 0, \tag{9}$$
$$\hat{n}\cdot(\tau_l - \tau_e)\cdot\hat{n} = -\gamma\nabla\cdot\hat{n}, \tag{10}$$

where $\hat{\boldsymbol{t}}$ is the unit vector tangent to the interface, τ_l is the viscous stress tensor, τ_e is the electrostatic Maxwell stress tensor, and γ is the surface tension. The normal and tangential projections of the Maxwell stress tensor on the interface satisfy the equations

$$\hat{t}\cdot\tau_e\cdot\hat{n} = -\sigma\nabla\phi_v\cdot\hat{t}, \tag{11}$$
$$\hat{n}\cdot\tau_e\cdot\hat{n} = \frac{1}{2}\epsilon_0((\nabla\phi_v\cdot\hat{n})^2 - \epsilon(\nabla\phi_l\cdot\hat{n})^2) + \frac{1}{2}\epsilon_0\big((\epsilon-1)(\nabla\phi_v\cdot\hat{t})^2\big). \tag{12}$$

A hybrid direct simulation Monte Carlo and particle-in-cell (DSMC–PIC) solver is implemented to simulate the downstream rarefied plume, of which a complete description of the solver can be found by Cai [1]. In summary, DSMC is a widely implemented particle method used to calculate collisional dynamics within dilute gases. Analogously for plasmas, PIC is a kinetic method used to simulate the dynamics of charged particles under the influence of external and self–induced electromagnetic fields. Simultaneous implementation of both methods within a

DISTRIBUTION A: Distribution approved for public release.

unified kinetic solver allows the study of gases characterized by both material and Coulombic interactions.

Within the multiscale model, the DSMC–PIC solver is used to initialize a distribution of charged macroparticles at the liquid–vacuum interface as well as simulate their motion within the computational vacuum domain. The initial distribution is a function of the ion number density determined by the EHD meniscus solver. The emission velocity is sampled from a biased Maxwellian based on the propellant temperature. From there, macroscopic plume properties that contribute to single emitter failure mechanisms can be calculated and simulations can be designed to study configurations that minimize these mechanisms. For example, the primary failure mode of electrosprays is overspray of propellant at the site of emission, resulting in impingement of the electrodes that ultimately contribute to shorting and power processing unit failure [2]. By conducting a sensitivity analysis, the proposed model may be able to elucidate what elements of the parameter space contribute most to the plume divergence angle, minimizing the probability of electrode impingement.

A complete schematic of the computational domain is presented in Fig. 2. Fig. 2a presents a macro-scale, two-dimensional domain of a single emitter tip below two extractor electrodes A voltage differential is applied between the emitter and electrodes to induce electric fields strengths on the order required for direct ion evaporation at the propellant free surface. Field emission at the interface is numerically treated within a separate sub-scale domain at the emitter apex and is coupled to the macro-scale domain via the Γ_{sub} intersection. Fig. 2b presents a sub-scale domain of an emission site at the emitter apex presented in Fig. 2a. Steady, open channel flow is assumed for the propellant in Ω_{liq}, where a fully developed velocity profile is imposed at the Γ_{inl} inlet boundary. Geometry of the EHD meniscus, Γ_{int}, is numerically perturbed to find configurations that satisfy mechanical equilibrium, a prerequisite to solve for steady-state emission characteristics.

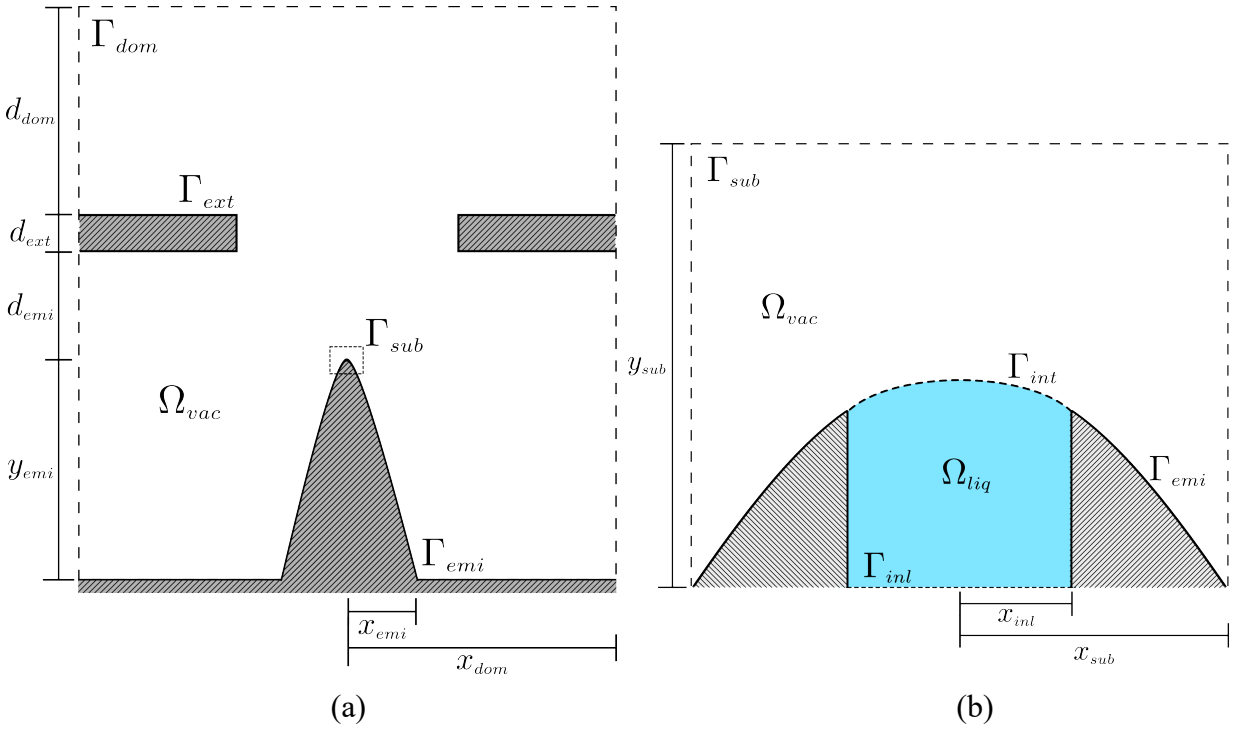


Figure 2. Computational domain.

DISTRIBUTION A: Distribution approved for public release.

2. Progress to Date

2.1 Numeric Implementation

The core developmental progress within the electrospray model has been within the Extraction Region. A finite element solver has been implemented using the Distributed and Unified Numerics Environment (DUNE), an open-source library for solving partial differential equations using grid-based methods. An algorithm has been developed that solves the coupled set of partial differential equations for a prescribed meniscus shape. The algorithm generally operates as follows:

The core Stokes and Laplace equations are solved in their respective domains. A multidomain module is configured to enforce boundary conditions that are dependent upon solutions across domains. An additional module is developed to enforce directionally dependent boundary conditions on the same interface. Consideration of electrostatic conditions, surface charge density transport, and stress balance at the free surface act as these unique multidomain boundary conditions. An iterative routine first solves the electric potential system until convergence, at which a global algorithm is implemented that solves the Stokes system and couples the domain together. A flowchart of this global algorithm is presented in Fig. 3. The result is a converged nonequilibrium solution for a prescribed meniscus shape. The current stage of development is expanding this to equilibrium solutions by including meniscus geometry perturbations in the global algorithm.

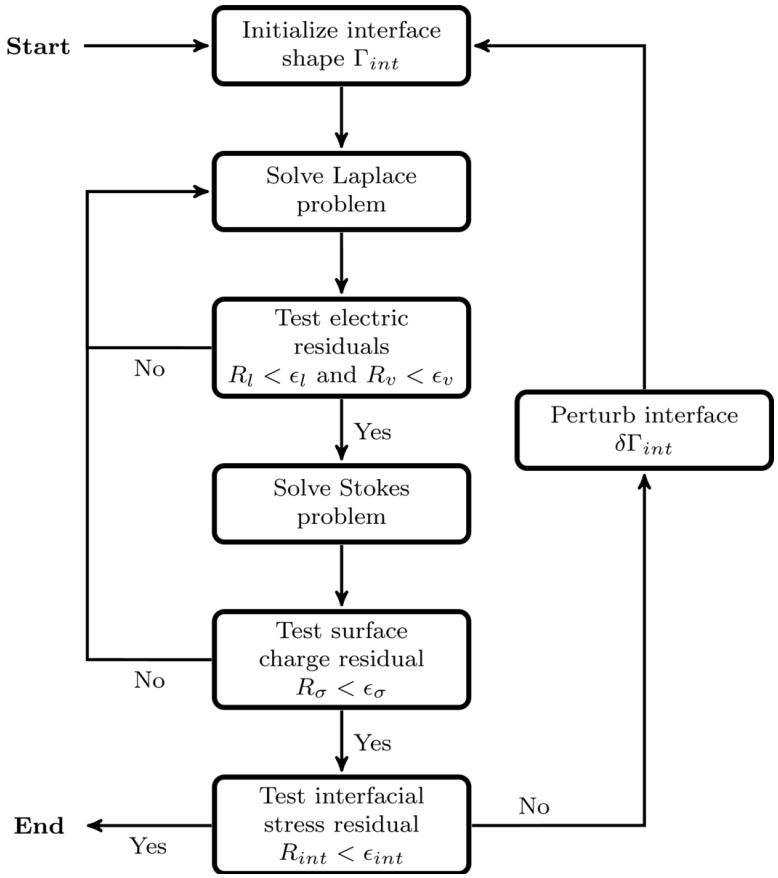


Figure 3. Algorithm to numerically solve for ion emission from the EHS meniscus within the Extraction Region.

DISTRIBUTION A: Distribution approved for public release.

2.2 Results

2.2.1 Simulation Parameters

Initial simulations within the Extraction and Plume region are conducted using similar operating parameters as those in [3]. Mapping of ion emission from the Extraction Region to the kinetic routine is not directly calculated. Experimental current values are used as input conditions into the kinetic routine via single cell injection at the emitter tip. The applied electric field condition within the EHD model is calibrated such that the integrated surface emission at the meniscus tip is of approximate order to the experimental current. Direct mapping of field emission from the EHD model within the Extraction Region to the kinetic model in the Plume Region is deferred to future work. A computational domain axial length of 0.1 μm and width of 0.1 μm is chosen for the Extraction Region, to emulate similar length scales of effective low paths within porous electrospray emitters. Meshes of the liquid and vacuum subdomains in the Extraction Region are shown in Fig. 3. A Taylor Cone angle of 49.29° is chosen for the emitter cone with a tip radius of 10 nm. Mesh elements at the emitter tip are refined in both subdomains to better resolve ion emission in this region. The computational domain of the Plume Region spans a radial distance of 500 μm and 1000 μm axially.

2.2.2 Electric Potentials

Electric potential distributions within the liquid and vacuum subdomains of the Extraction Region are presented in Fig. 4. A relatively linear progression is seen in the axial direction of both domains, with continuity between electric potentials at the interface. The potential within the liquid domain, Fig. 4a, can be seen enforced to zero where the fluid contacts the emitter electrode. A potential gradient tangential to the interface is also observed, suggesting a stronger electric field towards the meniscus center. This behavior is expected for a perturbed conductive fluid exposed to an external field, as the perturbation would result in a higher charge density at the tip and would result in a higher field strength. Continuity of electric potential across the liquid and vacuum domain interface is also observed. As the interfacial jump in electric displacement is innately enforced by the iteration scheme, all facets of the Laplace problem appear correctly represented within the semi-equilibrium potential distributions.

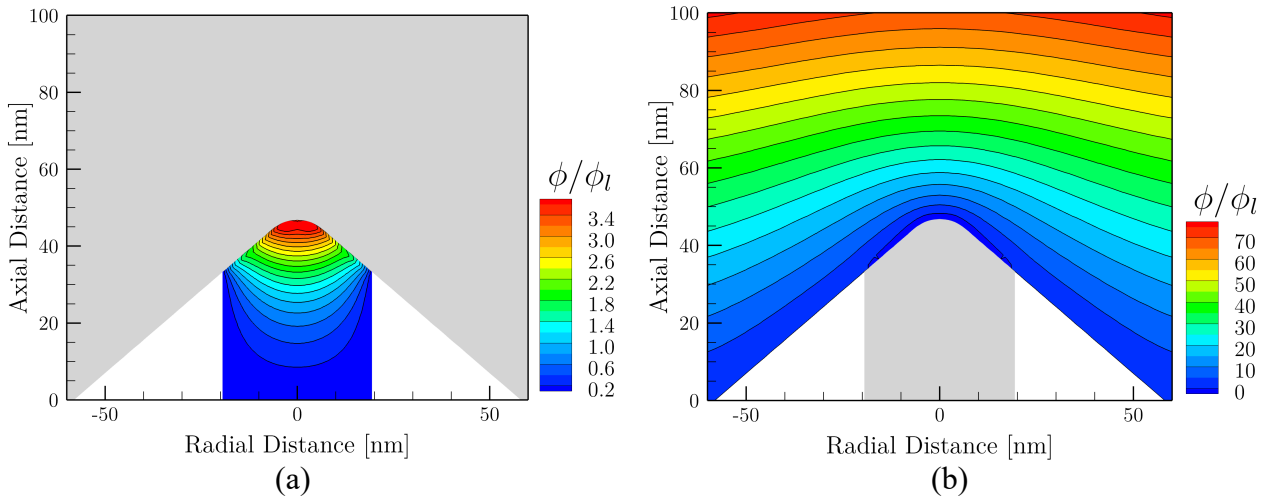


Figure 4. Electric potential distributions within the (a) liquid and (b) vacuum subdomains.

DISTRIBUTION A: Distribution approved for public release.

2.2.3 Stokes Flow and Ion Emission

Axial velocity contours within the liquid subdomain of the Extraction Region are presented in Fig. 5. Flow velocity of an ionic liquid meniscus operating in a purely ionic regime is known to scale with

$$v \sim \frac{I}{\pi\rho(q/m)(r^*)^2}, \tag{13}$$

where r^* is the characteristic length scale at the emitter tip and I is the emission current [4]. The Reynolds number scaling is then shown to be

$$Re \sim \frac{I}{\pi\mu(q/m)r^*} \sim 10^{-2}. \tag{14}$$

Using the single-emitter current for the -1562 V operational case ($I \approx 10^{-6}A$) in [3] and the fluid properties of EMI-BF_4 ($\mu \approx 10^{-2}$ Pa·s, $q/m \approx 10^6$ C/kg), the Reynolds number is shown to be significantly less than unity and thus Stokes flow is present. As mentioned, ion emission is only possible within a steady-state configuration if the normal fluid velocity at the intersection is nonzero. Field emission at the emitter tip is represented by arrows in the top-right plot of Fig. 5. It can be shown that the velocity at the emission tip is of approximate order to the emission velocity in the operational case, though it is important to note that the applied electric field, E_0, is adjusted in the Extraction Region to achieve this agreement.

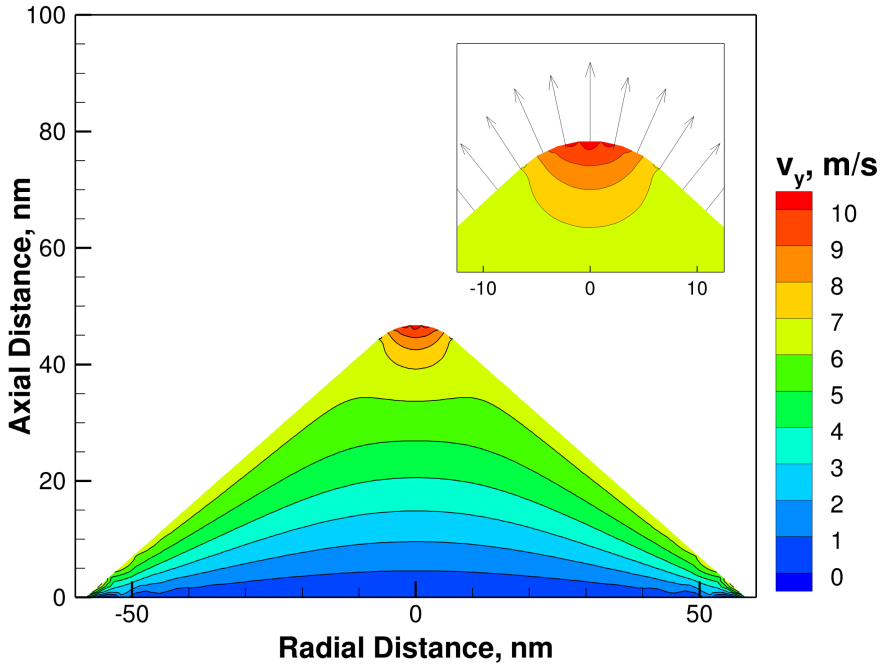


Figure 5. Axial velocity in the bulk fluid, with ion emission at the emitter tip shown in the inset.

DISTRIBUTION A: Distribution approved for public release.

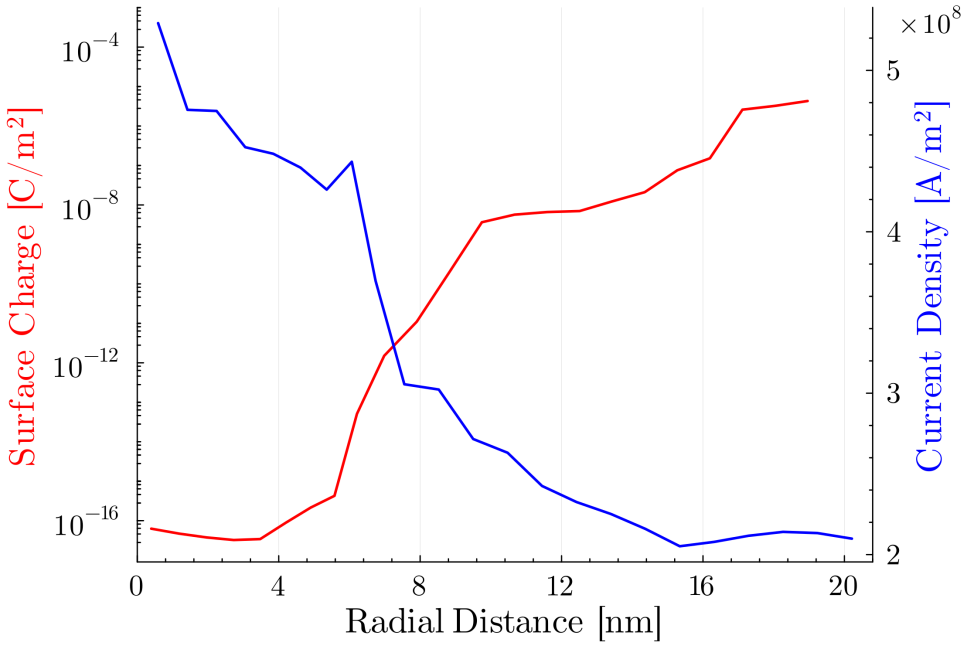


Figure 6. Interfacial surface charge and normal current density versus radial distance.

Characteristics of the Stokes problem can be observed through the interfacial current density, as it is linearly related to the normal fluid velocity at the meniscus. This current density in addition to the surface charge are plotted as a function of the radial distance in Fig. 6. As seen by the potential distribution, the emission centerline should correspond to the highest electric field, which in turn should result in the highest current density of emitted species. This is observed in Fig. 6, where the current density progressively declines with radial distance as the applied electric field weakens away from the centerline. The surface charge, on the other hand, appears to be inversely related to the current density with respect to radial distance. This is due to the continuity law of Eqn. (7), stating the surface charge represents the balance of current conducted to the interface and current evaporating from the interface. This balance is depicted in Fig. 6, where the surface charge is minimum at the interfacial locations corresponding to the highest ion emission, and vice versa. Additional quantitative validation of the EHD solver with occur once the interfacial perturbation scheme is implemented.

2.2.4 Plume Simulations

Independent simulations of the DSMC–PIC solver were conducted as well. As the coupling with the EHD meniscus solver has yet to be implemented, the simulations were initialized using experimental data of Natisin et al. [3]. Similarly, EMI-BF4 is chosen as the propellant. Within the simulation, the plume is assumed to consist of a 1:1 mixture of single-charged EMI^+ ions and EMI-BF4 neutrals. Ions colliding with any solid surfaces are reflected as neutral molecules. Emission current and thrust are calculated about the plane approximately 1000 μm away from the emitter base and are linearly scaled to match the experimental configuration where 576 emitters were operated in parallel. Within the plume, EMI^+ ion speeds (m/s) were calculated and are presented in Fig. 7, while comparisons of the numerical and measured values for emission current

DISTRIBUTION A: Distribution approved for public release.

and thrust are presented in Fig. 8. Agreement is shown between the numerical and experimental data across a range of extractor voltages, suggesting that downstream characteristics of the plume can be accurately simulated given sufficient initial conditions.

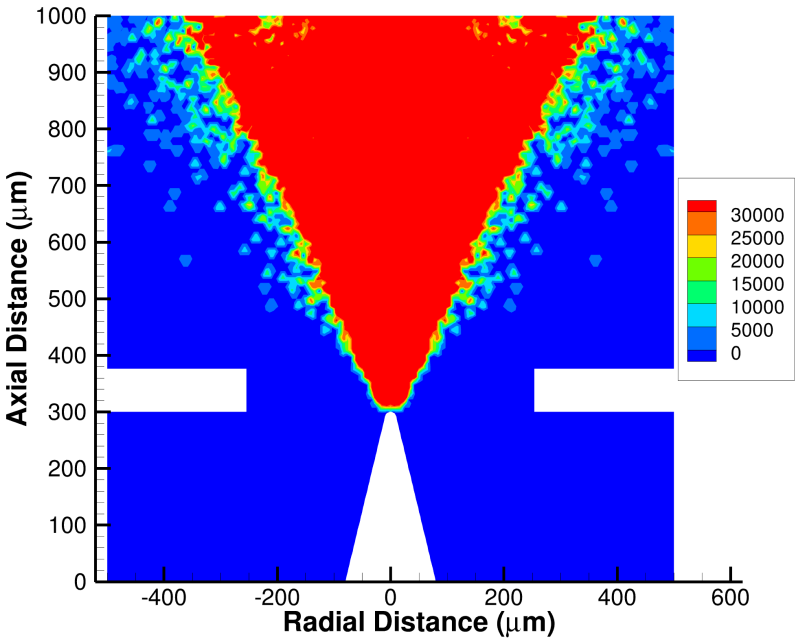


Figure 7. EMI+ ion speeds (m/s)

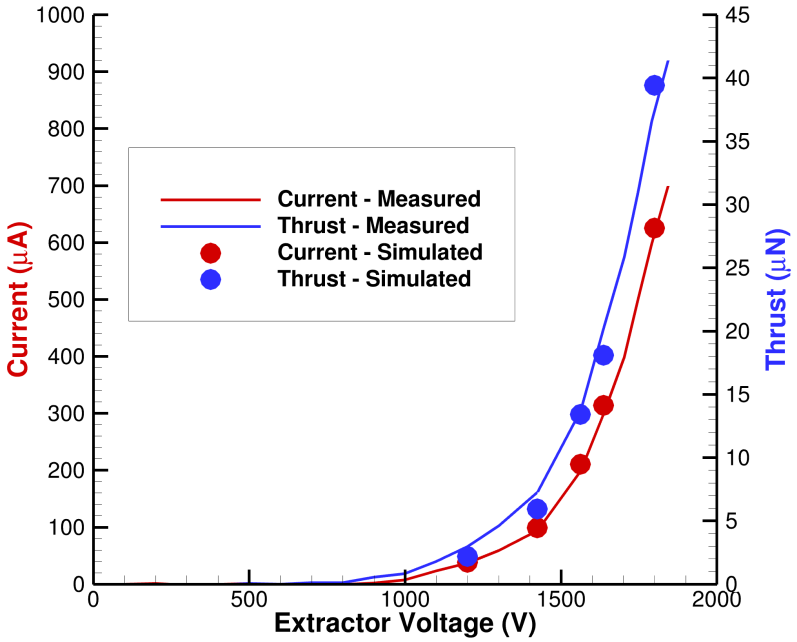


Figure 8. Comparison of emission current and thrust between experimental measurements by Natisin et al. [3] and DSMC–PIC simulation output.

DISTRIBUTION A: Distribution approved for public release.

3. Future Objectives

The majority of model development thus far has been within the Extraction Region. Implementing a normal stress balance routine at the interface, Eqn. (10), is the final module required for completion of the field emission model. This stress is a function of the surface tension, and thus the geometry of the meniscus. To complete this, a meniscus perturbation module must be developed that evolves the shape into one that satisfies equilibrium. Currently, the solver determines a nonequilibrium solution for a prescribed meniscus shape. With the addition of the meniscus perturbation module, the final equation of the field emission model is resolved, completing the Extraction Region component of the model. Development time for this module is estimated to take 1-2 months.

The kinetic model within the Plume Region is solved using an in-house direct simulation Monte-Carlo and particle-in-cell solver, and thus no core development is required. As such, the final task for the single emitter electrospray model is coupling the subscale routine in the Extraction Regime with the macroscale kinetic routine in the plume. To achieve a two-way coupling, the output of each submodel must be fed as boundary conditions to the other. Development time for this coupling module is estimated to take an additional month.

When the high-fidelity electrospray model is complete, its applications can be explored in parallel. First, the model must be benchmarked by comparing simulations with experimental measurements. Experimental measurements are nominally taken for electrosprays operating in arrays in the order of 100-1000, challenging validation of single emitter models as coupling effects cannot be accounted for. To overcome this, the Air Force Research Laboratory (AFRL) is conducting a Single Emitter Air Force Electrospray Thruster (SEAFET) program, providing data that can be directly used as validation for the single emitter model. The program has conducted a preliminary qualitative analysis of select emitters [5], with additional data to be made available in the coming months.

Further collaboration with the SEAFET program can allow exploration of the dependencies certain operating conditions have in life-limiting mechanisms. Once an initial benchmarking has been conducted, simulations spanning large parameter sweeps can be conducted to better quantify how perturbations in operations conditions such as geometry, voltage and material selection affect emission characteristics that directly contribute to failure modes. Experimental data could be taken for select configurations for calibration and further validation of the single emitter model. As the primary mechanism contributing to electrospray failure is emission impingement at the electrodes, exploring which facets of electrospray design and operation that directly contribute to overspraying at the grid will be the initial focus of the study.

The availability of both single emitter and multiplexed emitter data also allow for study of coupling effects within these systems. Experiments have demonstrated that emission characteristics of multiplexed arrays are not linear extrapolations of single emitter characteristics, alluding to possible inter-emitter dependencies. Once a single emitter model is validated, simulations can be configured to explore possible macroscopic effects that may occur from operating emitters in parallel. Again, these simulations may help elucidate what components of design and operation are contributing to this phenomenon by conducting parameter sweeps that are otherwise infeasible to perform experimentally. The results of which may then support select configurations of interest where experimentation can be conducted, optimizing the iterative routine towards building electrosprays whose mission capabilities vastly expand beyond those that are available today.

DISTRIBUTION A: Distribution approved for public release.

References

[1] C. Cai, "Theoretical and numerical studies of plume flows in vacuum chambers.," Ph.D. Dissertation, University of Michigan, Ann Arbor, 2005.

[2] A. Thuppul, P. L. Wright, A. L. Collins, J. K. Ziemer, and R. E. Wirz, "Lifetime Considerations for Electrospray Thrusters," *Aerospace*, vol. 7, no. 8, p. 108, Aug. 2020.

[3] M. Natisin, H. Zamora, W. McGehee, N. Arnold, Z. Holley, M. Holmes, and D. Eckhardt, "Fabrication and characterization of a fully conventionally machined, high-performance porous-media electrospray thruster," *Journal of Micromechanics and Microengineering*, vol. 30, no. 11, p. 115021, 2020.

[4] C. S. Coffman, "Electrically-assisted evaporation of charged fluids: Fundamental modeling and studies on ionic liquids," Ph.D. dissertation, Massachusetts Institute of Technology, 2016.

[5] W. A. McGehee, N. Arnold, M. R. Natisin, Z. A. Holley, and D. Eckhardt, "The single emitter air force electrospray thruster (SEAFET) Program: Goals and initial results," in *37th International Electric Propulsion Conference*, Massachusetts Institute of Technology, Cambridge, MA USA, Jun. 2022.

DISTRIBUTION A: Distribution approved for public release.